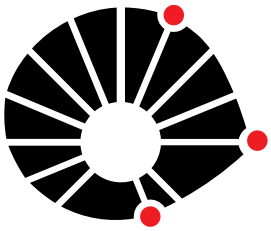

UNICAMP

UNIVERSIDADE ESTADUAL DE CAMPINAS

Instituto de Matemática, Estatística e Computação Científica

LUIS PEDRO LOMBARDI JUNIOR

Mathematical modeling of the Tumor-Host-Immunity interaction encompassing heterogeneity and evasion mechanisms

Modelagem matemática da interação Tumor-Hospedeiro-Imunidade abordando heterogeneidade e mecanismos de evasão

Campinas

2022

Luis Pedro Lombardi Junior

Mathematical modeling of the Tumor-Host-Immunity interaction encompassing heterogeneity and evasion mechanisms

Modelagem matemática da interação Tumor-Hospedeiro-Imunidade abordando heterogeneidade e mecanismos de evasão

Tese apresentada ao Instituto de Matemática, Estatística e Computação Científica da Universidade Estadual de Campinas como parte dos requisitos exigidos para a obtenção do título de Doutor em Matemática Aplicada.

Thesis presented to the Institute of Mathematics, Statistics and Scientific Computing of the University of Campinas in partial fulfillment of the requirements for the degree of Doctor in Applied Mathematics.

Orientador: Hyun Mo Yang

Este trabalho corresponde à versão final da Tese defendida pelo aluno Luis Pedro Lombardi Junior e orientada pelo Prof. Dr. Hyun Mo Yang.

Campinas

2022

Ficha catalográfica
Universidade Estadual de Campinas
Biblioteca do Instituto de Matemática, Estatística e Computação Científica
Ana Regina Machado - CRB 8/5467

Lombardi Junior, Luis Pedro, 1993-
L838m Mathematical modeling of the Tumor-Host-Immunity interaction encompassing heterogeneity and evasion mechanisms / Luis Pedro Lombardi Junior. – Campinas, SP : [s.n.], 2022.

Orientador: Hyun Mo Yang.
Tese (doutorado) – Universidade Estadual de Campinas, Instituto de Matemática, Estatística e Computação Científica.

1. Modelagem matemática. 2. Evasão tumoral. 3. Atividade antitumoral. 4. Equações diferenciais ordinárias. 5. Imunoterapia. I. Yang, Hyun Mo, 1959-. II. Universidade Estadual de Campinas. Instituto de Matemática, Estatística e Computação Científica. III. Título.

Informações Complementares

Título em outro idioma: Modelagem matemática da interação tumor-hospedeiro-imunidade abordando heterogeneidade e mecanismos de evasão
Palavras-chave em inglês:
Mathematical modeling
Tumor evasion
Antitumor activity
Ordinary differential equations
Immunotherapy
Área de concentração: Matemática Aplicada
Titulação: Doutor em Matemática Aplicada
Banca examinadora:
Hyun Mo Yang [Orientador]
Jose Fernando Fontanari
Artur César Fassoni
Giuseppe Romanazzi
Carlos Alberto dos Santos Braumann
Data de defesa: 07-10-2022
Programa de Pós-Graduação: Matemática Aplicada

Identificação e informações acadêmicas do(a) aluno(a)
- ORCID do autor: https://orcid.org/0000-0001-8029-6662
- Currículo Lattes do autor: http://lattes.cnpq.br/8892272071020808

Tese de Doutorado defendida em 07 de outubro de 2022 e aprovada pela banca examinadora composta pelos Profs. Drs.

Prof(a). Dr(a). HYUN MO YANG

Prof(a). Dr(a). JOSE FERNANDO FONTANARI

Prof(a). Dr(a). ARTUR CÉSAR FASSONI

Prof(a). Dr(a). GIUSEPPE ROMANAZZI

Prof(a). Dr(a). CARLOS ALBERTO DOS SANTOS BRAUMANN

A Ata da Defesa, assinada pelos membros da Comissão Examinadora, consta no SIGA/Sistema de Fluxo de Dissertação/Tese e na Secretaria de Pós-Graduação do Instituto de Matemática, Estatística e Computação Científica.

Agradecimentos

À Deus acima de tudo, pela minha vida e por todos que estão presentes nela, por tudo que obtive nesta caminhada, por todas as portas que me foram abertas e por me guiar em todos os meus caminhos.

Aos meus pais Luis Pedro e Rosângela e à minha irmã Simone, por todo o apoio, incentivo, carinho e paciência. Muito obrigado por tudo que me proporcionaram, sem vocês nada disto faria sentido.

Ao professor Hyun Mo Yang, pela compreensão, dedicação, pelo exemplo de professor e pesquisador e por todo o conhecimento que pude obter ao longo deste doutorado.

À todos os meus professores , desde a graduação até este momento, que despertaram meu interesse pela matemática aplicada e sempre me deram o incentivo necessário para progredir e conquistar meus objetivos.

Aos meus amigos e entes queridos, pelo companheirismo e apoio nos momentos difíceis.

Aos colegas do laboratório EPIFISMA, pela companhia toda semana, sempre me auxiliando quando necessário.

Aos funcionários do IMECC (biblioteca, secretaria, limpeza, etc), pelos diversos auxílios prestados ao longo do tempo.

O presente trabalho foi realizado com apoio da Coordenação de Aperfeiçoamento de Pessoal de Nível Superior - Brasil (CAPES) - Código de Financiamento 001

RESUMO

O conceito de imunovigilância postula que o sistema imune é capaz de detectar e eliminar células anormais no nosso organismo. Este processo é bastante complexo, envolvendo um grande número de diferentes tipos de células e citocinas que de maneira organizada podem combater o surgimento e desenvolvimento de tumores. A imunoterapia busca melhorar esta resposta imune de maneira a usar as próprias células do hospedeiro no combate ao câncer, aliada a outras terapias como quimioterapia e radioterapia. Nesta tese, propomos modelos matemáticos baseados em equações diferenciais ordinárias para descrever o desenvolvimento de um tumor avascular no organismo do hospedeiro e suas interações com as células imunes. No primeiro capítulo, propomos um modelo simples que descreve a dinâmica entre tumor e tecido saudável levando em consideração a existência de duas linhagens de células tumorais distintas a depender do acúmulo de mutações. Através da análise qualitativa e simulação do modelo, observa-se que quando a mutação ocorre de maneira lenta tem-se a formação de uma massa tumoral heterogênea, em que as duas linhagens podem coexistir, mas a medida que esta taxa aumenta a célula mais mutada tende a sobrepor a outra. No capítulo 2 propomos um modelo que representa o ciclo da imunidade tumoral desde a captura dos neoantígenos pelas células dendríticas até a ativação dos linfócitos efetores. Por meio da análise dos pontos de equilíbrio do sistema e suas respectivas estabilidades de acordo com o conjunto de parâmteros, observa-se que quando a resposta tecidual do hospedeiro é forte, o crescimento do tumor pode ser interrompido e as células tumorais eliminadas, no entanto dependendo da agressividade do mesmo, se a resposta imune não for eficiente o tumor irá se desenvolver. Quando a resposta tecidual é fraca a cura deixa de ser uma possibilidade, mas o tumor pode ser levado a um estado de remissão, a depender da resposta imune. Entretanto, quanto maior a agressividade do tumor, mais resistente ele é ao sistema imune, de modo a requerer uma eficácia cada vez maior para entrar em remissão. O efeito do tratamento imunoterápico foi testado simulando o modelo proposto, pacientes com tumores muito agressivos ou sistemas imunes comprometidos não se beneficiam do tratamento. Quando o tratamento surte efeito, ele deve se estender até que o tumor atinja um tamanho crítico a partir do qual não será capaz de se desenvolver novamente e entrará em remissão.

Palavras-chave: modelagem matemática, evasão tumoral, atividade antitumoral, equações diferenciais ordinárias, imunoterapia.

ABSTRACT

The concept of immunosurveillance postulates that the immune system can detect and eliminate abnormal cells in our body. This process is quite complex, involving a large number of different types of cells and cytokines that, in an organized way, can fight the emergence and development of tumors. Immunotherapy seeks to improve this immune response to use the host's cells to fight cancer, combined with other therapies such as chemotherapy and radiotherapy. In this thesis, we propose mathematical models based on ordinary differential equations to describe the development of an avascular tumor in the host organism and its interactions with immune cells. In the first chapter, we propose a simple model that describes the dynamics between tumor and healthy tissue, taking into account the existence of two distinct tumor cell lines depending on the accumulation of mutations. According to qualitaive analysis and model simulation, when the mutation occurs slowly, there is the formation of a heterogeneous tumor mass, in which the two lineages can coexist, but as this rate increases, the most mutated cell tends to overlap the other. In chapter 2 we propose a model that represents the cycle of tumor immunity from the capture of neoantigens by dendritic cells to the activation of effector lymphocytes. Based on the analysis of the equilibrium points of the system and their respective stabilities according to the parameter set, it is observed that when the tissue response of the host is strongWhen the host tissue response is strong, tumor growth can be stopped and tumor cells eliminated, however depending on the aggressiveness of the host, if the immune response is not efficient the tumor will develop. When the tissue response is weak, the cure is no longer a possibility, but the tumor can be controlled, however the greater the aggressiveness of the tumor, the more resistant it is to the immune system so that it requires increasing efficiency to enter remission. The effect of immunotherapy treatment was tested by simulating the proposed model, patients with very aggressive tumors or compromised immune systems do not benefit from the treatment. When the treatment is effective, it must extend until the tumor reaches a critical size beyond which it will not be able to grow again and will go into remission.

Keywords: mathematical modeling, tumor evasion, antitumoral activity, ordinary differential equations, immunotherapy.

LISTA DE ILUSTRAÇÕES

LISTA DE TABELAS

SUMÁRIO

Introdução

Em todos os países do mundo o câncer é a principal causa de morte e uma importante barreira para o aumento da expectativa de vida da população (1). De acordo com a Organização Mundial da Saúde (OMS), o câncer é a primeira ou segunda maior causa de morte antes dos 70 anos em 112 dos 183 países do mundo (2). Por conta disso, a busca por novas e melhores terapias é constantemente alvo de pesquisas.

O tratamento com drogas anticancerígenas é comumente categorizado em quatro classes diferentes: quimioterapia, que envolve um grande grupo de drogas citotóxicas que interferem na divisão celular e na síntese de DNA; terapia hormonal, que envolve medicamentos que interferem na sinalização do crescimento por meio de receptores hormonais nas células cancerígenas; terapia alvo, que consiste em um novo grupo de anticorpos e inibidores de quinase de pequenas moléculas que visam especificamente proteínas que estão envolvidas em vias de sinalização de crescimento em células cancerígenas; e imunoterapia, que visa a indução ou aumento de respostas imunes anticancerígenas (3). Este último, vem ganhando espaço e interesse ao longo das ultimas décadas, de forma que precisamos cada vez mais compreender todos os mecanismos envolvidos na resposta imune antitumoral.

A modelagem matemática é uma ferramenta importante no estudo dos mais diversos problemas médicos e biológicos. Usando tais modelos podemos testar diferentes cenários, hipóteses e teorias, na tentativa de confirmar ou mesmo refutá-las, sem nos preocupar, por exemplo, com questões éticas além de diminuir o uso de animais em testes, o que torna este tipo de abordagem vantajosa e prática. Estudos teóricos também são importantes e úteis pois geram insights a respeito dos mecanismos complexos existentes nos processos biológicos.

A oncologia matemática visa o estudo dos problemas relacionados ao crescimento tumoral utilizando ferramentas matemáticas e computacionais. Por meio dos mais diversos modelos propostos, é possível dar luz aos diversos questionamentos sobre o surgimento e desenvolvimento do câncer. De fato, a modelagem matemática e computacional é de grande importância para testes experimentais e protocolos de tratamento, com a vantagem

de poderem ser repetidos inúmeras vezes, sem possíveis danos a saúde dos pacientes e sem o alto custo financeiro decorrente dos experimentos em laboratório e testes clínicos.

Nesta tese propomos e analisamos modelos matemáticos baseados em equações diferenciais ordinárias para representar o crescimento tumoral e sua intereção com as células do hospedeiro além da resposta imune desencadeada. O objetivo principal é gerar informação teórica a respeito da dinâmica envolvendo tumor-hospedeiro-imunidade, o que nos permite elucidar as possibilidades de cura, remissão e até mesmo recidiva tumoral, além de dar suporte à simulação de protocolos de tratamento, em especial os imunoterápicos.

No Capítulo 1 consideramos a interação entre tumor e células saudáveis do hospedeiro, por meio de um modelo que considera a competição entre estas células e a pressão seletiva que uma exerce sobre a outra. Além disso, dois fenótipos diferentes de células tumorais foram considerados no modelo, diferenciados pela quantidade de mutações que cada um carrega. Assumimos que o acúmulo de mutação em um dos tipos de células faz com que, ao longo do tempo, ela se diferencie em um segundo tipo que apresenta diferentes parâmetros em relaçõ a primeira. O intuito é estudar as condições e situações em que a massa tumoral será formada por somente um ou ambos tipos de células. Esta informação é importante pois diferentes linhagens de células tumorais podem apresentar diferentes imunogenicidades e resistência a tratamentos, impactando na dinâmica e possíveis terapias a serem aplicadas.

No Capítulo 2 propomos e analizamos um modelo para o ciclo da imunidade tumoral, considerando os mecanismos envolvidos na ativação da resposta imune antitumoral, deste a captura dos neoantígenos pelas células dentríticas até a apresentação dos mesmos aos linfócitos no linfonodo regional. Avaliamos também os impactos dos mecanismos de evasão usados pelo tumor para escapar da resposta imune e como eles afetam a dinâmica do sistema. Finalmente, o modelo proposto pode ser usado para simular o uso de imunoterapias no tratamente de tumores, avaliar seus impactos e também limitações.

Por fim, apresentamos as conclusões desta tese e indicamos perspectivas futuras para continuação desta pesquisa. Os capítulos foram escritos em formato de artigo, em inglês, para publicação em periódicos internacionais. As demais partes da tese, como introdução e conclusão, estão escritas em português.

Chapter 1

A Mathematical Model of Tumor Growth Considering Mutation Accumulation

Abstract. Tumor heterogeneity describes differences between the abnormal cells within a tumor. As a result of this heterogeneity, the bulk tumor might include different cells harboring distinct molecular signatures with differential levels of sensitivity to treatment. In this work, we propose a mathematical model for cancer onset and progression, considering three populations: normal cells, type-1 tumor cells, which carry only a few mutations, and type-2 tumor cells, which carry more mutations. The genetic instability was included by a linear flux from type-1 to type-2 cells. Mathematical analysis was performed in detail. Results indicate that cancer onset can be prevented if the host body response is strong against both types of tumor cells. The formation of heterogeneous or homogeneous tumors depends on the mutation rate. For fast mutation accumulation, the model predicts a homogeneous tumor mass, since the mutated cells overpower the nonmutated ones. On the other hand for a low mutation rate, both types of cells can coexist and a heterogeneous tumor mass is predicted. Both situations may occur for an intermediary mutation rate according to tissue response and tumor aggressiveness.

Keywords: tumor heterogeneity; genetic instability; tumor growth, stability; bifurcations.

1.1 INTRODUCTION

Tumor heterogeneity is the observation that different tumor cells show distinct phenotypic features, including cellular morphology, metabolism, gene expression, proliferation, and metastatic potential. For instance, whenever a cell divides, a few mutations are acquired leading to a diverse population of cancer cells (4, 5, 6). These subpopulations may possess an evolutionary advantage over the others within the tumor microenvironment, and these subclones may become dominant in the tumor over time (7, 8). Also, hetero-

geneity is a significant challenge in cancer treatment since the tumor cells may exhibit different sensitivities to therapeutic drugs. Therefore, understanding and characterizing heterogeneity may guide the creation of more refined treatment strategies to yield higher efficacy (9).

Mutations in tumor cells can also generate neoantigens which may be recognized by the host immune system and trigger an antitumor immune response (10). The total number of mutations found in the DNA of cancer cells is called tumor mutational burden (TMB). Recent studies have suggested that tumors that have a high number of mutations appear to be more likely to respond to certain types of immunotherapy (11, 12, 13, 14), so the TMB is being used as a type of predictive biomarker.

Mathematical models have been used to help address questions associated with carcinogenesis and cancer evolution through multiple stages, in which somatic mutations accumulate to initiate malignancy (15). The models in literature have used different approaches, such as ordinary differential equations (16, 17, 18, 19, 20), partial differential equations (21, 22) and also computational models (23). Spencer et al.(16) developed a model considering angiogenesis, apoptosis, and genetic instability to investigate which pathway instigated the fastest tumor growth based on breast cancer data. Alvarez, Barbuto e Venegeroles(20), in turn, proposed a model for the cancer immunosurveillance which focused on the phenotypic heterogeneity of tumor cells, regarding the differences of immunogenicities. The model considers two types of tumor cells and two kinds of effector cells and describes phenomena such as tumor dormancy, robustness, and immunoselection over tumor heterogeneity, the immunoediting hypothesis (24, 25). The model proposed here is similar to the model in (19), where an Ordinary Differential Equation based model was developed considering three populations: normal, premalignant, and cancer cells, including genetic instability as an enabling characteristic of tumor progression. Their results indicate that apoptosis and tissue repair system are the first barriers against tumor progression, and also show that the presence of aggressive cancer cells opens the way to the survival of less adapted premalignant cells. The differences between the models include the mutation rate, which is considered linear in our study, and the interaction between tumor cells: we consider that both types of tumor cells compete for the same carrying capacity and such competition has several consequences in the system behavior.

In this study, we address the role of mutations in tumor evolution using a model of clonal evolution within a growing tumor. The model is based on a system of three nonlinear ordinary differential equations, describing three cell populations: normal cells, type 1 of tumor cells, which carry only a few mutations, and type 2 of tumor cells, which carry more mutations. The genetic instability of tumor cells is included in the model by the transition from type 1 cells to type 2 due to mutation accumulation. Our goal is to perform qualitative and quantitative extensive analyses in the parameter space to

entirely describes the model behavior, providing insightful information about the role of heterogeneity in cancer onset. The paper is organized as follows. In Section 1.2 the model is presented. In Section 1.3 the analysis of the model is performed. Discussions and conclusion are presented in Section 1.4.

1.2 MATHEMATICAL MODELLING

We propose a mathematical model consisting of a system of ordinary differential equations describing the interactions between tumor cells and healthy tissue cells. The tumor cells are divided into two phenotypes according to the number of mutations they carry, the tumor mutational burden TMB. More mutated tumor cells tend to be recognized by the host body more easily, while less mutated cells may go unnoticed. The model does not include several aspects of tumor growth and immune response but can provide us information about the dynamics between these cells, which are useful to understand more complex and accurate models.

Three state variables are considered: $N(t)$ represents the normal cells or healthy tissue cells, $A_1(t)$ corresponds to the tumor cells which presents low tumor mutational burden (TMB), and $A_2(t)$ stands for the mutated tumor cells presenting high TBM. The hypothesis behind the model are the following.

The production of normal cells is related to the maintenance of a homeostatic state, through the natural replenishment of old and dead cells, and it does not depend directly on the total number of living normal cells, but is an intrinsic property of the tissue (26). For this reason, we consider a constant recruitment r_n of normal cells and a natural mortality rate μ_n, which implies in a homeostatic state given by r_n/μ_n. Also, the presence of tumor cells causes several negative effects in the tissue, like suppression of immune cells (27, 15), the release of death signals (15) and also increasing the local acidity (28, 29). Parameters b_1 and b_2 encompass all these effects or, simply, they represent the competition between tissue and tumor. The equation describing the dynamics of healthy tissue is given by

$$\frac{dN}{dt} = \underbrace{r_n}_{\text{Recruitment}} - \underbrace{(b_1 A_1 N + b_2 A_2 N)}_{\text{Competition}} - \underbrace{\mu_n N}_{\text{Natural mortality}} \tag{1.1}$$

The proliferation of tumor cells is independent of the tissue's structure, and they keep their growth program due to the self-sufficiency in growth signals (30). So we consider a logistic growth to tumor cells, being r_1 and r_2 the intrinsic growth rates for A_1 and A_2 cells, μ_1, μ_2 the respective mortality rates and K the tumor carrying capacity for both types of tumor cells.

In the same way that the tumor harms healthy cells, normal cells also cause damage to tumor cells, due to competition by space or nutrients for example, which we will call tissue response and is represented by the parameters c_1 and c_2. Due to genetic instability, A_1 cells mutate and turn into A_2 cells according to the mutation rate α. TO keep the model tractable and as simple as possible, we assumed α as a constant flux which representing that the mutation accumulation is a natural process which do not depends on external factors.

The equations for tumor cells dynamics are given by:

$$\frac{dA_i}{dt} = \underbrace{r_i A_i \left(1 - \frac{A_1 + A_2}{K}\right)}_{\text{Tumor growth}} - \underbrace{c_i N A_i}_{\text{Competition}} + \underbrace{(-1)^i \alpha A_1}_{\text{Mutational accumulation}} - \underbrace{\mu_i A_i}_{\text{Natural mortality}}, \tag{1.2}$$

for $i = 1, 2$. The mutation accumulation term represents the flux, positive or negative, between A_1 and A_2 cells.

In Figure 1.1 we present a flowchart describing the interactions among the cell populations.

Figure 1.1 – Flow diagram of heterogeneous tumor growth model.

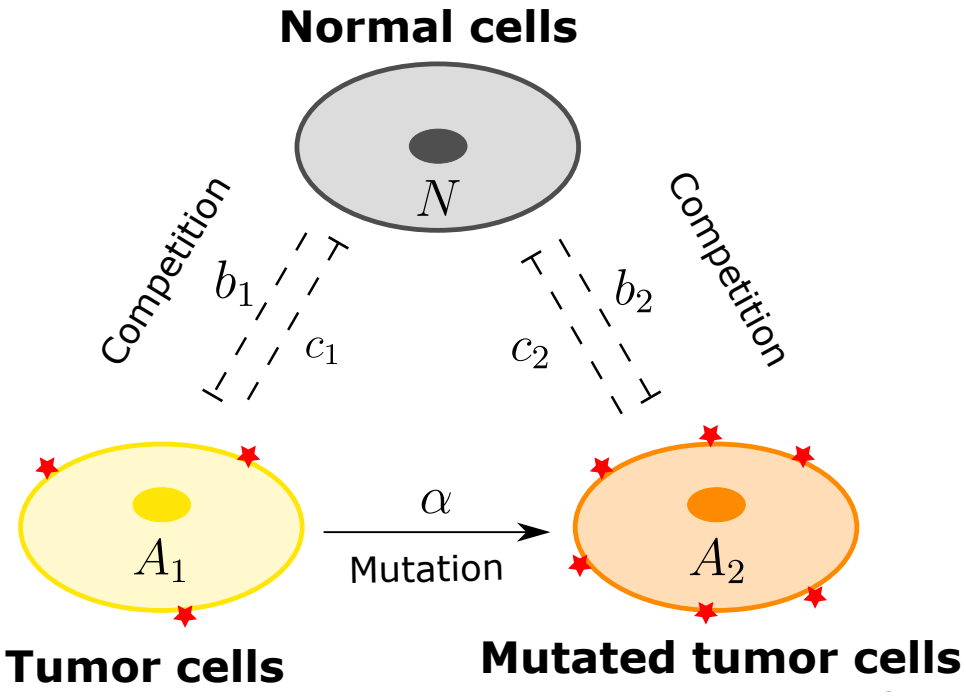

The model parameters are described in table 1.1.

Finally, the full model is given by:

Table 1.1 – Parameters of heterogeneous tumor growth model

Parameter	Description	Value	Unity
r_n	Healthy cells recruitment rate	10^2	cell day^{-1}
μ_n	Healthy cells natural mortality rate	0.01	day^{-1}
r_1	Type 1 tumor cells intrinsic growth rate	0.05	day^{-1}
r_2	Type 2 tumor cells intrinsic growth rate	0.04	day^{-1}
μ_1	Type 1 tumor cells natural mortality rate	0.02	day^{-1}
μ_2	Type 2 tumor cells natural mortality rate	0.03	day^{-1}
K	Tumor carrying capacity	7.5×10^3	cells
b_1, b_2	Tumor cells aggressiveness	Variable	cell day^{-1}
c_1, c_2	Tissue response to tumor cells	Variable	cell day^{-1}
α	Mutation rate	Variable	day^{-1}

$$\begin{cases} \dfrac{dN}{dt} &= r_n - b_1 A_1 N - b_2 A_2 N - \mu_n N \\ \dfrac{dA_1}{dt} &= r_1 A_1 \left(1 - \dfrac{A_1 + A_2}{K}\right) - c_1 N A_1 - \alpha A_1 - \mu_1 A_1 \\ \dfrac{dA_2}{dt} &= r_2 A_2 \left(1 - \dfrac{A_1 + A_2}{K}\right) - c_2 N A_2 + \alpha A_1 - \mu_2 A_2 \end{cases} \tag{1.3}$$

In the next sections, the analysis and numerical simulations of system (1.3) will be performed to describe the existence and stability of equilibrium points.

1.3 MODEL ANALYSIS

In this section, a mathematical analysis of system (1.3) is performed. The equilibrium points are obtained by setting derivatives in (1.3) equal to zero and the stability analysis is performed by the eigenvalues of the Jacobian Matrix $J(N, A_1, A_2)$ evaluated at each equilibrium.

Before we start the equilibrium points analysis, consider Ω as the subset of $\mathbb{R}^3$ defined by

$$\Omega = \left\{ (N, A_1, A_2) \in \mathbb{R}^3_+ \mid N \leqslant \frac{r_n}{\mu_n} \text{ and } A_1 + A_2 \leqslant \frac{IK}{r} \right\}, \tag{1.4}$$

where $I = r - \mu$, being $r = \max\{r_1, r_2\}$ and $\mu = \min\{\mu_1, \mu_2\}$.

Theorem 1 (Invariant Set)**.** *Model (1.3) is invariant in Ω, that is, taking an initial condition in Ω, the solutions remain in Ω.*

Proof. We need to show that the flow of the system (1.3) at the borders of Ω points into the region, that is, to analyze the signal of the derivatives at the border of Ω and show that, taking an initial condition in Ω, the state variables can not assume negative values nor goes to infinity. Figure 1.2 illustrates the invariant set Ω.

Figure 1.2 – Invariant set Ω for system (1.3)

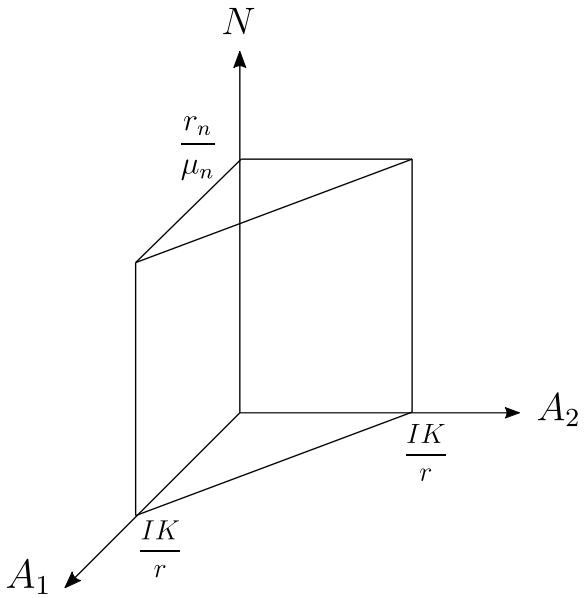

Let us analyse the five borders described in Figure 1.2 $(i)N = 0$, $(ii)A_1 = 0$, $(iii)A_2 = 0$, $(iv)N = r_n/\mu_n$ and $(v)A_1 + A_2 = IK/r$.

(i) If $N = 0$ then from the first equation in (1.3) we obtain $dN/dt = r_n > 0$, so $N = 0 \Rightarrow dN/dt > 0$ and N can not assume negative values.

(ii) Clearly, $A_1 = 0 \Rightarrow dA_1/dt = 0$, which means that the orbits remain at the border and A_1 is nonnegative in Ω.

(iii) If $A_2 = 0$ then $dA_2/dt = \alpha A_1 \geqslant 0$. So, A_2 is also nonnegative.

(iv) If $N = r_n/\mu_n$ then $dN/dt = (-b_1A_1 - b_2A_2)r_n/\mu_n \leqslant 0$. Moreover, if $N \geqslant r_n/\mu_n \Rightarrow dN/dt \leqslant 0$ and the orbits goes into Ω.

(v) If $A_1 + A_2 = IK/r$ then

$$\begin{aligned}
\frac{d(A_1 + A_2)}{dt} &= (r_1A_1 + r_2A_2)\left(1 - \frac{A_1 + A_2}{K}\right) - N(c_1A_1 + c_2A_2) - \mu_1A_1 - \mu_2A_2 \\
&\leqslant r(A_1 + A_2))\left(1 - \frac{A_1 + A_2}{K}\right) - \mu(A_1 + A_2) \\
&= I(A_1 + A_2)\left(1 - \frac{r}{IK}(A_1 + A_2)\right) \\
&= 0,
\end{aligned}$$

so, $A_1 + A_2 = IK/r \Rightarrow \dfrac{d(A_1 + A_2)}{dt} \leqslant 0.$

Therefore, the flow of system (1.3) at the border of Ω points into Ω, and the solutions can not scape from the invariant set. □

1.3.1 TUMOR-FREE EQUILIBRIUM

The trivial equilibrium or tumor-free equilibrium is given by

$$P_0 = (N_0^*, A_1^*, A_2^*) = \left(\frac{r_n}{\mu_n}, 0, 0\right). \tag{1.5}$$

The Jacobian Matrix evaluated at P_0 can be written as

$$J(P_0) = \begin{bmatrix} -\mu_n & -b_1\dfrac{r_n}{\mu_n} & -b_2\dfrac{r_n}{\mu_n} \\ 0 & r_1 - \alpha - \mu_1 - c_1\dfrac{r_n}{\mu_n} & 0 \\ 0 & \alpha & r_2 - \mu_2 - c_2\dfrac{r_n}{\mu_n} \end{bmatrix},$$

whose eigenvalues are

$$\lambda_1 = -\mu_n, \quad \lambda_2 = \frac{r_n}{\mu_n}(c_1^{th} - c_1), \quad \lambda_3 = \frac{r_n}{\mu_n}(c_2^{th} - c_2)$$

where

$$c_1^{th} = \frac{\mu_n}{r_n}R_1 \quad c_2^{th} = \frac{\mu_n}{r_n}R_2 \tag{1.6}$$

for $R_1 = (r_1 - \alpha - \mu_1)$ and $R_2 = (r_2 - \mu_2)$, which can be interpreted as the net reproduction rate of tumor cells A_1 and A_2, respectively. We assume that these net rates are positive, otherwise the tumor cells will be extinct.

So, the tumor-free equilibrium point P_0 is stable if, and only if, $c_2 > c_2^{th}$ and $c_1 > c_1^{th}$, which means that if the tissue response against both tumor cells is high, then the normal cells can eliminate the tumor cells. Notice that the host body needs to present a good response against both phenotypes of tumor cells, and not only one. The net rates R_i increase the thresholds c_i^{th} and the risk of tumor onset, that is, more proliferative tumors settle in the host more easily. Moreover, the fraction μ_n/r_n which appears in both thresholds can be written as $\mu_n/r_n = 1/N_0^*$, where N_0^* is the normal cells equilibrium state in absence of a tumor, or the homoeostatic state. So, increasing the homoeostatic state decreases the thresholds c_i^{th} and consequently decreases the risk of tumor onset.

1.3.2 BOUNDARY EQUILIBRIUM POINTS

The boundary equilibrium is obtained when one of the tumor populations is zero, which corresponds to a homogeneous tumor mass. Since there is the flux α from A_1 to A_2, there is no equilibrium point such that $A_1 \neq 0$ and $A_2 = 0$, which means that, the proposed model allows the existence of homogeneous tumor composed only by high TBM cells, which is supposed to be easily recognized by the immune system.

The boundary equilibrium is obtained taking $A_1 = 0$, and can be written as

$$P_b = (N^*, A_1^*, A_2^*) = \left(\frac{r_n}{b_2 A_2^* + \mu_n}, 0, A_2^*\right).$$

where A_2^* is a root of the second degree polynomial $p_2(A_2^*) = a_2(A_2^*)^2 + a_1 A_2^* + a_0$, whose coefficients are given by

$$a_2 = \frac{b_2 r_2}{K}, \qquad a_1 = (r_2 - \mu_2)(b_2^{th} - b_2), \qquad a_0 = r_n(c_2 - c_2^{th}), \tag{1.7}$$

and the parameters b_2^{th} and c_2^{th} are

$$b_2^{th} = \frac{\mu_n r_2}{K(r_2 - \mu_2)} \quad \text{and} \quad c_2^{th} = \frac{\mu_n(r_2 - \mu_2)}{r_n}.$$

1.3.2.1 EXISTENCE

The existence of boundary equilibria is determined by the analysis of polynomial $p_2(A_2^*)$ in (1.7) and using the Descartes rule of signs (31). The discriminant of $p_2(A_2^*)$ is given by

$$\Delta = (r_2 + \mu_2)^2(b_2^{th} - b_2)^2 - \frac{4b_2 r_2}{K} r_n(c_2 - c_2^{th}).$$

Let us define $b_{2\Delta}^{th}$ as the biggest value of b_2 (if there are more than one possible) such that $\Delta = 0$, which can be written as

$$b_{2\Delta}^{th} = b_2^{th} + 2\tau + 2\sqrt{\tau(b_2^{th} + \tau)}, \qquad \text{for } \tau = \frac{r_2 r_n(c_2 - c_2^{th})}{K(r_2 - \mu_2)^2}$$

The existence of boundary equilibriums is summarized as follow:

1. If $c_2 > c_2^{th}$ and $b_2 < b_{2\Delta}^{th}$, then there is no boundary equilibrium.
2. If $c_2 > c_2^{th}$ and $b_2 > b_{2\Delta}^{th}$, then there are two boundary equilibriums, P_b^1 and P_b^2.
3. If $c_2 < c_2^{th}$ there will always be a single boundary equilibrium P_b^2.

Notice that the existence of boundary equilibriums is determined by the interaction between normal cells N and high TMB tumor cells A_2. Parameters related to the A_1 cells do not interferer in the existence of boundary equilibrium points.

When the tissue response against cancer is strong and the tumor aggressiveness is low (case 1 above), the boundary equilibrium does not exist. Increasing b_2 two boundary equilibrium states appear in the dynamics (case 2). Finally, if the tissue response is weak (case 3) a single boundary equilibrium exists regardless of the aggressiveness parameter b_2.

1.3.2.2 STABILITY

Let P_b^1 and P_b^2 be the boundary equilibrium points determined in the previous subsection. The Jacobian Matrix evaluated at the boundary equilibrium is given by

$$J(P_b^i) = \begin{bmatrix} -b_2 A_2^* - \mu_n & -b_1 N^* & -b_2 N^* \\ 0 & r_1\left(1 - \dfrac{A_2^*}{K}\right) - c_1 N^* - \alpha - \mu_1 & 0 \\ -c_2 A_2^* & \alpha - \dfrac{r_2 A_2^*}{K} & -\dfrac{r_2 A_2^*}{K} \end{bmatrix} \tag{1.8}$$

The characteristic polynomial of the matrix in (1.8) can be written as

$$p^b(\lambda) = p_1^b(\lambda) p_2^b(\lambda) \tag{1.9}$$

where

$$\begin{aligned} p_1^b(\lambda) &= r_1\left(1 - \frac{A_2^*}{K}\right) - c_1 N^* - \alpha - \mu_1 - \lambda \\ p_2^b(\lambda) &= \lambda^2 + \left(b_2 A_2^* + \mu_n + \frac{r_2 A_2^*}{K}\right)\lambda + A_2^*\left(2a_2 A_2^* + a_1\right). \end{aligned}$$

So, the boundary equilibrium points will be stable if both polynomials, p_1^b, and p_2^b, have negative real-part roots.

Firstly, let us analyse p_2^b. We already know that there up two boundary equilibriums, $A_2^{1*} = \dfrac{-a_1 + \sqrt{\Delta}}{2a_2}$ and $A_2^{2*} = \dfrac{-a_1 - \sqrt{\Delta}}{2a_2}$. Notice now that, if $(2a_2 A_2^* + a_1) < 0$, then, by Descartes' rule os signs, p_2^b has a positive real root. On the other hand if $(2a_2 A_2^* + a_1) > 0$, then p_2^b has roots with negative real part. Substituting the expressions for A_2^{1*} and A_2^{2*} we have

$$A_2^{1*}\left(2a_2 A_2^{1*} + a_1\right) = -A_2^{1*}\sqrt{\Delta} < 0 \quad \text{and} \quad A_2^{2*}\left(2a_2 A_2^{2*} + a_1\right) = A_2^{2*}\sqrt{\Delta} > 0.$$

So, we conclude that the boundary equilibrium P_b^1, when it exists, is always unstable. On the other hand, P_b^2's stability is determined by the eigenvalue related to polynomial p_1^b, since p_2^b has roots with negative real part.

Now, let us analyze the polynomial p_1^b. Notice that this polynomial contains parameters related to the A_1 cells, so the interaction between the two types of tumor cells will determine if the boundary equilibrium is stable or not. Increasing r_1 (or equivalently decreasing c_1 and α) the eigenvalue related to p_1^b tends to become positive, which means that, if the tumor microenvironment is favorable to A_1, the boundary equilibrium must be unstable, and a heterogeneous tumor mass is expected. On the other hand, if the environment does not benefit the less mutated cells A_1, then the mutated cells A_2 may eliminate (by competition) the other cells and the boundary equilibrium becomes stable, corresponding to a homogeneous tumor.

When A_1 cells are suppressed from model (1.3), the system of equations is the same presented in (32), and the analysis of the boundary equilibria is quite similar. The

main difference is related to the polynomial p_1^b which represents the interaction between the two types of tumor cells. In (32), the stability of the tumor state can be easily determined and depends on the relation between A_2 and N, however when A_1 cells are included, the competition between tumor cells plays a role to determine if the tumor phenotypes will coexist or not, that is, the boundary equilibria is stable or not.

1.3.3 INTERNAL EQUILIBRIUM POINTS

In this section we analyse the existence and stability of the internal equilibrium points $P^* = (N^*, A_1^*, A_2^*)$ of system (1.3). Due to the complexity to find the expressions for N^*, A_1^* and A_2^*, we assume that $b_1 = b_2 = b$ and $c_1 = c_2 = c$, that is, the competition terms between tumor and healthy tissue are equal for both types of tumor cells.

The internal equilibrium point $P^* = (N^*, A_1^*, A_2^*)$ has entries

$$N^* = \frac{r_n}{b_1 A_1^* + b_2 A_2^* + \mu_n}, \qquad A_1^* = A_2^* \frac{(r_1 - r_2)\left(1 - \frac{A_2}{K}\right) + \mu_2 - \mu_1 - \alpha}{(r_1 - r_2)A_2^*/K + \alpha} \tag{1.10}$$

where A_2^* is a root of the polynomial

$$p_I(A_2^*) = q_0 + q_1 A_2^* + q_2 (A_2^*)^2 6 \tag{1.11}$$

whose coefficients are given by

$$\begin{aligned} q_0 &= \alpha^2 r_n (c - c_1^{th}) \\ q_1 &= \frac{\alpha}{K}\left(2R r_n (c - c_1^{th}) + (R + U) R_1 K (b_1^{th} - b)\right) \\ q_2 &= \frac{1}{K^2}\left(cR^2 r_n + (R(\alpha + \mu_1) + r_1 U)(bK(R + U) + R\mu_n)\right) \end{aligned} \tag{1.12}$$

with $R = r_1 - r_2$, $U = \mu_2 - \mu_1$, $R_1 = r_1 - \mu_1 - \alpha$ and

$$b_1^{th} = \frac{r_1 \mu_n}{K R_1}, \qquad c_1^{th} = \frac{R_1 \mu_n}{r_n}. \tag{1.13}$$

Two options must be considered regarding the parameters R and U. In the first one, we assume that the mutations are unfavorable to tumor cells, that is, the less mutated tumor cells A_1 are more proliferative and presents a smaller mortality rate than the A_2 cells, which means that $r_1 > r_2$ and $\mu_1 < \mu_2$, implying $R > 0$ and $U > 0$. The other option is to consider that the mutations are favorable to tumor cells, increasing the proliferation and decreasing the apoptosis of A_2 cells, that is, $r_2 > r_1$, $\mu_2 < \mu_1$, implying $R < 0$ and $U < 0$.

Let us first analyze the unfavorable mutation case, in which $R, U > 0$. Tumor cells that present more mutation can be, in general, more easily recognized and eliminated by the immune system, and also are more sensitive to the immunotherapies, so the case in which $R > 0$ and $U > 0$ corresponds to the worst situation for treatment successful since

we assuming that the A_1 cells, which are more resistant to immune response, are also more proliferative ($r_1 > r_2$ and $\mu_1 < \mu_2$), which turn them even more hard to eliminate. The favorable case will be commented after.

By the Descartes' Rule of Signs, polynomial $p_I(A_2^*)$ has the following behaviour:

1. If $c < c_1^{th}$ than there is a single positive root A_2^*.
2. If $c > c_1^{th}$ and $b < b_{1\Delta}^{th}$ then there is no positive roots.
3. If $c > c_1^{th}$ and $b > b_{1\Delta}^{th}$ then there are two positive roots.

where $b_{1\Delta}^{th}$ is the value of b, with $b_{1\Delta}^{th} > b_1^{th}$, such that the discriminant of polynomial (1.11) is equal to zero.

Notice that the roots above described not necessarily are biological-feasible equilibrium points of system (1.3) since the expression for A_1^* in (1.10) can be negative for some values of A_2^*. So, after determine the roots, we need to verify is the expression for A_1 is positive.

As we pointed, the existence of internal equilibrium points is determined by the position of b and c in comparison to b_1^{th} and c_1^{th}, while for the existence of boundary equilibrium points we need to compare b and c with b_2^{th} and c_2^{th} respectively. Since each parameters must be compared to two thresholds, it is important to know the relative position between b_1^{th} and b_2^{th}, and between c_1^{th} and c_2^{th} in order to determine the existence of boundary and internal equilibrium points for different combinations of the parameters b and c.

Firstly, for c_1^{th} and c_2^{th} we have that

$$\begin{aligned} c_1^{th} - c_2^{th} &= \frac{\mu_n}{r_n}(r_1 - \mu_1 - \alpha + r_2 - \mu_2) \\ &= \frac{\mu_n}{r_n}(R + U - \alpha) \\ &= \frac{\mu_n}{r_n}(\alpha_c - \alpha). \end{aligned}$$

So, the relative position between c_1^{th} and c_2^{th} are determined by the mutation rate α. If $\alpha > \alpha_c = R + U$, then $c_2^{th} > c_1^{th}$, or if $\alpha < \alpha_c$, then $c_2^{th} < c_1^{th}$.

For b_1^{th} and b_2^{th} we have that

$$\begin{aligned} b_1^{th} - b_2^{th} &= \frac{\mu_n}{r_n}\left(\frac{r_1}{R_1} - \frac{r_2}{R_2}\right) \\ &= \frac{r_2\mu_n}{r_n R_1 R_2}\left(\alpha - \frac{r_1\mu_2 - r_2\mu_1}{r_2}\right) \\ &= \frac{r_2\mu_n}{r_n R_1 R_2}\left(\alpha - \alpha_b\right). \end{aligned}$$

Thus, denoting $\alpha_b = \dfrac{r_1\mu_2 - r_2\mu_1}{r_2}$ we obtain that, if $\alpha > \alpha_b$ then $b_1^{th} > b_2^{th}$, or if $\alpha < \alpha_b$, then $b_1^{th} < b_2^{th}$.

Now, let us compare α_c and α_b as follows:

$$\begin{aligned}
\alpha_c - \alpha_b &= (r_1 - r_2) + (\mu_2 - \mu_1) - \left(\frac{r_1\mu_2 - r_2\mu_1}{r_2}\right) \\
&= \frac{1}{r_2}\left(r_1r_2 - r_2^2 + r_2\mu_2 - r_2\mu_1 - r_1\mu_2 + r_2\mu_1\right) \\
&= \frac{1}{r_2}(r_1 - r_2)(r_2 - \mu_2) \\
&\geqslant 0
\end{aligned}$$

Therefore, $\alpha_c > \alpha_b$. Using this, we must analyze three different cases according to the mutation rate α, which are

1. $\alpha > \alpha_c$, which implies $c_1^{th} < c_2^{th}$ and $b_1^{th} > b_2^{th}$.
2. $\alpha < \alpha_b$, which implies $c_1^{th} > c_2^{th}$ and $b_1^{th} < b_2^{th}$.
3. $\alpha_b < \alpha < \alpha_c$, which implies $c_1^{th} > c_2^{th}$ and $b_1^{th} > b_2^{th}$.

CASE 1: HIGH MUTATION RATE ($\alpha > \alpha_c$)

Let us first consider the case in which the A_1 cells rapidly turn into A_2 cells, that is, α is high.

The existence of internal equilibrium points is determined by the roots of polynomial (1.11). In addiction, we need to verify if, given a root A_2^*, the expression for A_1^* is positive. So, observe that, since we assume $R, U > 0$ and $\alpha > \alpha_c$, from the expression for A_1^* in (1.10) we have that

$$\begin{aligned}
A_1^* \geqslant 0 \quad &\Leftrightarrow \quad A_2^*\frac{(r_1 - r_2)\left(1 - \frac{A_2}{K}\right) + \mu_2 - \mu_1 - \alpha}{(r_1 - r_2)A_2/K + \alpha} \geqslant 0 \\
&\Leftrightarrow \quad R\left(1 - \frac{A_2}{K}\right) + U - \alpha \geqslant 0 \\
&\Leftrightarrow \quad A_2^* \leqslant \frac{K}{R}(\alpha_c - \alpha) < 0
\end{aligned}$$

So, to obtain $A_1^* > 0$, it is necessary that $A_2^* < 0$, which means that when $\alpha > \alpha_c$ there is no internal equilibrium, and the model dynamics contains only the trivial and the boundary equilibriums. Therefore, when a high mutation rate is considered, the less mutated cells A_1 are excluded from the system dynamics, and only one type of tumor cells may coexist with the healthy cells. Therefore, considering a high mutation rate causes the formation of a homogeneous tumor mass.

To confirm that behavior, we perform numerical simulations considering several values of b and c. For each combination, we analyze the existence and the stability (by the Jacobian matrix) of the tumor-free state, the boundary equilibrium points, and the internal equilibrium points. The results are depicted in Figure 1.3, where P_0 stands for the trivial equilibria, P_b^1 and P_b^2 stands for the boundary equilibrium points. The equilibrium points inside squares are stable, while the others are unstable.

Figure 1.3 – Existence and stability diagram for $\alpha > \alpha_c$

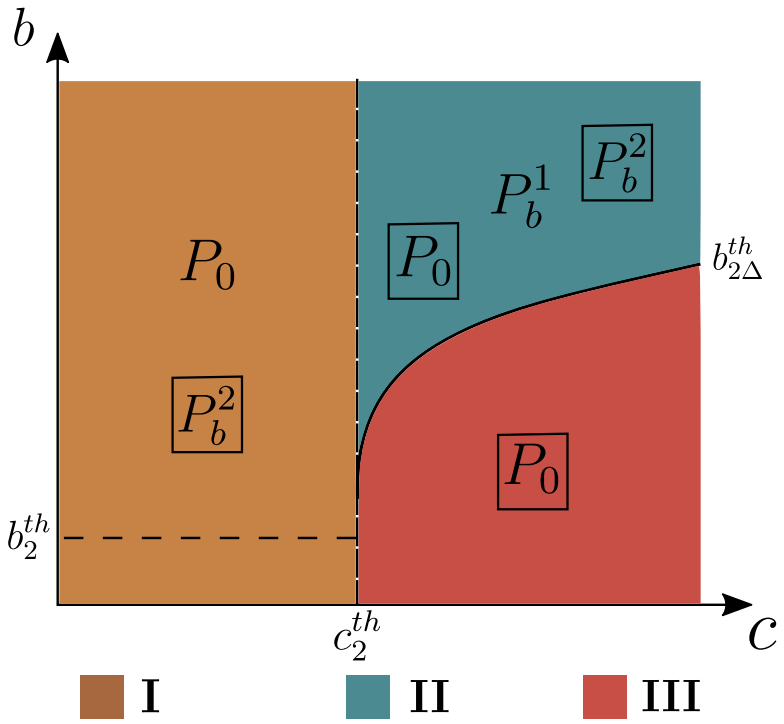

Three distinct regions can be observed in Figure 1.3. In region I, when $c < c_2^{th}$, the boundary equilibria P_b^2 is globally stable, while the tumor-free state is unstable. In region II we have that $c > c_2^{th}$ and $b > b_{2\Delta}^{th}$, so there are two boundary equilibrium points and there is bistability between the tumor-free state P_0 and the boundary equilibria P_b^2, while P_b^1 is an unstable boundary equilibrium point which divides the basins of attraction, so the initial condition determines if tumor will progress or disappear. Finally, region III, which is also called the cure regime, corresponds to the situation where tumor onset is not possible since the tumor-free state is the only one equilibrium point in the dynamics, and also it is stable.

To illustrate the transitions between these regimes, Figure 1.4 presents a bifurcation diagram. In 1.4a we horizontally go through Figure 1.3, fixing b and varying the tissue response c, transiting from I to II and III. In 1.4b we vertically go through Figure 1.3, fixing c and varying the tumor aggressiveness b, transiting from region III to II. The blue color corresponds to stable points, while the red color represents the unstable ones.

Figure 1.4 – Bifurcation diagram for $\alpha > \alpha_c$.

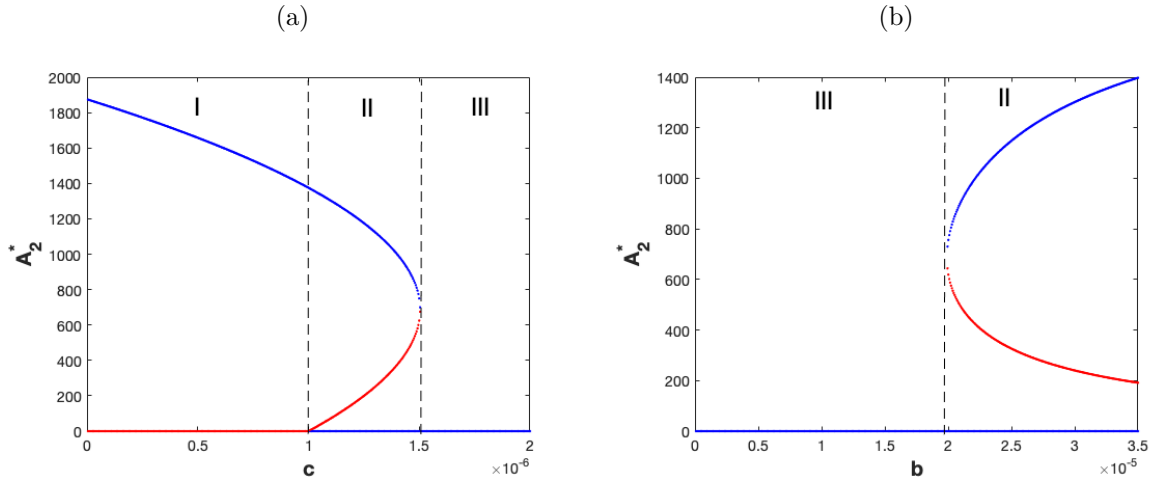

Figure 1.4a shows that, as we increase the tissue response c, system (1.3) approaches the curing regime III, passing through regimes I and II. On the other hand, from Figure 1.4b, increasing the tumor aggressiveness b, the model exists the curing regime III and approach II, exemplifying the tumor onset.

CASE 2: LOW MUTATION RATE ($\alpha < \alpha_b$)

Let us consider now a small flux α from A_1 to A_2 such that $\alpha < \alpha_b$, that is, tumor cells slowly accumulate mutations. As we previously described, in this case we have that $c_1^{th} > c_2^{th}$ and $b_1^{th} < b_2^{th}$.

The stability analysis of the equilibrium points and the existence of internal equilibria (considering the condition imposed in expression (1.10)) was done by numerical simulations. For several combinations of parameters b and c, we analyzed the existence and the stability (using the eigenvalues of Jacobian Matrix) of the trivial equilibrium point P_0, the boundary equilibriums P_b^1 and P_b^2, and also the internal equilibriums P_1 and P_2.

Figure 1.5 illustrates the qualitative behavior of system (1.3). Equilibrium points inside squares are stable, while the others are unstable.

In all the simulations, for several values of α, the positivity condition for A_1^* in the internal equilibria (1.10) is always satisfied, so the low flux $\alpha < \alpha_b$ allows the existence of the internal equilibria for every combination of parameters c and b.

When the tissue response is weak, $c < c_2^{th}$ (regime I in Figure 1.5), even though the boundary equilibria exists, it is unstable, while the internal equilibria P_2 is stable. Taking $c_2^{th} < c < c_1^{th}$ we observe two regimes which are delimited by $b_{2\Delta}^{th}$: above this curve, region II, the internal equilibria is stable and two boundary equilibriums appear, but both are unstable, while for $b < b_{2\Delta}^{th}$, region III, the boundary states do not exists.

Figure 1.5 – Existence and stability diagram for $\alpha < \alpha_b$

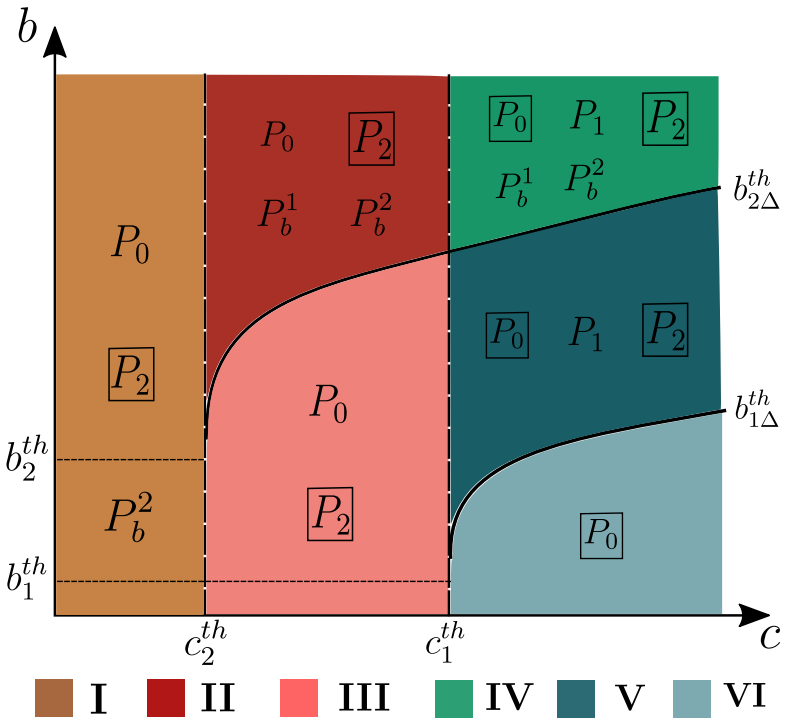

Finally, when the tissue response is strong, $c > c_1^{th} > c_2^{th}$, the tumor-free state becomes stable. For $b < b_{1\Delta}^{th}$, region VI, the cure state P_0 is globally stable (tumor onset is not possible). Increasing b such that $b > b_{1\Delta}^{th}$, the internal equilibria appears and there is bistability between P_2 and P_0. When $b > b_{2\Delta}^{th}$ the boundary states appear, however they are always unstable.

Furthermore, observe in Figure 1.5 that whenever the internal equilibrium P_2 exists, it is stable. On the other hand, the boundary equilibrium points, P_1 and P_2, are always unstable, when they exist. So, when a slow mutation rate is considered, the boundary equilibrium points do not interfere in the system's qualitative behavior, which is guided only by the trivial equilibria and the internal equilibrium points. In other words, when α is small, there always be two types of tumor cells interacting and always a heterogeneous tumor mass.

Similarly to the previous case, we present in Figure 1.6 a bifurcation diagram illustrating the transition among the regimes. In Figure 1.6a we horizontally go through Figure 1.5, fixing b and varying the tissue response c, transiting from the region I to II, then III, V, and VI. In Figure 1.6b we vertically go through Figure 1.5, fixing c and varying the tumor aggressiveness b, transiting from region VI to V and VI. The blue color corresponds to stable points, while the red color represents the unstable ones.

Even if the boundary equilibrium exists, it is not interfering in the dynamics since it is always unstable, represented by the red curves on the left in Figure 1.6a and on the right in 1.6b. Since these states are always unstable, the dynamics considering

Figure 1.6 – Bifurcation diagram for $\alpha < \alpha_b$.

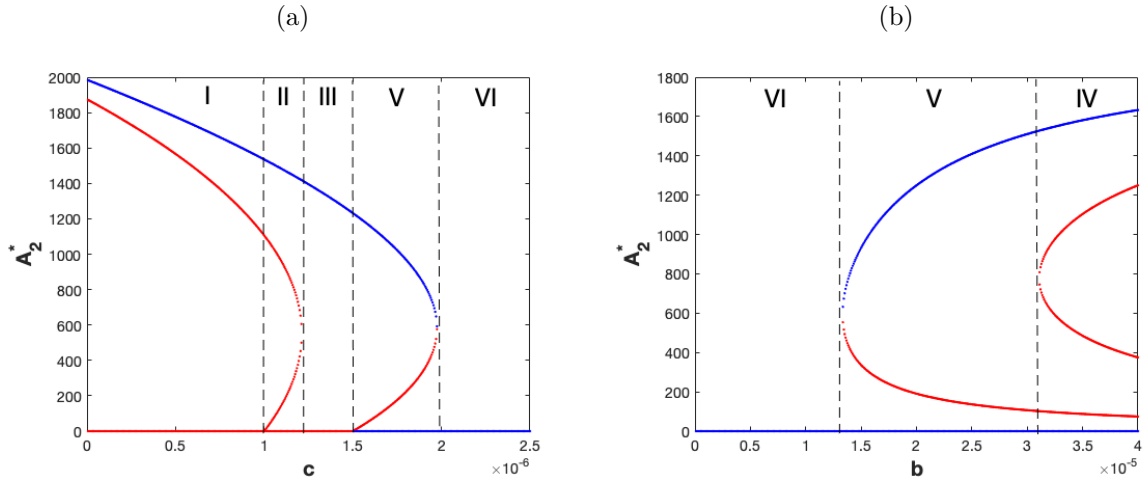

$\alpha < \alpha_b$ can be summarized in only three different regimes: in the first one, when $c < c_1^{th}$, the internal equilibria P_2 is globally stable (regions I, II, and III). In the second one, the tumor-free state is globally stable (region VI), and finally the third regime presents bistability between P_2 and P_0 (regimes IV and V).

Although the existence of the boundary equilibrium does not affect the dynamics, their presence is important for two reasons. First, even though it is unstable, it is still an equilibrium point, so if we manage to eliminate the A_1 cells, using chemotherapy for example, they will not proliferate again. Second, the boundary equilibrium must exist so that we can transition from case 1 ($\alpha > \alpha_c$) to case 2 ($\alpha < \alpha_b$) as we decrease the mutation rate, that is, the boundary equilibria is no longer stable, but it still exists. This situation will be better clarified during the next session.

CASE 3: INTERMEDIARY MUTATION RATE ($\alpha_c > \alpha > \alpha_b$)

As showed, when $\alpha > \alpha_c$, system dynamics is guided by the boundary points, on the other hand, when $\alpha < \alpha_b$, the internal points guide the system dynamics. Equivalently, a fast mutation generates a homogeneous tumor, while slow mutation generates a heterogeneous one. Now, let us deal with the case with an intermediary mutation rate: $\alpha_c > \alpha > \alpha_b$. In this case, we already showed that $c_1^{th} > c_2^{th}$ and $b_1^{th} > b_2^{th}$.

Similar to the previous case, the analysis was done using numerical simulations in which we determine the existence and the stability of the boundary equilibrium points and the internal equilibrium points for several combinations of parameters b and c. The simulations show that different behaviors occur according to the value of α, as it gets closer to the threshold α_c.

Firstly, let us start with $\alpha_c > \alpha > \alpha_b$, but α close to the inferior threshold α_b. Figure 1.4 illustrates the system behavior. The curve denoted by s is related to the

condition for $A_1^* > 0$ and above this curve one of the internal equilibria disappear since the biological-feasible condition is no longer satisfied. Again, P_0 stands for the trivial equilibria, P_b^1 and P_b^2 stand for the boundary equilibrium points, and P_1 and P_2 stand for the internal equilibrium points. The equilibrium points inside squares are stable, while the others are unstable.

Figure 1.7 – Existence and stability diagram for $\alpha_b < \alpha < \alpha_c$, when α is close to α_b

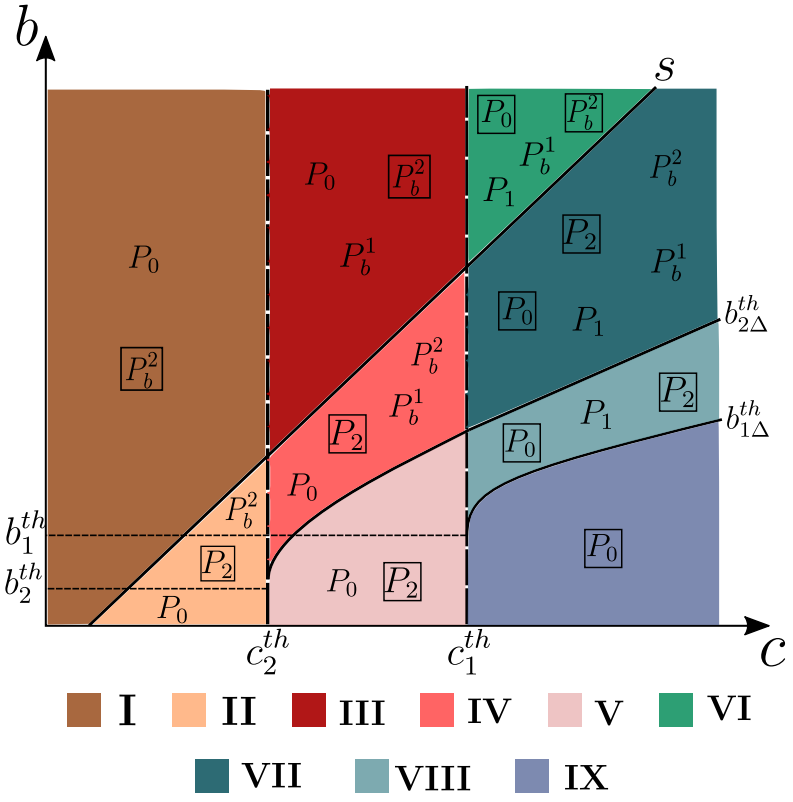

Nine different regimes are observed in Figure 1.7. Taking $c < c_2^{th}$ we have regions I and II which are separated by the curve s: under the curve (I) the internal equilibria P_2 is stable while the boundary equilibria are unstable, crossing s (II), P_2 disappear and the boundary equilibria becomes stable.

If $c_2^{th} < c < c_1^{th}$ and $b < b_{2\Delta}^{th}$, then the internal equilibria is stable (region V). Increasing b such that $b > b_{2\Delta}^{th}$, two boundary equilibriums appear, both unstable. Finally, increasing even more b and crossing the positivity condition s (region III), the internal equilibria disappear and the boundary state P_b^2 becomes stable.

When $c > c_1^{th}$ the tumor-free state P_0 is stable. In this case four regions appear, delimited by $b_{1\Delta}^{th}$, $b_{2\Delta}^{th}$ and s. In region IX ($b < b_{1\Delta}^{th}$), P_0 is globally stable; in region VIII ($b_{1\Delta}^{th} < b < b_{2\Delta}^{th}$) two internal equilibrium points appear, being one stable and the other unstable. Increasing b such that $b > b_{2\Delta}^{th}$ (VII) the boundary points P_b^1 and P_b^2 appear as unstable states. Finally, above s(region VI), P_2 disappears and the boundary equilibria P_b^2 becomes stable.

Remember that, when $\alpha > \alpha_c$ the condition for A_1^* in the internal equilibria is not satisfied, so the dynamics approach the boundary equilibria. On the other hand, when $\alpha < \alpha_b$ that condition is always satisfied and system (1.3) approaches the internal equilibria. However, in Figure 1.7 we observe that the curve s divide the dynamics: above that curve, the boundary equilibria is always stable, while under curve s the internal equilibria are the stable one. So, depending on the parameters c and b, the model can approach both types of equilibrium points.

The transition among the different regions is illustrated in Figure 1.8 by bifurcation diagrams. In Figure 1.8a we vertically go through Figure 1.7, varying the tumor aggressiveness b, fixing c such that $c_2^{th} < c < c_1^{th}$, and transiting from region V to IV and III. In Figure 1.8b we also vary b, but fixing $c > c_1^{th}$, transition among regions IX, VIII, VII and VI. In Figures 1.8c and 1.8d we vary the parameter c for two different choices of b, horizontally going through Figure 1.7.

Figure 1.8 – Bifurcation diagrams for $\alpha_b < \alpha < \alpha_c$.

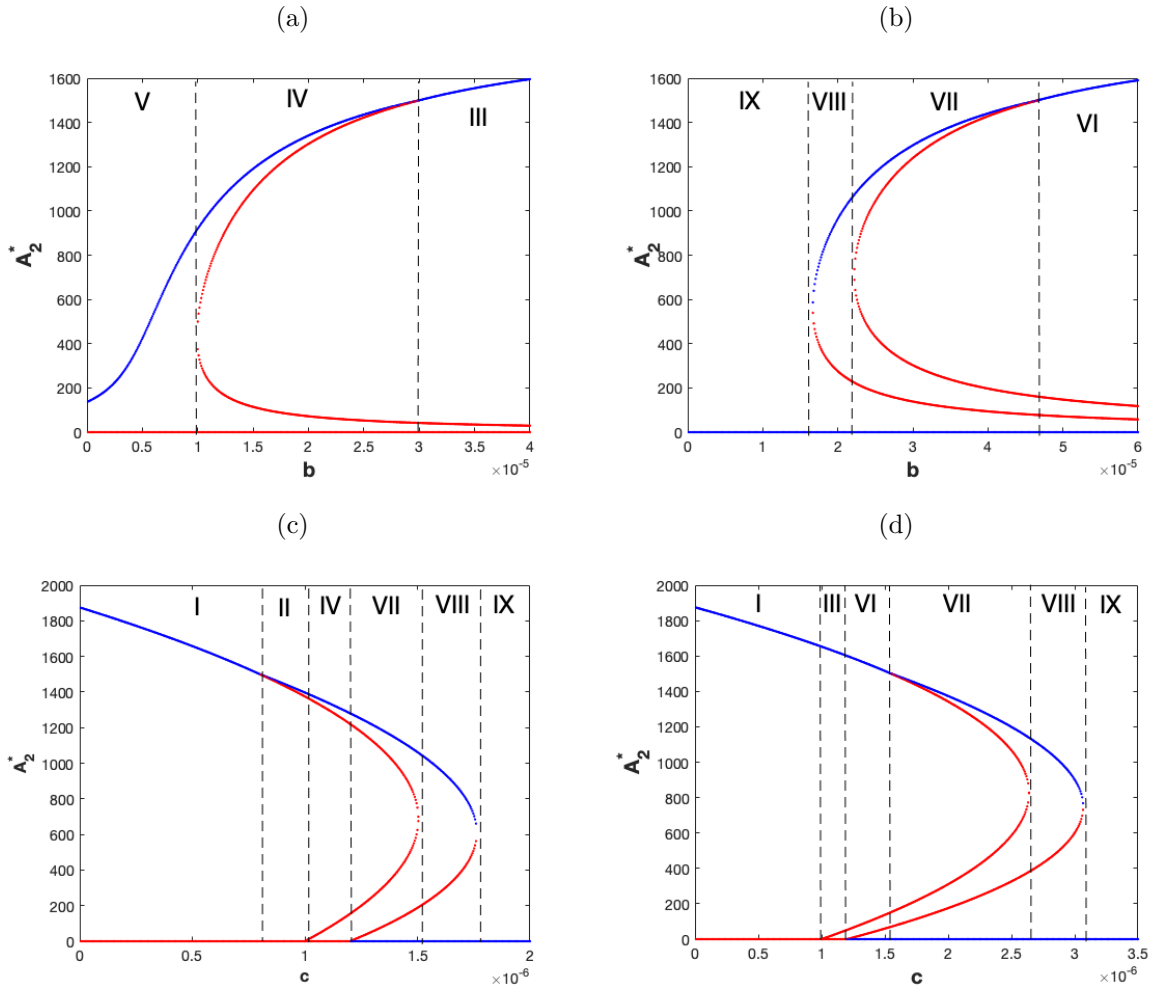

In all figures, we notice the existence of two curves, one is related to the boundary equilibria, and the other is related to the internal equilibria. In Figures 1.8a

and 1.8b, we start in a region where the internal equilibria is stable and the boundary equilibrium points do not exist. Then, the boundary equilibrium points appear as unstable states in the regions IV, for Figure 1.8a, and VII for 1.8b. Finally, the bifurcations for boundary and internal equilibria collapses, and the boundary equilibria become stable (regions III and VI for 1.8a and 1.8b, respectively).

Figures 1.8c and 1.8d are similar, but starting with a stable boundary equilibria in region I. Then, the internal equilibria appear and the boundary equilibria lose their stability. In these figures, we also observe when the trivial state P_0 becomes stable in regions VI, VII, VIII, and IX.

When α gets close to the superior threshold α_c, the qualitative behavior may change. Notice that, increasing α, the the value of c_1^{th} decreases and b_1^{th} increases, so the curve $b_{1\Delta}^{th}$ approach $b_{2\Delta}^{th}$ and region IX (where there is only P_0) advances over regions V and VIII. Furthermore, increasing α, the positivity condition $A_1^* > 0$ in (1.10) becomes more difficult to be satisfied, which means that the curve s is somehow displaced to the right, and regions II, IV, and VII decrease in size. Summarizing, if α approach the upper threshold α_c, regions II, IV, V, VII and VIII start to disappear. Notice that these are the regions in which the internal equilibrium is stable, thus as α approaches α_c, Figure 1.7 becomes similar to Figure 1.3, in which $\alpha > \alpha_c$.

To exemplify the transition from $\alpha < \alpha_b$ to $\alpha > \alpha_c$, we took the bifurcation diagram in Figure 1.6b, corresponding to the case $\alpha < \alpha_b$, and start to increase α until $\alpha > \alpha_c$. Our goal is to observe the transition between the diagrams 1.6b, for $\alpha < \alpha_b$, and 1.4b, in which $\alpha > \alpha_c$.

Figure 1.9 depicts the transition among the cases as we increase the mutation rate α. Figure 1.9a corresponds to the case in which $\alpha < \alpha_b$ and is exactly the same figure that we presented in 1.6b. Notice that in this figure, the curve which represents the boundary equilibria is inside the curve representing the internal equilibria, and these two curves do not intercept.

Increasing α we go to Figure 1.9b, in which the upper branch of the internal equilibria curve touches the upper branch of the boundary equilibria curve, and from this point the boundary equilibria become stable. As we increase α, the point at which the curves intersect moves to the left, along the upper branch of the boundary equilibria curve. In Figures 1.9d and 1.9e, the internal equilibria curve starts from the lower branch of the boundary equilibria curve, so in these two figures the stable internal equilibria disappear and there is only the unstable one. Finally, when α surpasses the threshold α_c, represented in Figure 1.9f, the internal equilibria curve collapses in the lower branch of the boundary equilibria curve. This is the same figure we presented in 1.4b

Thus, increasing α the internal equilibria curve approaches the boundary

Figure 1.9 – Transition from case 2, $\alpha < \alpha_b$, to case 1, $\alpha > \alpha_c$. For the parameters in Table (1.1) we obtained $\alpha_b = 0.0175$ and $\alpha_c = 0.02$

(a) $\alpha = 0.015$ ($\alpha < \alpha_b$)

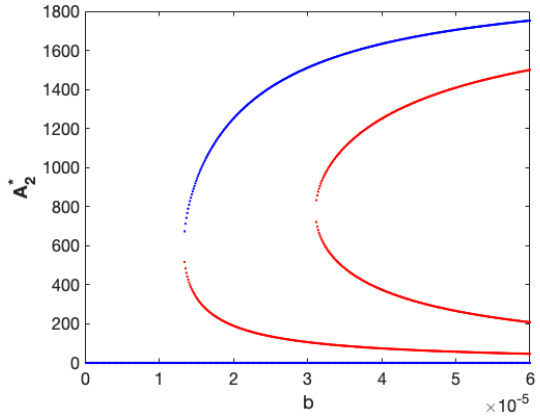

(b) $\alpha = 0.0181$ ($\alpha_c > \alpha > \alpha_b$)

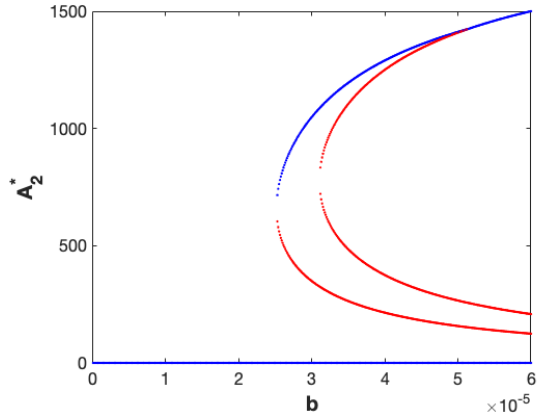

(c) $\alpha = 0.0187$ ($\alpha_c > \alpha > \alpha_b$)

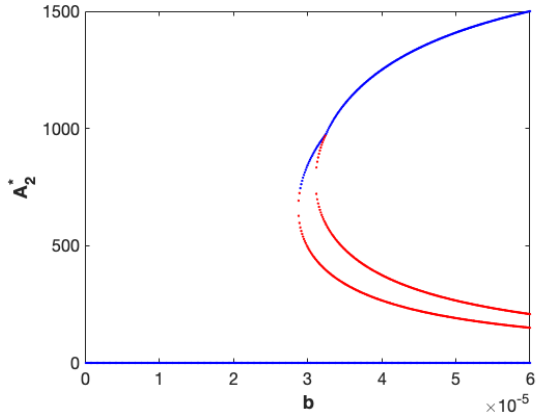

(d) $\alpha = 0.0192$ ($\alpha_c > \alpha > \alpha_b$)

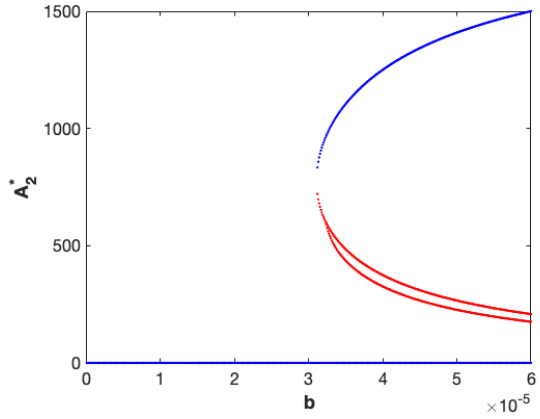

(e) $\alpha = 0.0195$ ($\alpha_c > \alpha > \alpha_b$)

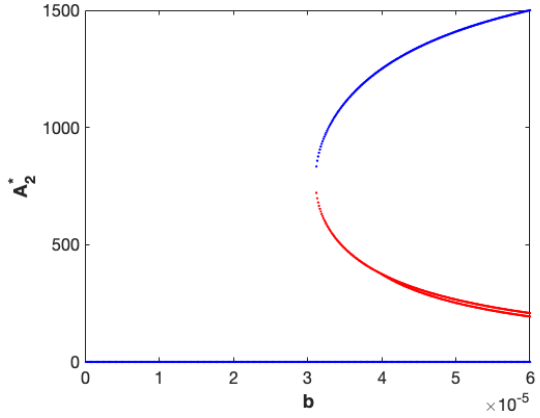

(f) $\alpha = 0.022$ ($\alpha > \alpha_c$)

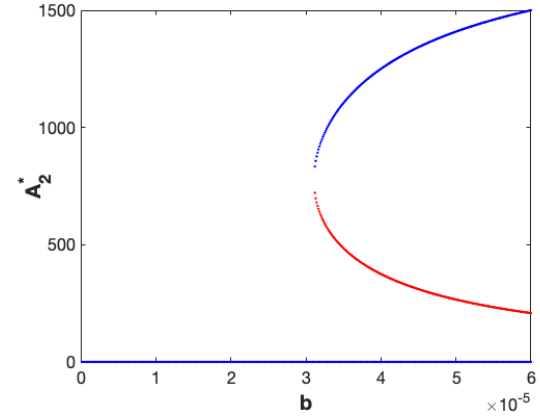

equilibria curve in such a way that the curves collapse and the internal equilibria disappear, illustrating the transition from case 2 ($\alpha < \alpha_b$) to case 1 ($\alpha > \alpha_c$). Observe that, as we increase the mutation rate, the boundary equilibria firstly appears as an unstable state, to then becomes stable when α is high enough, which also causes the exclusion of the internal

equilibria.

In all the diagrams, we are assuming that the mutations are unfavorable to tumor cells ($r_1 > r_2$ and $\mu_1 < \mu_2$). Now, let us briefly discuss what happens if we assume that the mutations in tumor cells increase their proliferation and decrease the apoptosis, which means that, the mutated cells A_2 are benefited. In the model, this assumption is equivalent to take $r_2 > r_1$ and $\mu_2 < \mu_1$, which implies $R, U < 0$ in the polynomial $p_I(A_2^*)$ in (1.11).

Taking $R, U < 0$ we have that $\alpha_b, \alpha_c < 0$ which implies $c_1^{th} < c_2^{th}$ and $b_1^{th} > b_2^{th}$ regardless the mutation rate α, and a single case must be analyzed. Furthermore, by numerical simulations, we observed that in this situation the positivity condition given in (1.10) is not satisfied for any value of α, b and c, so there are no internal equilibria and the qualitative behavior is the same described Figure 1.3 related to the case 1: $\alpha > \alpha_c$. Therefore, when the mutations benefit the A_2 cells, system (1.3) has no internal equilibria, which means that the more mutated cells can eliminate the others since the environment is favorable to them. Equivalently, A_1 cells have to be more efficient than A_2 cells (regarding proliferation and apoptosis) to remain in the TME and not be excluded by competition.

1.4 DISCUSSION AND CONCLUSIONS

A mathematical model consisting of a system of ordinary differential equations was proposed to describe cancer onset and establishment at a normal tissue, considering two types of tumor cells according to the number of mutations they carry. The proliferation of each type of tumor cell is independent of the other, however, both types compete by the same carrying capacity. Also, a continuous flux from the less mutated cells to the more mutated ones was considered to capture the effects of genetic instability as a factor that enhances the probabilities of mutations.

The model considering the same tumor aggressiveness and tissue response for both tumor cells was studied in detail. The analysis predicts that tumor onset can be prevented if the host body response is strong against both types of tumor cells. The higher the healthy cells homeostatic state, the lower the risk of tumor onset, or equivalently, the higher the net growth rate of tumor cells, the higher the risk of tumor onset. Even though the tumor-free state is stable, increasing the aggressiveness of tumor cells (which is related to the amount of damage caused to the tissue), the model presents bistability between the trivial state and a nontrivial one (boundary or internal, depending on the parameters). Therefore, since the tumor-free state is locally stable, only a few abnormal cells do not cause tumor onset, which is possible only in the presence of numerous mutated cells.

The existence of nontrivial equilibria was characterized in the entire parameter space, and the stability analysis of these equilibria was done numerically. The boundary

equilibrium points correspond to the situation where one type of tumor cells can not survive in the tumor microenvironment (TME), which causes the formation of a homogeneous tumor mass. The internal points, in turn, present the coexistence of both types of tumor cells, characterizing tumor heterogeneity. If tumor cells take advantage of those mutations, increasing their proliferation ($R < 0$) and decreasing their apoptosis ($U < 0$), then the mutated tumor cells overpower the others and exclude them from system dynamics, that is, there are no heterogeneity in this case. In contrast, when the mutations do not benefit tumor cells, the coexistence of type-1 and type-2 tumor cells becomes possible, and the mutation rate plays a role to determine the existence of a homogeneous or heterogeneous tumor. Under high genomic instability ($\alpha > \alpha_c$), that is, when tumor cells rapidly accumulate mutations and transit from type-1 cells to type-2, the less mutated tumor cells are not able to survive and the remaining tumor is composed by only one type of tumor cells, so a fast mutation generates homogeneous tumors. On the other hand, a small mutation rate ($\alpha < \alpha_b$) allows the survival of less mutated cells and, in this case, we observed the formation of a heterogeneous tumor. The intermediary case ($\alpha_b < \alpha < \alpha_c$) corresponds to a transition between the two cases presented above. There is a relation between tumor aggressiveness and tissue response, given by the curve s in figure 1.7, which determines tumor heterogeneity: above this relation, we observe the formation of a homogenous tumor composed of the more mutated cells, on the other hand, under this relation the tumor is heterogeneous and both types of cells coexist in TME. As the mutation rate is increased, we observed that the regime presenting heterogeneity starts to disappear, while the regime presenting homogeneity increases, illustrating the transition between the cases with low and high genetic instability.

Due to complexity, the full model considering different aggressiveness and tissue responses for each type of tumor cells was not completely analyzed in this study. Including different tissue responses c_1 and c_2 means that one type of tumor cells is more resistant to the tissue pressure. Therefore, we expect that when $c_1 < c_2$ the probability of coexistence is increased, on the other hand, if $c_2 < c_1$, then the boundary equilibria must appear more frequently, so choosing different combinations of c_1 and c_2 we benefit one of the tumor cells phenotypes and the system behavior must change. Appendix 1.A contains a brief analysis of the case $c_1 \neq c_2$.

This study contributes to the understanding of tumor onset and progression regarding tumor heterogeneity, and it can also be used as a basis for building more accurate models by incorporating other phenomena. In the next works, we will extend it by including the antitumor immune response and treatments, like chemotherapy and immunotherapy.

APPENDIX

1.A MODELING DIFFERENT TISSUE RESPONSES FOR TUMOR CELLS

The full model considering different aggressiveness ($b_1 \neq b_2$) and different tissue responses ($c_1 \neq c_2$) for each type of tumor cells was not completely analyzed in this study. To give an example of how these assumptions may change the model dynamics, we analyze in this section the case in which there are different tissue responses against the two types of tumor cells, that is, $c_1 \neq c_2$. The mutations in tumor cells affect their growth and death processes, the expression of neoantigens and/or their resistance to drugs and immune response (7, 8), but not necessarily these cells become more (or less) aggressive, so for simplicity, we keep the assumption that $b = b_1 = b_2$.

When we consider $c = c_1 = c_2$, we have one parameter (c) to be compared with two thresholds, c_1^{th} and c_2^{th}, so we need to know the relative position between these thresholds, which is affected by the mutation rate α: if $\alpha > \alpha_c$ then $c_2^{th} > c_1^{th}$, and if $\alpha < \alpha_c$, then $c_2^{th} < c_1^{th}$, as we discuss in Section 1.3.3. However, if we consider $c_1 \neq c_2$, then the parameter c_1 must be compared with c_1^{th}, while c_2 must be compared with c_2^{th}, so the relative position between the thresholds is no longer necessary. So, the three cases that we analysed in Section 1.3.3 must appear mixed when we consider different c_1 and c_2. Also, notice that the expressions for c_1^{th} and c_2^{th} in (1.6) do not change when we consider different tissue responses c_1 and c_2.

Moreover, taking different tissue responses also affects the existence of internal equilibrium points. The positivity condition for A_1^* given in (1.10) can know be written as

$$A_1^* = A_2^* \frac{\left(\frac{r_1 c_2}{c_1} - r_2\right)\left(1 - \frac{A_2}{K}\right) + \mu_2 - \frac{(\mu_1+\alpha)c_2}{c1}}{\left(\frac{r_1 c_2}{c_1} - r_2\right)A_2^*/K + \alpha}. \tag{1.14}$$

being A_2^* a positive root of a second degree polynomial which we will not present here due to its complexity. In (1.10) the parameter c appears only in the expression for A_2^*, but now c_1 and c_2 appear explicitly in the expression for A_1^*.

Different from Section 1.3.3, when $c_1 \neq c_2$, we can not divide the analysis in cases according to α. Furthermore, by numerical simulations, we observed several scenarios for different combinations of c_1, c_2 and α. We are not interested in presenting a full analysis, but only give an example of the model dynamics when different tissue responses are considered. So, we present in this appendix a particular case considering $\alpha = 0.022$, which is the same value used in the high mutation rate case in Section 1.3.3.

In Figure 1.10 we present the system behavior taking $\alpha = 0.022$ and varying c_1 for a fixed $c_2 < c_2^{th}$ (a) and $c_2 > c_2^{th}$ (b).

Figure 1.10 – Existence and stability diagram for $c_1 \neq c_2$ considering $\alpha = 0.022$ and fixed c_2.

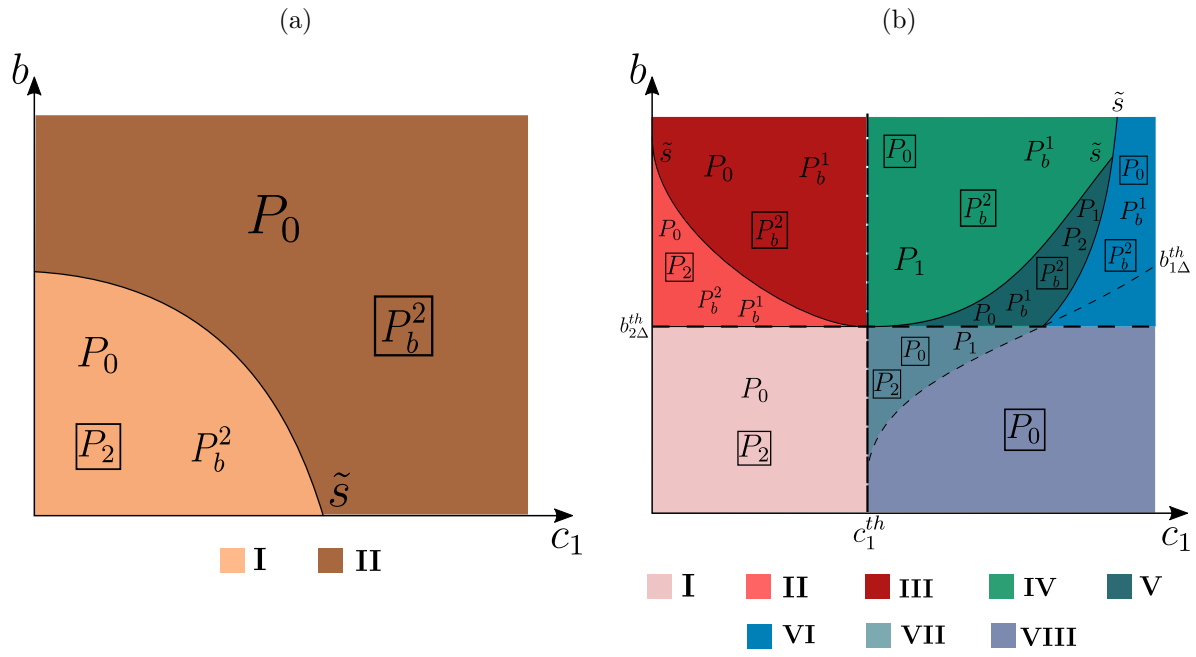

When $c_2 < c_2^{th}$, Figure 1.10a, we observe two regimes, in the first one (I) the tissue pressure under A_1 cells is weak, allowing their survival and the formation of a heterogeneous tumor mass. As we increase c_1, the A_2 cells overpower the others and the internal equilibria disappear while the boundary one becomes stable (II). Therefore, the coexistence of both tumor cells is possible under high genetic instability since c_1 is small, which not occurs when $c_1 = c_2$. The curve denoted by $\tilde{s}$ corresponds to the positivity condition given in (1.14).

In Figure 1.10b we observe the dynamics for $c_2 > c_2^{th}$. Notice that this figure is similar to the transitory case presented in Figure 1.7, but containing a new regime in which there is no internal equilibria, denoted by region VI. Remember that when we consider $c_1 = c_2$ and $\alpha = 0.022$ (see figure 1.3) the internal equilibria does not appear in the dynamics, however using the same mutation rate we obtained a different behavior for $c_1 \neq c_2$, which is similar to the transitory case (considering intermediary α). As we increase c_1, due to high pressure under A_1 cells, the internal equilibrium points lose stability and then disappear from the dynamics, remaining only the tumor-free state and the boundary equilibria, similar to Figure 1.3 (high mutation rate case). Therefore, Figure 1.10 is, in a way, a mix of cases 1 ($\alpha > \alpha_c$) and 3 ($\alpha_b < \alpha < \alpha_c$) presented in Section 1.3.3.

Now, let us present in Figure 1.11 the existence and stability for $c_1 \neq c_2$ but fixing c_1 and varying c_2.

In Figure 1.11 we vary c_2 and obtained the same regions that we obtained in Figure 1.10, but in different positions. Increasing c_1 we are benefiting the A_2 cells, so the

Figure 1.11 – Existence and stability diagram for $c_1 \neq c_2$ considering $\alpha = 0.022$ and fixed c_1.

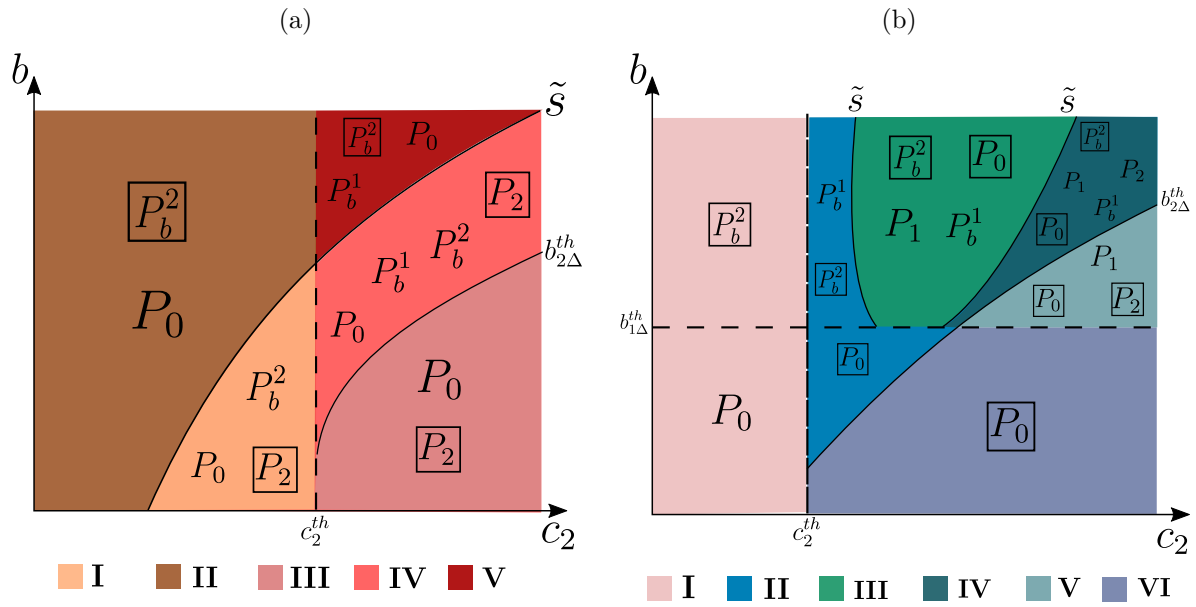

boundary equilibria becomes stable in rightmost regions. On the other hand, increasing c_2 the A_1 cells are benefited and the coexistence becomes possible, so the internal equilibria appears in the rightmost regions of Figure 1.11. Therefore, different combinations of these parameters can benefit one or another type of tumor cells, so the internal (or boundary) equilibria can arise in cases where this was not possible when we assume $c_1 = c_2$.

Although we present only one particular case in this appendix, it is useful to understand the role of c_1 and c_2 in the heterogeneity of the tumor mass and give us insights for new studies.

Chapter 2

Mathematical Modelling of Tumor-Immune Cycle Encompassing Tumor Evasion

Abstract. Cancer can be characterized by the uncontrolled development of abnormal cells as a result of the accumulation of genetic alterations and the loss of normal cellular regulatory processes. These cells generate neoantigens which can be detected by the immune system, triggering T cell responses that recognize and eliminate cancer cells. However, tumor cells may use several mechanisms to avoid the immune response. In this work, we propose a mathematical model for tumor-immune interaction and tumor evasion consisting in a system of ordinary differential equations. Results predict that nonaggressive tumors can be controlled by the tissue pressure and by the action of the immune cells, while the aggressive ones overpower the healthy cells and show resistance to immune response, which is increased by the tumor evasion mechanisms. The model also predicts that the tumor aggressiveness, the evasion mechanisms, and other factors play a role in the efficacy of immunotherapeutic treatments.

Keywords: tumor growth, immune response, tumor evasion, bifurcations, basins of attraction.

2.1 INTRODUCTION

Cancer is a leading cause of death worldwide, accounting for an estimated 9.6 million deaths in 2018 (33). Cancer arises from the uncontrolled proliferation and spread of abnormal cells that have lost their normal cellular regulatory processes. The lethality of malignant tumors is associated with their unregulated proliferative activity, the resistance to death and the ability to invade host tissues and metastasize (34, 35).

The concept of immunosurveillance was proposed by Macfarlane Burnet in the 1950s and state that the host immune system is capable of recognizing and destroying

transformed cells (36). The main response of the immune system to tumors is by T-cells, the neoantigens are presented on MHC class I molecules like viral antigens, which allows the cytotoxic T lymphocytes to recognize the tumor cells as abnormal and kill them (37, 38, 39, 34).

Chen e Mellman(10) describes the Cancer-Immunity cycle as a series of stepwise events that must be initiated and allowed to proceed and expand iteratively in order to lead to effective killing of cancer cells. The neoantigens released by tumor cells are captured by dendritc cells (DCs), which, in turn, present it on MHCI and MHCII molecules to T-cells in the regional lymph node, resulting in the priming and activation of effector $CD4^+$ and $CD8^+$ lymphocytes. Finally, these effector T cells traffic to the tumor site, where recognizes the target tumor cells and kill them.

However, the anticancer immune response is not optimized. The tumor antigens may not be recognized and correctly presented, T cells may be inhibited from infiltrating the tumor and several other mechanisms are used to avoid the immune system (40). For example, tumor cells express the programmed death-ligand 1 (PD-L1), which engages the programmed death-1 (PD-1) receptor on activated T cells, transducing a signal to inhibit T cell proliferation and function. By secreting cytokines like TGF-β, IL-10, IL-4 and IL-13, tumor cells inhibit the activity of macrophages and lymphocytes, creating an immunossupressive tumor microenvironment (41, 42).

Several mathematical models of tumor-host-immune interactions have been proposed in recent literature. Fassoni e Yang(32) developed a toy model for the interaction between healthy cells and cancer cells without the immune response. The model exibits three regimes: cancer cure, cancer onset and an intermediary regime with bistability between these two states. Although this model do not consider immune cells, it provide theoretical insights about cancer onset which can be compared to the model proposed here.

Pillis, Radunskaya e Wiseman(43) proposed a model based on a system of ODEs considering the adaptative immune response, by $CD8^+$ lymphocytes, and the innate response, by natural killers cells. Several regimes of tumor growth, control, and elimination were found, and the model tracked the different roles played by both responses in tumor elimination, suggesting that interactions between other immune cell types have an effect on the response. A similar model was proposed in (44), but considering the dynamics of binding/detachment of $CD8^+$ lymphocytes to tumor cells, which lead to tumor escape from immune system. Another tumor scape machanisms was examined in (45), in which the effects of $TGF-\beta$ suppression on T-cell response were considered, and in (46), in which the role of regulatory T cells was analysed together the effect of some cytokines in tumor dynamics, like $TGF-\beta$, IL-10 and IL-2.

In the context of state variables and compartments, the model proposed in this

paper has similarities with the the model in (47), in which the cells interactions occur in two different levels, the prostate gland compartment, which consider the interactions among tumor cells, macrophages and immune cells, and the lymphoid tissue compartment, which concerns the T-cell priming and differentiation.

According to these assumptions, we proposed a tumor growth model based on a system of nonlinear ordinary differential equations considering the antigen presentation, T cell priming and the tumor evasion mechanisms, which occur in two levels: the tumor microenvironment level and in lymph node level. The model is presented in section 2.2 and the results are in section 2.3. In section 2.4 we discuss the results and its implications in cancer immunotherapy. The conclusions are in section 2.5.

2.2 MATERIALS AND METHODS

2.2.1 MATHEMATICAL MODELING

We proposed a mathematical model consisting of a system of ODEs to represent the tumor immune cycle including the evasion mechanisms. Two levels are considered in the model: the tumor microenvironment (TME), which corresponds to the tissue where the tumor cells are proliferating, and the lymph node (LN) level, representing the regional lymph node where T-cell priming occurs.

In the TME level, six state variables are considered: $A(t)$ represents the tumor cells, $N(t)$ stands for the normal cells, $C(t)$ corresponds to the cytotoxic T lymphocytes (CTL), $C_d(t)$ stands for the disabled CTLs by tumor cells, $D(t)$ denotes the immature dendritic cells (DCs), and $D_a(t)$ stands for the activated (mature) DCs. The antigen presentation and T-cell activation occur in the lymph node (LN) level, in which five other state variables are considered: the lymph node DCs $D_{al}(t)$, the naïve $CD4^+$ and $CD8^+$ lymphocytes, denoted respectively by $H_v(t)$ and $C_v(t)$, and the effector $CD4^+$ and $CD8^+$ lymphocytes at the lymph node: $H_l(t)$ and $C_l(t)$.

We start by presenting the dynamics of these populations, then we present the model parameters, and finally the model equations.

A constant production of healthy tissue cells N, dendritic cells D, and naïve immune cells (H_v and C_v) is considered in the vital dynamics, denoted respectively by r_n, r_d, r_h and r_c, instead of a density-dependent one. The production of new cells is not related to living cells in the tissue, but it is related to the maintenance of a homeostatic state, through the natural replenishment of old and dead cells (26), so the constant recruitment rate was considered in the model. Moreover, all of the cells considered in the model presents a natural mortality rate μ_*, changing the sub-index according to each state variable.

On the other hand, tumor cells proliferate independent of the tissue structure in which they are located, so we consider a density-dependent growth for tumor cells by logistic law, being r_a the intrinsic growth rate, μ_a the natural mortality rate and K the tumor carrying capacity. This assumption means that the tumor cells have limited resources and can not proliferate indistinctly, which is a reasonable assumption for avascular tumors. To keep the model as simple as possible, we are not considering the phenomena of angiogenesis, i.e., the formation of new blood vessels to feed the tumor cells (48, 49).

The tumor cells and healthy cells damage each other according to the parameters b and c, which in a simple way, represents all the negative effects caused by tumor cells in the tissue and vice-versa, like the competition by nutrients and space, toxicity, and so on (15, 28, 29, 27).

Antigen presentation occurs in the following way: the immature DCs (D) catch neoantigens and become mature ones (D_a) according to the parameter γ. Then, these cells transit to the regional lymph node at a flux ϕ_d and present the neoantigens at a rate σ_h to the naïve $CD4^+$ lymphocytes, which differentiate into effector $CD4^+$ lymphocytes.

The effector $CD4^+$ lymphocytes stimulate the differentiation of naïve $CD8^+$ cells into effector cytotoxic T-lymphocytes (CTLs) at a rate σ_c. Finally the effector $CD8^+$ cells transit back to the TME at a flux ϕ_c, where they kill tumor cells, being β the killing rate.

The effector lymphocytes in the lymph node can clone themselves, which is called clonal expansion (34). In the model, the parameters θ_h and θ_c correspond to the lymphocytes cloning rates, and the clonal expansions of $CD4^+$ and $CD8^+$ cells are included in our model respectively by the terms

$$\Theta_h = \theta_h D_{al}\left(1 - \frac{H_l}{Q_h}\right) \quad \text{and} \quad \Theta_c = \theta_c H_l\left(1 - \frac{C_l}{Q_c}\right).$$

Notice that, the $CD4^+$ clonal expansion depends on D_{dal}, that is, depends on the presence of neoantigens, which means that the greater the number of DCs carrying neoantigens, the greater the cloning expansion, furthermore there is no clonal processes in the absence of neoantigens. The clonal expansion of $CD8^+$ cells, in turn, depends on the cytokines produced by the $CD4^+$ cells, like the interleukin-2, IL2 (34). For both lymphocytes, we assume that the clonal expansion can not occur indefinitely, but It is limited by the carrying capacities Q_h and Q_c.

As previously described, tumor cells can avoid the immune response in several ways. In this model, two evasion mechanisms are included: first, tumor cells disrupt the maturation processes of DCs, being ν the disruption rate. Second, tumor cells may inhibit CTLs in the TME, turning them into disabled CTLs (C_d). Parameter ρ represents the inhibition rate of CTLs by tumor cells. The disabled CTLs stay at the TME, however

they do not interfere in tumor control. Also, these cells may be reactivated at a rate τ.

The flowchart in Figure 2.1 illustrates the system dynamics highlighting the parameters related to cellular interactions and transitions between the different levels. The parameters corresponding to cellular production, proliferation and natural death are omitted.

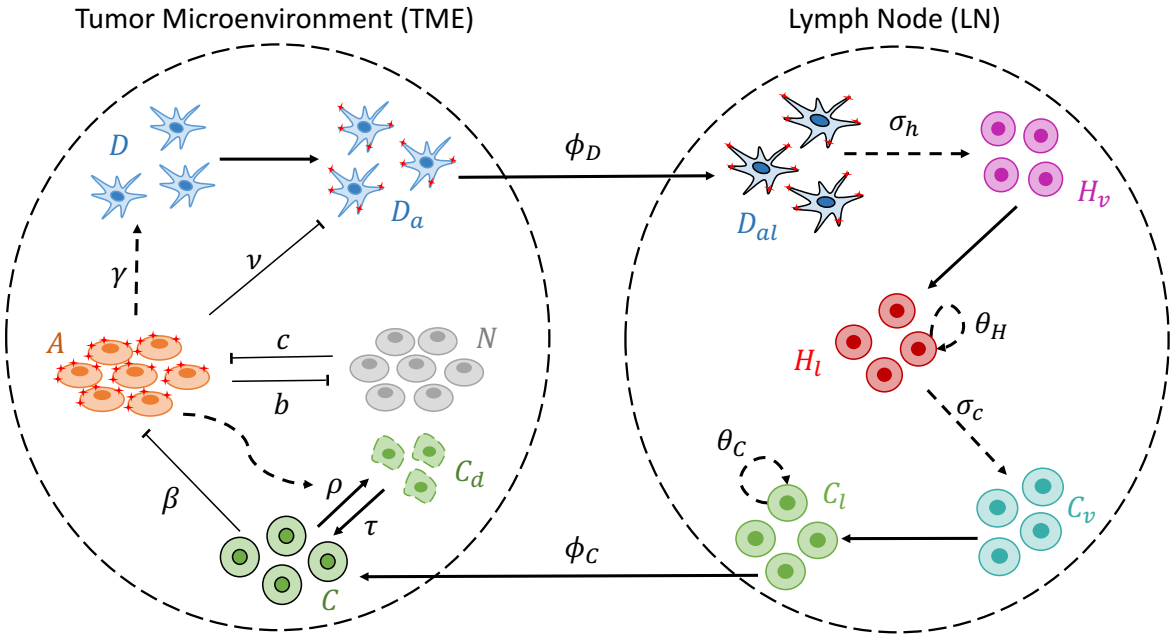

Figure 2.1 – The tumour-immune interactions and T-cell priming. Dashed lines indicate proliferation/activation or inhibition. Blocked arrows indicate killing/blocking. Sharp arrows indicate transition/differentiation.

Based on the above descriptions and in the flowchart given by Figure 2.1, we propose the following model to describe the tumor-immune cycle:

$$\text{TME}\begin{cases} \dfrac{dN}{dt} &= r_n - bNA - \mu_n N \\ \dfrac{dA}{dt} &= r_a A\left(1-\dfrac{A}{K}\right) - cAN - \beta AC - \mu_a A \\ \dfrac{dC}{dt} &= q\phi_c C_l - \rho AC - \mu_c C + \tau C_d \\ \dfrac{dC_d}{dt} &= \rho AC - (\tau + \mu_c) C_d \\ \dfrac{dD}{dt} &= r_d - \gamma AD - \mu_d D \\ \dfrac{dD_a}{dt} &= \gamma AD - \nu AD_a - (\phi_d + \mu_{da}) D_a \end{cases} \tag{2.1}$$

$$\text{LN}\begin{cases} \frac{dD_{al}}{dt} &= p\phi_d D_a - \mu_{dal} D_{al} \\ \frac{dH_v}{dt} &= r_h - \sigma_h H_v D_{al} - \mu_{hv} H_v \\ \frac{dH_l}{dt} &= \sigma_h H_v D_{al} + \Theta_h H_l - \mu_{hl} H_l \\ \frac{dC_v}{dt} &= r_c - \sigma_c C_v H_l - \mu_{cv} C_v \\ \frac{dC_l}{dt} &= \sigma_c C_v H_l + \Theta_c C_l - (\phi_c + \mu_{cl}) C_l \end{cases} \tag{2.2}$$

Table 2.1 contains the state variables used in the model, where vol_t corresponds to the volume of the tissue where cancer is installed, for instance lung, kidneys, etc, and vol_{ln} corresponds to the volume of the regional lymph node where T-cell activation occurs.

Since DCs and CTLs traffic between TME and LN, and each level has different characteristics (like volume, density, etc), we introduce two parameters, p and q, related to the density fitness during level transition. Table 2.1 contains the units used for each variable. Notice that C has unit depending on the volume of the TME, however these cells come from C_l cells, whose unit depends on the LN volume. So, to correct the variable's dimensions, the flux ϕ_c of CTLs entering in the TME must be multiplied by the correction factor p, whose unit is vol_t/vol_{ln}, in order to fit the dimension of CTLs equation. Similarly, the flux of DCs entering in the lymph node must be multiplied by the factor p, whose unit is vol_{ln}/vol_t. We can also assume $p, q < 1$ to represent the lose of cells during the traffic.

Table 2.1 – State variables of the tumor-immune model (2.1)-(2.2)

	Description	Unit
TME Variables		
A	Tumor cells	$cell/vol_t$
N	Healthy tissue cells	$cell/vol_t$
C	Cytotoxic T Lymphocytes	$cell/vol_t$
C_d	Disabled CTLs	$cell/vol_t$
D	Immature Dendritic cells	$cell/vol_t$
D_a	Mature dendritic cells	$cell/vol_t$
LN Variables		
H_v	Naïve $CD4^+$ cells	$cell/vol_{ln}$
H_l	Effector $CD4^+$ cells in LN	$cell/vol_{ln}$
C_v	Naïve $CD8^+$ cells	$cell/vol_{ln}$
C_l	Effector $CD8^+$ cells in LN	$cell/vol_{ln}$
D_{al}	Mature dendritic cells in LN	$cell/vol_{ln}$

The model parameters are summarized in table 2.2

Since the main idea of this work is provide theoretical information about cancer onset and its interaction with the immune system, we keep the model as general as possible

Table 2.2 – Tumor-immune model parameters.

Parameter	Description	Value	Reference
r_n	Recruitment rate of Normal cells	10^5 $[cell]day^{-1}$	(50, 51, 52)
r_d	Recruitment rate of DCs	5×10^2	(53)
r_c, r_h	Recruitment rate of Naive lymphocytes	10^3	(53)
r_a	Tumor intrinsic growth rate	4.3×10^{-1}	(54)
μ_a	Tumor natural death rate	0.143	Assumed
μ_n	Normal cells natural death rate	0.143	(55)
μ_d	DCs natural death rate	0.01	(53)
μ_{da}, μ_{dal}	Mature DCs natural death rate	0.02	(53)
μ_{hv}, μ_{cv}	Naive lymphocytes natural death rate	0.1	(53)
μ_h, μ_c	Effector lymphocytes natural death rate	0.3	(53, 56)
K	Tumor carrying capacity	5.25×10^5	Assumed
b	Tumor cells aggressiveness		Allowed to vary
c	Tissue response to tumor cells		Allowed to vary
γ	Antigen presentation coefficient	10^{-4}	(54)
ϕ_d	DCs flux to lymph node	0.9	(57, 58)
ϕ_c	Effector $CD8^+$ flux to TME	0.9	(53)
p, q	Density fitness coefficients	0.5	(57, 58)
σ_h, σ_c	Naïve lymphocytes activation rate	10^{-3}	(59)
$\theta_h, \theta_c,$	Effector $CD4^+$ and $CD8^+$ cloning rates		Allowed to vary
Q_h, Q_c	$CD4^+$ and $CD8^+$ carrying capacity in LN	10^{10}	(60)
τ	Disabled CTLs recovery rate	0	-
β	Tumor killing rate by CTLs		Allowed to vary
ρ	CTLs blocking coefficient by tumor cells	10^{-6}	Assumed
ν	DCs disruption coefficient by tumor cells	5×10^{-5}	Assumed

and do not consider a specific kind of cancer, however the equations and parameter values can be adapted to represent the tumor proliferation in different organs and tissues. Moreover, the proposed model does not consider the innate immune response and the presence of, for instance, natural killer cells. In appendix 2.A we present a toy model considering such kind of cells and determine that the efficiency of the innate response may control or not tumor progression, therefore we are assuming in model 2.1-2.2 that this innate response was already overpowered by tumor cells.

The analysis of system (2.1)-(2.2) will be discussed in the following section.

2.2.2 MODEL ANALYSIS

For the mathematical analysis we assume for simplicity that the disabled CTLs can not be reactivated, $\tau = 0$. Thus, the equation for C_d can be decoupled from model (2.1)-(2.2) and will be omitted in the analysis from now on. Also, we firstly consider that $\theta_h, \theta_c = 0$, that is, there is no clonal expansion, since it significantly increase the complexity of the system equations and difficult the qualitative analysis related to the existence and stability of equilibrium points. In section 2.3.3 we discuss the effect of clonal expansion in

the tumor-immune dynamics.

In appendix 2.B we show that model 2.1-2.2 is well-posed and biologically feasible, that is, the state variables will not assume negative values neither goes to infinity once we choose a valid initial condition.

The equilibrium points are obtained by setting the derivatives in system (2.1)-(2.2) equal to zero. To solve the related algebric system, we determined an expression for the equilibrium point of each variable in terms of the tumor population A^* and obtained a polynomial equation related to that variable. Finding the positive roots of this equation we are able to determine the other variables and the equilibrium points of system (2.1)-(2.2).

To analyse the polynomial equation related to A^* we use the Descartes Rule of Signs (61), that is, the signal alternations among the coefficients gives us the possible number of positive roots and consequently the number of equilibrium points, which will depend on the combination of the model parameters.

To stability analysis of the equilibrium points, we numerically obtained the eigenvalues of jacobian matrix of system (2.1)-(2.2) evaluated at each equilibrium point. Using bifurcations diagrams we determined the equilibrium points and obtained the related eigenvalues, classifying them as stable, when all the eigenvalues has negative real part, or as unstable, otherwise.

Let us show here a summary of the mathematical analysis, whose detailed presentation are available at 2.C. Firstly, we introduce the trivial equilibrium point, or tumor-free state, and then the possibilities of existence of nontrivial equilibrium points.

2.2.2.1 TRIVIAL EQUILIBRIUM POINT

Let us present the analysis of the trivial equilibrium point, or tumor-free state, which is given by

$$P_0 = \left(\bar{N}, \bar{A}, \bar{C}, \bar{D}, \bar{D}_a, \bar{D}_{al}, \bar{H}_v, \bar{H}_l, \bar{C}_v, \bar{C}_l\right) = \left(\frac{r_n}{\mu_n}, 0, 0, \frac{r_d}{\mu_d}, 0, 0, \frac{r_h}{\mu_{hv}}, 0, \frac{r_c}{\mu_{cv}}, 0\right). \tag{2.3}$$

in which there is only the healthy cells, immature DCs and naïve lymphocytes in their respective homoeostatic states. This equilibrium point always exists, and its stability is determined by the following result:

Theorem 2. *The tumor-free state P_0 in (2.3) is locally stable if, and only if $c > c^{th}$, where*

$$c^{th} = \frac{\mu_n R_A}{r_n} = \frac{R_a}{N_0}, \text{ with } R_A = r_a - \mu_a. \tag{2.4}$$

Proof. Let $J_0 = J(P_0)$ be the Jacobian Matrix evaluated at P_0, whose spectrum is given by

$$\sigma_J(J_0) = \left\{-\mu_c, -\mu_{cv}, -\mu_d, -\mu_{dal}, -\mu_{hl}, -\mu_{hv}, -\mu_n, -(\mu_{cl} + \phi_c), -(\mu_{da} + \phi_d), \frac{r_n(c^{th} - c)}{\mu_n}\right\},$$

Therefore, all eigenvalues are real negatives, except $\dfrac{r_n(c^{th}-c)}{\mu_n}$, which will be negative if, and only if, $c > c^{th}$, condition that which guarantee the tumor-free state stability. □

The term R_A corresponds to the net reproduction rate of tumor cells, which we are assuming to be positive, while N_0 is the homoeostatic state of healthy cells in the absence of tumor population. Therefore, if and only if the host body response against cancer is strong, then this state is stable and the cure is possible.

2.2.2.2 NONTRIVIAL EQUILIBRIUM POINT

Let $\bar{P} = \left(\bar{N}, \bar{A}, \bar{C}, \bar{D}, \bar{D}_a, \bar{D}_{al}, \bar{H}_v, \bar{H}_l, \bar{C}_v, \bar{C}_l\right)$ be an arbitrary equilibrium point of system (2.1)-(2.2). The trivial equilibrium point P_0 is obtained taking $\bar{A} = 0$, while the nontrivial states, or tumor states, have $\bar{A} \neq 0$.

Setting the system equations equal to zero and solving the related algebric system we obtained that the expressions for $\bar{N}$, $\bar{D}$, $\bar{D}_a$, $\bar{D}_{al}$, $\bar{H}_v$, $\bar{H}_l$, $\bar{C}_v$, $\bar{C}_l$ and $\bar{C}$ can be written in terms of $\bar{A}$, which, in turn, is a root of the fifth-degree polynomial given in (2.9). In previous section we observed that the host body response determines if the cure is possible or not, according to the threshold c^{th}. Tumor onset, on the other hand, also depends on its aggressiveness according to the threshold $b^{th} = \dfrac{\mu_n r_a}{R_a K}$. We classify the tumor as aggressive if $b > b^{th}$ and nonaggressive if $b \leqslant b^{th}$.

The existence of tumor states will be presented considering the combinations of host body response and tumor aggressiveness in the following way:

CASE 1: $c > c^{th}$ AND $b < b^{th}$

There is no signal alternation among the coefficients of polynomial (2.9), therefore, by the Descartes rule of signs, there is no tumor state in this situation.

CASE 2: $c > c^{th}$ AND $b > b^{th}$

According to the coefficients of polynomial (2.9) two tumor states appear when the aggressiveness b reach a critical value, denominated $\tilde{b^{th}}$, with $\tilde{b^{th}} > b^{th}$. The stability of each equilibrium point was determined analysing the eigenvalues of the Jacobian matrix evaluated at each point, being one of them stable and the other unstable.

In this case there is bistability between the tumor-free state and the stable tumor state. The unstable one, in turn, divides the basins of attraction of the stable equilibrium points, which means that, the unstable state is a critical value for the initial tumor size: if it is bigger than the stable state, tumor progress, but if it is smaller than the critical value, tumor will be eliminated. Figures 2.6 and 2.8 in Appendix 2.C presents a bifurcation

diagram illustrating the appearance of the equilibrium points as the aggressiveness is increased.

CASE 3: $c < c^{th}$ AND $b > b^{th}$

When we consider that $c < c^{th}$ there always be at least one signal alternation among the polynomial coefficients, therefore, there is at least one tumor state in this situation.

Considering $b > b^{th}$, we observed the existence of one or three tumor equilibrium points, depending on the immune response. Let β_1^c and β_2^c be the critical values for the citotoxic action of lymphocytes β, defined in (2.8) in Appendix 2.C, which determine three distinct situations, which are:

i. Low Immune Action ($\beta < \beta_1^c$): there is a single tumor equilibrium point, which is stable.

ii. Medium Immune Action ($\beta_1^c < \beta < \beta_2^c$): there is three tumor equilibrium points. The first one, with more tumor burden, is stable; the second one, with medium burden, is unstable; the last one is stable and has only a fell tumor cells. The unstable state divides the basins of attraction of the other two tumor states, so the initial tumor size determines if it will grow to the bigger state, or shrink to the smallest state.

iii. High Immune Action ($\beta > \beta_2^c$): there is only one tumor state, but with a low tumor burden.

To illustrate the transition among these situations and the appearance/disappearance of the tumor states according to β, Figure 2.7 in appendix 2.C contains a bifurcation diagram. The behavior observed here is compatible with the hysteresis phenomenon presented in (61). In the course of the work, we will discuss this occurrence in more detail.

CASE 4: $c < c^{th}$ AND $b < b^{th}$

Similar to previous case, there will always be at least one tumor state in this situation. When the evasion parameters ν and ρ are small, then there is a single tumor state, which is stable.

However, as these parameters are increased, two other tumor states may appear and the systems bevahior is the same discussed above: for $\beta < \beta_1^c$ there s a single tumor state, for $\beta_1^c < \beta < \beta_2^c$ there are three tumor states, two of them are stable and one is unstable. Finally, when $\beta > \beta_2^c$ there is only one tumor state, which is stable. Therefore, if we consider ν and ρ high, then the case 4 ($c < c^{th}$ and $b < b^{th}$) has the same behavior of

case 3 ($c < c^{th}$ and $b > b^{th}$), thus the evasion parameters ν and ρ induce the hysteresis phenomena in case 4, which does not exists in the absence (nor for small values) of these parameters.

Actually, ν and ρ are responsible for facilitating the establishment of the tumor in all the cases presented above, either increasing the size of the tumor state or increasing its basin of attraction, requiring better immune and tissue responses to control tumor growth.

All the situations presented are discussed and analyzed in detail in 2.C together with bifurcations diagrams illustrating the system's behavior. In the next section, we will present the biological interpretations of this mathematical analysis.

2.3 RESULTS

Let us interpret the mathematical results done in previous sections and present their biological implications.

Firstly, let us deal with the tumor-free state, given in (2.3) whose stability is determined by the threshold c^{th}. Parameter c corresponds to the host tissue response against cancer. According to theorem 2, if this response is strong ($c > c^{th}$) the tumor-free state P_0 is stable and the tumor onset may be avoided; on the other hand, if the host body response is weak $c < c^{th}$, then P_0 is unstable and the tumor progress. Furthermore, the higher the tumor net growth rate R_A, the higher c^{th}, so the tissue response c needs to be bigger to control cancer onset, that is, more proliferative tumors require better tissue responses to be suppressed. On the other hand, if the homoeostatic N_0 is high, then c^{th} is small and healthy cells can control tumor cells more easily.

Moreover, the stability of P_0 does not depend on the immune system, and the possibility of cure is determined only by the host body response. It happens because T-cells are triggered only in the presence of tumor cells. Although the immune system does not determine P_0's stability, it is important in tumor control, which will be discussed throughout this work.

The host body and immune system may lead cancer to cure, when all the abnormal cells are eliminated, or to remission, when the tumor cells are decreased and not be detected, and symptoms disappear, although cancer still may be in the body. The cancer may come back to the same place as the original (primary) tumor or to another place in the body, which is called a recurrent cancer (62).

Since the possibility of cure is determined by c^{th}, we divided the results in two cases according to the tissue response parameter: strong response $c > c^{th}$ and weak response $c < c^{th}$.

2.3.1 STRONG TISSUE RESPONSE ($c > c^{th}$)

When we combine a strong tissue response ($c > c^{th}$) with a nonaggressive tumor ($b < b^{th}$), them the tumor-free state is the only one equilibrium point of system (2.1)-(2.2), therefore the tumor onset is not possible. We can interpret this situation as a healthy host with a non-aggressive tumor, therefore the host body can control tumor progression and eliminate it since P_0 is the unique biological-feasible stable steady state of the dynamical system.

When the tumor is aggressive ($b > \tilde{b^{th}}$) two tumor equilibrium points appear, one stable and the other unstable, as presented in 2.2.2.2. Let A^+ be the tumor burden of the stable state, while A^- is the tumor burden of the unstable state. In this situation if the tumor initial size is lesser than A^-, then the host body eliminates the abnormal cells, going to the tumor-free state. On the other hand if the initial size is bigger than A^-, the host body can not control tumor progression, which will grow to the stable state A^+. Furthermore, the more aggressive the tumor is, the lesser is A^-, which means that smaller tumors may also progress if they are strongly aggressive. Figure 2.2 illustrates the systems behavior for the strong tissue response case.

Figure 2.2 – Possible outcomes considering the tumor initial size and its aggressiveness for the strong tissue response case ($c > c^{th}$)

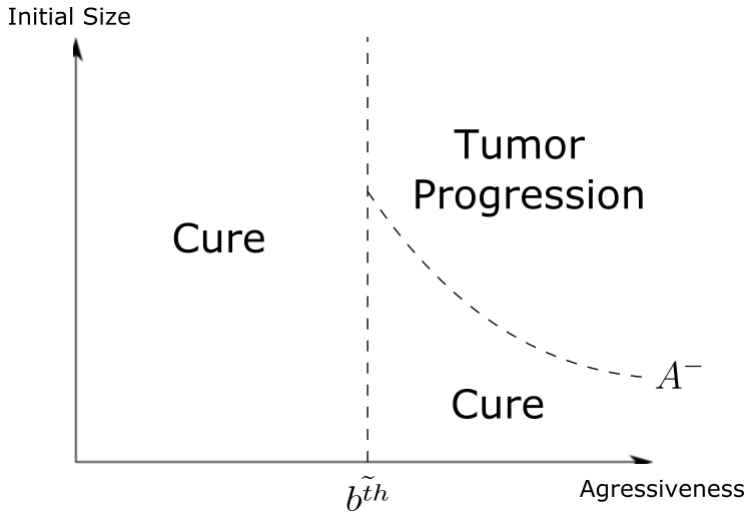

The introduction of the immune response affects tumor onset and progression in several ways. Firstly, increasing the killing rate β also increases the critical value $\tilde{b^{th}}$, therefore the stronger the cytotoxic action of lymphocytes, the more aggressive the tumor needs to be in order to escape and grow, otherwise, it will be eliminated by the host's response. Furthermore, the immune response decreases the value of A^+, that is, it decreases the size of the tumor in equilibrium, and also increases the value of A^-, thus hindering tumor growth, since its initial size will need to be bigger.

However, the evasion mechanisms work to do the opposite. Increasing the

parameters ν and ρ decreases the value of $\tilde{\beta^{th}}$, so more evasive tumors can progress even with low aggressiveness. Furthermore, these parameters also affect tumor equilibrium, increasing A^+ and decreasing A^-, thus allowing tumors to grow even if they are initially small. In Appendix 2.C we present the analysis of system behavior and the role of parameters β, ν and ρ in details, also the Figures 2.6 and 2.8 illustrate the cases discussed above.

2.3.2 WEAK TISSUE RESPONSE ($c < c^{th}$)

Now, let us deal with the weak tissue response ($c < c^{th}$). In this situation, the tumor-free state is unstable, thus there is no possibility of cure, but tumor can be controlled in a remission situation, as we will present.

Firstly, let us consider a nonaggressive tumor, $b < b^{th}$. In this case, there always be a single tumor state, therefore, the abnormal cells will always achieve this equilibrium since the tumor-free state is unstable. However, the cytotoxic action of lymphocytes decreases the tumor size in the equilibrium, therefore, improving the killing rate β the tumor size can be small and remain in remission. The evasion mechanisms, on the other hand, inhibit the immune response and difficult tumor control, so the effort of the lymphocytes needs to be bigger to lead to the remission in case of evasive tumors.

On the other hand, if we consider an aggressive tumor, $b > b^{th}$, three different situations may occur according to the immune response, as we discuss in section 2.2.2.2. Figure 2.3 illustrates the possibilities in the weak tissue response case considering the three levels for immune response and the tumor initial size.

Figure 2.3 – Possible outcomes considering the tumor initial size and the lymphocytes cytotoxic action for the weak tissue response case ($c < c^{th}$)

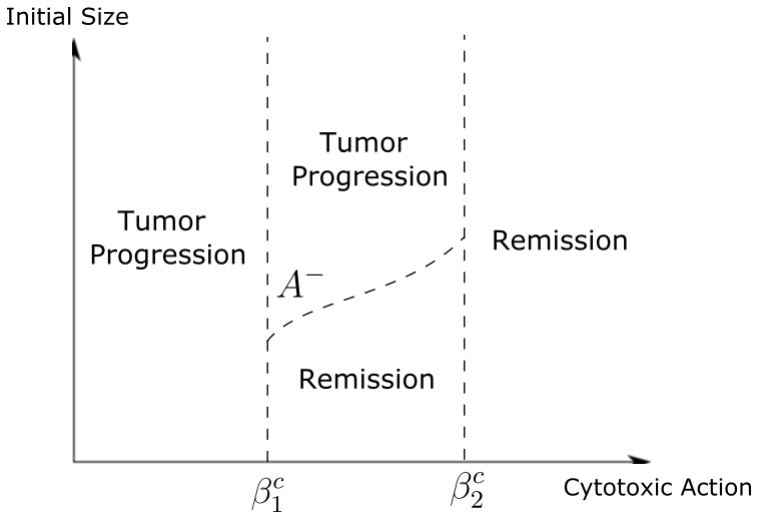

When we consider low immune action ($\beta < \beta_1^c$) there is a single tumor equilibrium point with a huge number of cells, lets say A^+. Since the lymphocytes can not

control the tumor grow, it will increase its size until achieve the equilibrium. For medium immune action ($\beta_1^c < \beta < \beta_2^c$), three tumor states appear: the first one, similar to previous case, is stable and has numerous cells, denoted also by A^+. The second one, also stable, has only a few cells, which we characterize as the remission state. Finally the third one is an unstable state whose tumor burden is denoted by A^-. If the tumor initial size is bigger than A^-, than it will grow to the value A^+, however, if the initial size is lesser than A^-, then the tumor cells go to the remission state. Finally, for high immune action ($\beta > \beta_2^c$) there is only the remission state, therefore the lymphocytes always control the tumor and keep it at low level.

The Figure 2.3 also shows us that, when it comes to aggressive tumors, there is resistance to remission. For instance, consider a situation where the immune response is low (the left region in figure) and the tumor mass is big, close to its equilibrium value. Suppose that the action of lymphocytes is improved (by therapies, for instance) walking then to the central region of the figure. Although there is a possibility of remission in this region, the tumor does not regress because its size is bigger than the value of A^-, since we start from a tumor close to equilibrium. The remission only happens when we reach the right region of the figure, that is, when $\beta > \beta_2^c$. So, the existence of the intermediary regime (mathematically equivalent to the hysteresis) implies tumor resistance.

Now, consider a host with high immune action and a tumor in remission, that is, we start in the right region of the figure. If the lymphocytes loose strength somehow, due to tumor interference or external facts, reducing the parameter β and entering in central region, the tumor cells remain in low level until the microenvironment becomes favourable, that is, until $\beta < \beta_1^c$. At this point the abnormal cells start to proliferate and tumor goes from the remission state to the equilibrium value occurring a tumor relapse.

As we discussed, nonaggressive tumors ($b < b^{th}$) do not have such an intermediary regime, since there is a single nontrivial equilibrium point. Thus, they are not resistant, which means that increasing lymphocytes action leads to remission without passing through the hysteresis region. The evasion mechanisms ν and ρ, however, affect this behavior and induce the appearance of the transient region even for nonaggressive tumors. Figure 2.9 in the appendix shows this transition as we increase ν and ρ. Thus, when there is evasion, even less aggressive tumors resist remission, showing the same behavior as aggressive ones. Furthermore, increasing the value of the parameters ν and ρ also increases the value of β_2^c, that is, the central region of the Figure 2.3 gets bigger, needing stronger cytotoxic action to lead the tumor to remission.

2.3.3 ASSESSING THE EFFECTS OF CLONAL EXPANSION IN TUMOR-IMMUNE INTERACTIONS

In this section we briefly discuss the effects of clonal expansion in the systems behavior and its biological implications, so we investigate how parameters θ_h and θ_c change the diagrams 2.2 and 2.3. Similar to previous section, we divide the results considering strong and weak tissue response.

STRONG TISSUE RESPONSE

Since the cloning processes increases the lymphocytes population, it is expected that tumor control will be facilitated as we increase the cloning rates θ_h and θ_c. Indeed, the value of $\bar{\beta^{th}}$ is increased when we include the cloning rates, which means that the tumor must be more aggressive to avoid elimination. Figure 2.10b in appendix illustrates how the cloning rates displace $\bar{\beta^{th}}$ forward, hindering tumor progression in the host body.

In addition to increasing the value of $\bar{\beta^{th}}$, clonal expansion also affects the critical value A^- which determines, from the initial tumor population, whether it will grow or be eliminated. We observed that, once a certain aggressiveness b is fixed, the higher the cloning rate, the higher the value of A^-, that is, the initial size of the tumor mass needs to be bigger to settle down in host body. However, at a certain point, increase even more the cloning rate does not increase A^-, instead of it, a new stable tumor equilibrium point arises, which is illustrated in Figure 2.12 of the appendix 2.C.3. In this case, the clonal expansion creates an intermediary tumor state, therefore, even if the host body can not eliminate the cancer cells, it may keep them in a middle level instead of allows it grown to the tumor state and reach a bigger size.

Several simulations were done to understand the model dynamics in this situation. In general, we observe that the tumor always presents a rapid growth at the beginning, due to high aggressiveness, which in turn generates a strong immune response because of the high clonal expansion, thus controlling the tumor growth. At this point, depending on the initial population of tumor cells and the host body parameters, we observe the three outcomes highlighted above: i) the tumor is able to recover and evades the immune response, growing and achieving tumor equilibrium; ii) the immune response can be efficient and eliminate it; iii) when there is a certain balance of forces, the tumor goes into intermediate equilibrium, with a relatively low tumor burden.

In the appendix 2.C.3 we present in more detail the dynamics that arise with the high cloning rate, the emergence of this new equilibrium and the dependence on initial conditions.

WEAK TISSUE RESPONSE

The model bahavior in this case is presented in Diagram 2.3 and summarized as follows: regime I with $\beta < \beta_1^c$ presents tumor progression; regime II with $\beta_1^c < \beta < \beta_2^c$ presents two outcomes, tumor progression and tumor remission, depending on the initial burden; and regime III with $\beta > \beta_2^c$ always leads to tumor remission.

Including the clonal expansion, we observed that the values of β_1^c and β_2^c decrease, so the first region corresponding to tumor progression becomes smaller, while the second and third regions are displaced backward. Therefore, even for low values of the killing rate β, the immune response is able to lead the tumor to remission and avoid its progression. In Appendix 2.C the Figure 2.12 illustrates the curves being displaced backward as we increase θ_h and θ_c. Notice that when these parameters are high enough the tumor progression region I does not exists, therefore, when the clonal expansion is strong, the remission state exists regardless the value of β and tumor can be easily controlled.

However, we observe that considering a high cloning rate, a limit cycle arises around the remission equilibrium point. This means that the tumor population will not be constant at the remission state, but it will oscillate around the equilibrium point, periodically. In figures 2.13 and 2.14 of the appendix 2.C we discuss the emergence and mathematical implications of this type of solution, here we will pay attention to the biological interpretation.

When the tumor population starts to increase beyond the state of remission, the immune response is triggered and quickly proliferate (due to the high cloning rate) eliminating the tumor cells. When the tumor is almost eliminated (below the state of remission), the immune response also diminishes, allowing the tumor to grow again. When it reaches a high value, a new immune response will be activated, restarting the cycle described above.

Since these oscillations occur around the remission state, which has only a few tumor cells, the periodically increase and decrease of tumor size may not be detectable, depending on the limit cycles amplitude. In the appendix 2.C we observe that the amplitude of the oscillations is associated with the killing rate β so that the smaller this parameter, the greater the oscillation, that is, the more the tumor can grow before being slowed down by the immune response. On the other hand, the bigger β, the smaller the oscillation, since tumor cells are quickly controlled by lymphocytes. This is also related to the period of the cycle, the greater the oscillation, the longer the time needed for the tumor to recover and grow again (the time between two oscillations), while for high β the oscillations are small and therefore the time between them is short. Figure 2.15 illustrates the oscillations in the tumor population for different values of β.

2.4 DISCUSSION

2.4.1 IMMUNOTHERAPY: THEORETICAL INSIGHTS

The immunotherapy consists of mobilizing the immune system to treat cancer (63, 64). Promising new therapies have emerged in the treatment of selected cancers, including immune checkpoint inhibition therapies (65), like anti-PD-1 and anti-PD-L1 (66), the CAR T-cells therapies (67), non-specific immune stimulation and treatment vaccines, which improves the immune cells' skills to fight cancer .

In system (2.1)-(2.2), such therapies may interfere in the model parameters, especially in the killing rate β and in the tumor evasion parameters ν and ρ. Simply, let us simulate the use of, for instance, immune checkpoint inhibition therapies, assuming that the treatment is able to decrease the value of the evasion parameters ν and ρ. We are not considering equations for the drug concentration, neither complex interactions among these drugs and the immune cells; our purpose is to obtain insights about immunotherapy using model (2.1)-(2.2) as simple as possible.

Firstly, let us consider the strong tissue response case, $c > c^{th}$. We already know that when $b > \tilde{b^{th}}$ the tumor may grown or be eliminated, depending on its initial size. Also, ν and ρ allows the progression of less aggressive tumors, so when the therapy starts, ν and ρ will be decreased and consequently the the value of $\tilde{b^{th}}$ will be displaced forward. Figure 2.4a illustrates it, the black lines correspond to the dynamic without treatment, while the blue lines represent the dynamics during treatment. The curve A^- and $\tilde{A^-}$ correspond to the critical tumor initial size with no treatment and during treatment, respectively. Above each one, the tumor progress, while under them, the dynamics goes to cure.

To illustrate the treatment successful or failure, consider two patients, each one presenting a different tumor aggressiveness and a different initial tumor population, given in diagram 2.4a by the points P_1 and P_2.

Notice that, both patients, in the abscence of treatment (black line) has initial size bigger than A^-, therefore the tumor population will increase until achieve the tumor state. When the therapy is introduced (blue curve), the patient P_1 has tumor aggressiveness lesser then $\tilde{\beta^{th}}'$, so the only possbility is the cure state, therefore tumor cells start to decrease and approach zero.

When treatment stops, the dynamics goes back to the black lines, therefore if the remaining tumor population after treatment is bigger than A^-, the treatment will fail since the tumor will start to increase again, on the other hand, if after treatment there are less than A^- tumor cells, the treatment success and the dynamics goes to cure.

In Figure 2.4b we illustrate the treatment failure and successful: starting with the same initial condition, we present the simulation in which there is no treatment (so

Figure 2.4 – Immunotherapy scheme and simulation in the strong tissue response case

(a) Immunotherapy scheme

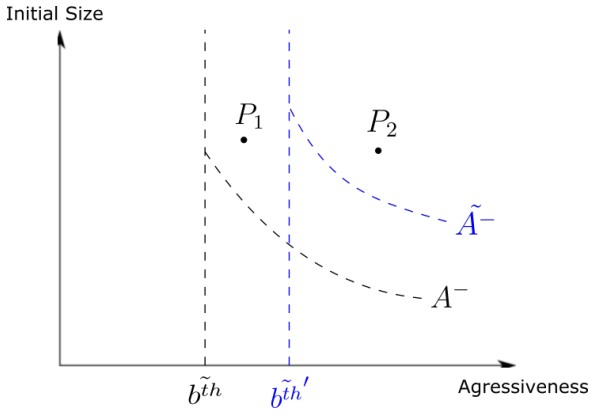

(b) Numerical simulations

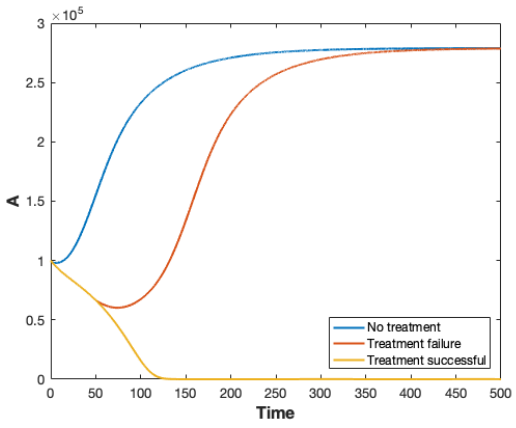

the population increases until the equilibrium) and two treatment simulations. In the first one, the treatment stops at $t = 50$, and the number of tumor cells increases since the reduction was not enough to achieve the critical value A^-, so treatment fails. In the second simulation, the treatment was extended up to $t = 100$, and after that, the tumor cells remain decreasing until its elimination, representing a treatment successful.

Now, notice that even during treatment, the patient P_2 remains in the tumor progression region, that is, to the right of $\tilde{\beta^{th}}'$ and with initial size bigger than $\tilde{A}^-$, so the tumor keeps proliferating and this patient does not respond to the treatment.

A similar analysis was done for the weak tissue response case, $c < c^{th}$, which is presented in Figure 2.5. Here, during treatment the the curves will be displaced backward, so lesser killing rates β will be able to reduce the tumor population to the remission state. Again, the black lines correspond to the absence of treatment, while the blue lines represents the dynamics during treatment.

Figure 2.5 – Immunotherapy scheme and simulation in the strong tissue response case

(a) Immunotherapy scheme

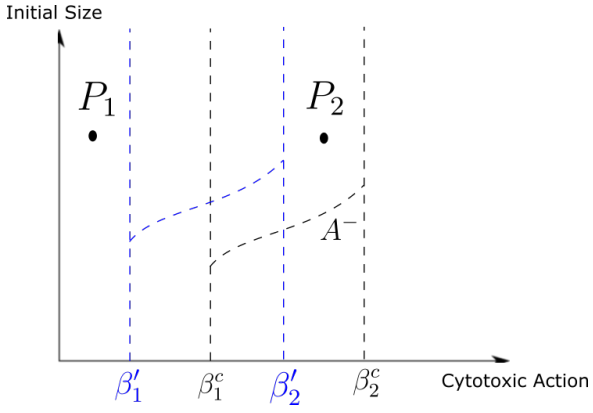

(b) Numerical simulations

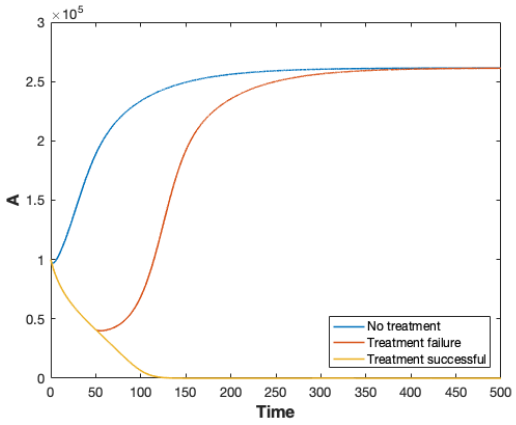

Firstly, consider the patient P_1. Since his/her killing rate β is such that $\beta < \beta_1^c$, the only one equilibrium point is the tumoral state, so when the treatment stops, whatever is the remaining tumor population, it will always increase and approach the tumoral state. In other words, treatment will fail in patients with a weak immune response, whose parameter β is lesser than β_1.

Now, for patient P_2. In the absence of treatment, this points belongs to the tumor progression region, since it has $\beta_1^c < \beta < \beta_2^c$ and the initial size is bigger than A^-, therefore the tumor will proliferate. During the treatment, the curves are displaced backward and now the patient belongs to the remission region, since $\beta > \beta_2'$, and so the tumor cells will decrease. Analogous to previous case, when the treatment stops, the systems dynamic goes back to the black lines; if the remaining tumor population is lesser than A^-, treatment will success, otherwise the abnormal cell will start to proliferate again. Figure 2.5b illustrates both situations.

Therefore, two key factors determine the successful of immunotherapy. The first one depends on the carachteristics of tumor cells and how the host body responds to them. Patients carrying aggressive and evasive tumors may not respond to treatment. The same occurs for weakened patients, who present low killing rate (β) and weak tissue response (c). The second factor is the treatment's duration: even if the relation tumor-host body allows immunotherapy success, if the treatment stops before the tumor size achieve the critical value A^-, treatment will fail. It is important to mention that this kind of therapy also has side effects, which are not included in our analysis. Therefore, there is a limit for the drug concentration in the host body and treatment duration, thus impairing the performance of immunotherapy.

Furthermore, other types of treatment can be used together, before or even after immunotherapy in an attempt to fight cancer, such as chemotherapy or targeted therapies. A more detailed study on immunotherapy, including the equations for drugs, toxicity, and joint treatments, will be carried out in future works.

2.4.2 THE ROLE OF THE IMMUNE SYSTEM IN CANCER DYNAMICS

In this study, we developed a mathematical model for the tumor-immune interaction considering T-cell priming and tumor evasion mechanisms. The model provides us information about how the tumor onset may be prevented or controlled by the tissue and T-cells, and also the effects of tumor evasion in the efficiency of the immune system.

The immune response has a direct effect on tumor cells, by β, but also an indirect effect which we will discuss now. In system (2.1)-(2.2), the competition terms between the tumor and the healthy tissue are given by cN in the tumor equation, and bA in the healthy tissue equation. Due to the killing rate β, the immune response decreases

the number of tumor cells A, then the competition term bA also decreases, that is, the population of healthy cells is less pressured by competition and can proliferate more. Since there are more healthy cells, the term cN of total competition in A increases, as if the effect of competition in A becomes stronger. Therefore, the immune response not only direct eliminates tumor cells but also interferes in the interaction of tumor-healthy tissue.

In the absence of an immune system, model (2.1)-(2.2) is quite similar to the model proposed by Fassoni e Yang(32), which corresponds to a mathematical model for the interaction between tumor cells and healthy tissue cells. This model exhibits three regimes: in the first one cancer onset is not possible since the cancer cure state is globally stable; the second regime presents bistability between cancer and the cancer cure states; in the third regime, the cancer state is globally stable. This qualitative behavior is similar to those presented here, since the immune response affects the competition terms as we discussed. The combination of an aggressive tumor with a weak tissue response is the worst situation for the host body. In the absence of an immune response, the healthy cells are overpowered by cancer cells and tumor progression occurs (32).

When the immune response is included, the CTLs can control tumor mass, leading the dynamics to a remission state. Nonaggressive tumors are more easily controlled by the immune cells, that is, a little increase in the killing rate β is enough to decrease the tumor state population to a small value. However, aggressive tumors present resistance to be destroyed due to the hysteresis effect. The number of tumor cells remains high until β reach a critical value β_2^c when the tumor state jumps down to the remission state. We also observed that the hysteresis may explain tumor recurrence cases since as β decreases, the tumor population remains at a low level until the point that the killing rate is small enough, and the equilibrium point jumps up from the remission state to the tumor state, and the tumor starts to proliferate.

Tumor evasion plays an important role in tumor onset and progression. Including such mechanisms in the dynamics, we observed an increase in the tumor equilibrium population, also facilitating tumor to settle down in host body, even the less aggressive ones. Furthermore, nonaggressive tumors presented the hysteresis phenomena, which is not noticed in the absence of evasion, which means that, due to these mechanisms, even nonaggressive tumors show resistance to be eliminated. Also, the effort of the immune system to control tumor needs to be even bigger when the evasion mechanisms are included.

The model proposed by Pillis, Radunskaya e Wiseman(43) considered the T-cell interactions with natural killer cells. Similar to the results in our model, the author found several regimes of tumor growth, control, removal and also periodic solutions. Although the model did not include any suppressive effects, the importance of the innate immune response in that work suggests that other immune cells, like the natural killer cells, have an effect on the tumor dynamics, and may be included in our future works. Arciero, Jackson e

Kirschner(45), in turn, focused in the suppressive effects, specially by the regulatory T-cells. These cells inhibit CTLs action in the TME, creating an immunosuppressed environment. The presence of these cells affects the tumor growth and control and also may be included in future works.

Furthermore, some tumor cells may be more immunogenic than the others due to the accumulation of mutation, measured by the mutation burden (11). In Chapter 1 we analyzed a simple model considering two distinct tumor phenotypes according to the mutational accumulation; our next step is to include this cell differentiation in system (2.1)-(2.2) together another aspects of the antitumor response.

2.5 CONCLUSION

We proposed a mathematical model describing the tumor-immune cycle considering antigen presentation, T cell priming and the evasion mechanisms used by tumor cells to avoid the CTLs and disrupt the antigen presentation. The results showed that the total tumor elimination is only possible in a healthy body host which presents a strong tissue response against tumor cells. Otherwise, the tumor cells can not be totally eliminated, but can be controlled and reduced to a low burden with the help of immune cells.

The damage caused by tumor cells in the healthy tissue plays a role in the tumor maintenance. Nonaggressive tumors, which cause less damage, can be controlled by the tissue pressure and by the immune cells action. Tumors which cause more damage, the aggressive ones, overpower the healthy cells and show resistance to immune response.

Tumor evasion is the main barrier faced by the immune system to fight cancer since these mechanisms increase tumor resistance. Nonaggressive tumors are more easily eliminated and have no resistance in the absence of tumor evasion. However, when including such mechanisms, it was noted that even nonaggressive tumors showed resistance to the action of CTLs. Aggressive tumors benefit even more from these mechanisms and make T-cell action even more difficult.

We also discussed about the use of immunotherapy, which is a good alternative in cancer treatment, however, some patients may not benefit from this type of treatment, whose efficiency depends on the combination of some factors: tumor aggressiveness, host body response, immune response, and the tumor ability to avoid immune system. In general, patients with weakened immune system and tissue response, together aggressive and evasive tumors patients with weakened immune systems do not respond well to immunotherapy. Also, the treatment's duration needs to be enough to decrease tumor population and change the basin of attraction, otherwise, the treatment fails.

Understanding the key processes in tumor–immune cycle is extremely important to the development and optimization of effective treatments, especially immunotherapies. The model presented here helps to understand these interactions, providing theoretical insights which are useful to the formulation of more complex and accurate models.

APPENDIX

2.A MODELLING THE INNATE IMMUNE RESPONSE

In this section we present a toy model considering the innate immune response against cancer. Only two state variables are considered: tumor cells A and the innate immune cells M, corresponding to macrophages, natural-killers and other cells which form the first barrier to eliminate pathogens. These cells circulate in the host body patrolling the tissues and searching viruses, bacterias and abnormal cells, therefore we assume in our model a constant recruitment r_m of circulating cells into the tumor microenvironment (TME). Tumor cells, on the other hand, proliferate according to the intrinsic growth rate r_a, and are limited by the TME carrying capacity K. The immune cells recognize and eliminate the tumor cells at a rate δ. Paremeters μ_a and μ_m stands for the natural mortality rate of tumor and immune cells, respectively.

Based on these assumption we proposed the following model for the interaction between cancer and innate immune response:

$$\begin{aligned} \frac{dA}{dt} &= r_a A\left(1-\frac{A}{K}\right) - \delta M A - \mu_a A \\ \frac{dM}{dt} &= r_m - \mu_m M \end{aligned} \tag{2.5}$$

The equilibrium points of model (2.5) are obtained setting its equations to zero and solving the corresponding system.

From the second equation we have that the value of M at the equilibrium is $M^* = r_m/\mu_m$. Substituting in the first equation, we obtain two equilibrium points: the tumor-free state $P_0 = (A^*, M^*) = (0, r_m/\mu_n)$ and the tumor equilibrium:

$$P^* = (A^*, M^*) = \left(\frac{K r_m}{r_a \mu_m}(\delta^{th} - \delta), \frac{r_m}{\mu_m}\right) \tag{2.6}$$

where $\delta^{th} = \mu_m(r_a - \mu_a)/r_m$. Therefore, the tumor state P^* is biologically feasible if, and only if, $\delta < \delta^{th}$, otherwise the tumor population are negative.

Let us analyse the stability of the two equilibrium points. Let $J(A^*, M^*)$ be

the Jacobian Matrix related to system (2.5) given by

$$J(A^*, M^*) = \begin{bmatrix} r_a\left(1 - \dfrac{A^*}{K}\right) - \dfrac{r_a A^*}{K} - \delta M^* - \mu_a & 0 \\ -\delta A^* & -\mu_m \end{bmatrix}$$

The eigenvalues of the Jacobian matrix evaluated at the tumor-free state ($J(P_0)$) are given by $\lambda_1 = -\mu_m$ and $\lambda_2 = (r_m/\mu_m)(\delta^{th} - \delta)$. So, the tumor-free state is stable if, and only if, $\delta > \delta^{th}$, and unstable otherwise. Similarly, the eigenvalues related to the tumor state P^* are $\lambda_1 = -\mu_m$ and $\lambda_2 = (r_m/\mu_m)(\delta - \delta^{th})$. Therefore, the tumor state is stable if, and only if, $\delta < \delta^{th}$, and unstable otherwise.

This result show us that, if the innate response is accurate ($\delta > \delta^{th}$) the tumor is eliminated by immune cells. On the other hand, if the response is not good enough, tumor evade from immune cells and settle down in the host body.

2.B INVARIANCE

Let Ω be the biologically-feasible domain for system (2.1)-(2.2), which is given by

$$\begin{aligned} \Omega \;=\; & \Big\{(N, A, C, D, D_a, D_{al}, H_v, H_l, C_v, C_l) \in \mathbb{R}^{10}_{+} \mid \; N \leqslant r_n/\mu_n;\; A \leqslant I_a K/r_a; \\ & D + D_a + D_{al} \leqslant r_d/\mu_d^{max};\; H_v \leqslant r_h/\mu_{hv};\; H_l \leqslant H_{max};\; C_v \leqslant r_c/\mu_{cv}; \\ & C_l \leqslant C_{max};\; C \leqslant \frac{q\phi_c C_{max}}{\mu_c}\Big\}. \end{aligned}$$

where $I_a = r_a - \mu_a$, $\mu_d^{max} = \max\{\mu_d, \mu_{da}, \mu_{dal}\}$, $H_{max} = \max\left\{Q_h, \dfrac{\sigma_h r_h r_d}{\mu_{hv}\mu_{hl}\mu_d^{max}}\right\}$ and $C_{max} = \max\left\{Q_c, \dfrac{\sigma_c r_c H_{max}}{\mu_{cv}(\phi_c + \mu_{cl})}\right\}$.

Let us show that the set Ω defined in (2.7) is an invariant set for system (2.1)-(2.2). We need to show that the flux of system (2.1)-(2.2) at the border of Ω points into the invariant set, that is, we analyse the derivatives at the borders of Ω.

First, It is easy to see that, if the state variable assumes zero, then the derivative of the corresponding equation is zero or positive, that is, if $x = 0$ then $dx/dt \geqslant 0$, for $x = N, A, D, D_a, D_{al}, H_v, H_l, C_v, C_l$ and C. Therefore the flux in these borders points into Ω, or equivalently, at $x = 0$, the derivatives are positive and the populations must increase, do not assuming negative values.

Now, let us show that each population are limited and can not go to infinity, remaining in the invariant set Ω.

For the healthy cells population, notice that

$$\frac{dN}{dt} = r_n - bNA - \mu_n N \leqslant r_n - \mu_n N,$$

so when $N = r_n/\mu_n$ we have that $\dfrac{dN}{dt} \leqslant 0$.

For the tumor cells population:

$$\begin{aligned}\frac{dA}{dt} &= r_a A\left(1-\frac{A}{K}\right) - cAN - \beta AC - \mu_a A \\ &\leqslant r_a A\left(1-\frac{A}{K}\right) - \mu_a A \\ &= I_a A\left(1-\frac{r_a}{I_a K}A\right).\end{aligned}$$

So, if $A = \dfrac{I_a K}{r_a}$ then $\dfrac{dA}{dt} \leqslant 0$.

For the DCs equation, we have that

$$\begin{aligned}\frac{d(D+D_a+D_{al})}{dt} &= r_d - \nu A D_a - (1-p)\phi_d D_a - \mu_d D - \mu_{da} D_a - \mu_{dal} D_{al} \\ &\leqslant r_d - (1-p)\phi_d D_a - \mu_d^{max}(D+D_a+D_{al}) \\ &\leqslant r_d - \mu_d^{max}(D+D_a+D_{al}), \text{ since we assume } p \leqslant 1.\end{aligned}$$

Therefore, at the border $D + D_a + D_{al} = \dfrac{r_d}{\mu_d^{max}}$ we have that $\dfrac{d(D+D_a+D_{al})}{dt} \leqslant 0$.

The H_v equation satisfies:

$$\frac{dH_v}{dt} = r_h - \sigma_h H_v D_{al} - \mu_{hv} H_v \leqslant r_h - \mu_{hv} H_v,$$

so, when $H_v = r_h/\mu_{hv}$ we have that $\dfrac{dH_v}{dt} \leqslant 0$.

Using that $H_v \leqslant r_h/\mu_{hv}$ and $D_{al} \leqslant r_d/\mu_d^{max}$ in Ω, the equation for H_l can be written as

$$\begin{aligned}\frac{dH_l}{dt} &= \sigma_h H_v D_{al} - \mu_{hl} H_l + \theta_h D_{al}\left(1-\frac{H_l}{Q_h}\right)H_l \\ &\leqslant \underbrace{\sigma_h \frac{r_h}{\mu_{hv}}\frac{r_d}{\mu_d^{max}} - \mu_{hl} H_l}_{\Diamond} + \underbrace{\theta_h \frac{r_d}{\mu_d^{max}}\left(1-\frac{H_l}{Q_h}\right)H_l}_{\triangle}.\end{aligned}$$

Notice that, if $H_l = H_{max}$, then we have that $H_l \geqslant Q_h$, which implies that the expression $\triangle$ is less than or equal to zero. Equivalently, $H_l = H_{max}$ implies $H_l \geqslant \dfrac{\sigma_h r_h r_d}{\mu_{hv}\mu_{hl}\mu_d^{max}}$ and consequently, the expression $\Diamond$ is less than or equal to zero. Therefore, at the border $H = H_{max}$ we have that $\dfrac{dH_l}{dt} \leqslant 0$.

For C_v, we have that

$$\frac{dC_v}{dt} = r_c - \sigma_c C_v H_l - \mu_{cv} C_v \leqslant r_c - \mu_{cv} C_v,$$

so, when $C_v = r_c/\mu_{cv}$ we have that $\dfrac{dC_v}{dt} \leqslant 0$.

We use the fact that $H_l \leqslant H_{max}$ and $C_v \leqslant r_c/\mu_{cv}$ and obtain that

$$\begin{aligned}\frac{dC_l}{dt} &= \sigma_c C_v H_l - (\phi_c + \mu_{cl})C_l + \theta_c H_l \left(1 - \frac{C_l}{Q_c}\right) C_l \\ &\leqslant \underbrace{\sigma_c \frac{r_c}{\mu_{cv}} H_{max} - (\phi_c + \mu_{cl})C_l}_{\Diamond} + \underbrace{\theta_c H_{max} \left(1 - \frac{C_l}{Q_c}\right) C_l}_{\triangle}.\end{aligned}$$

Similar to H_l, if we take $C_l = C_{max}$, then $C_l \geqslant Q_c$ and $C_l \geqslant \dfrac{\sigma_c r_c H_{max}}{\mu_{cv}(\phi_c + \mu_{cl})}$, which implies that the expressions $\Diamond$ and $\triangle$ are less than or equal to zero, resulting that $\dfrac{dC_l}{dt} \leqslant 0$.

Finally, for C:

$$\begin{aligned}\frac{dC}{dt} &= q\phi_c C_l - \rho A C - \mu_c C \\ &\leqslant q\phi_c C_{max} - \mu_c C,\end{aligned}$$

and if $C = \dfrac{q\phi_c C_{max}}{\mu_c}$, then $\dfrac{dC}{dt} \leqslant 0$

Therefore, the flux at the borders of system (2.1)-(2.2) points into Ω. That is, taking an initial condition in Ω, the solutions will not go to infinity, or assume negative values. Equivalently, the solutions can not escape from the domain Ω and the system (2.1)-(2.2) is invariant in this set.

2.C MATHEMATICAL ANALYSIS OF THE TUMOR-IMMUNE MODEL

In this section, we detailed show the mathematical analysis of system (2.1)-(2.2). We assume for simplicity that the disabled CTLs can not be reactivated, $\tau = 0$. Thus, the equation for C_d can be decoupled from model (2.1)-(2.2) and will be omitted in the analysis from now on.

The equilibrium points are obtained by setting the derivatives in system (2.1)-(2.2) equal to zero, and the stability analysis is performed by the eigenvalues of the Jacobian Matrix $J(N, A, C, D, D_a, D_{al}, H_v, H_l, C_v, C_l)$ related to the dynamical system.

Firstly we analyse the model without the evasion mechanisms and then introduce such parameters to observe how they may change the systems behavior. Finally, we analyse the cloning processes and its effect in the model dynamics.

2.C.1 SUBMODEL WITHOUT CLONAL EXPANSION AND TUMOR EVASION

Initially, to better understanding the effect of tumor evasion on system (2.1)-(2.2), it is important to analyze the behavior of this system without such mechanisms

($\nu = \rho = 0$). The clonal expansion is also removed in this section ($\theta_H = \theta_C = 0$) to simplify the model analysis.

Let $\bar{P} = \left(\bar{N}, \bar{A}, \bar{C}, \bar{D}, \bar{D_a}, \bar{D_{al}}, \bar{H_v}, \bar{H_l}, \bar{C_v}, \bar{C_l}\right)$ be an arbitrary equilibrium point of system (2.1)-(2.2).

The trivial equilibrium point P_0 was analysed in section 2.2.2.1, so here restrict the results here to the nontrivial equilibrium points, or tumor states. The expressions for $\bar{N}$, $\bar{D}$, $\bar{D_a}$, $\bar{D_{al}}$, $\bar{H_v}$, $\bar{H_l}$, $\bar{C_v}$, $\bar{C_l}$ and $\bar{C}$ can be written in terms of $\bar{A}$, which, in turn, is a root of the polynomial

$$p(\bar{A}) = a_0 + a_1\bar{A} + a_2\bar{A}^2 + a_3\bar{A}^3, \tag{2.7}$$

whose coefficients are

$$\begin{cases} a_0 &= \tilde{u}\mu_d r_n(c - c^{th}) \\ a_1 &= \tilde{w}\mu_n(\beta - \beta_1)\gamma + \tilde{u}\mu_d R_A(b^{th} - b) \\ a_2 &= \tilde{w}b(\beta - \beta_2)\gamma + \tilde{u}\mu_d b(r_a/K) \\ a_3 &= (\tilde{u} + \tilde{v})\gamma b(r_a/K) \end{cases}$$

where $\tilde{u} = \mu_c\mu_{cv}\mu_{dal}\mu_h\mu_{hv}(\mu_{cl} + \phi_c)(\mu_{da} + \phi_d)$, $\tilde{v} = p\sigma_h r_d\mu_c\phi_d(\mu_{cl} + \phi_c)(\sigma_c r_h + \mu_{cv}\mu_h)$ and $\tilde{w} = pq\sigma_h\sigma_c r_d r_c r_h\phi_c\phi_d$ are positive constants and

$$b^{th} = \frac{\mu_n r_a}{R_A K}, \qquad \beta_1 = R_A\frac{\tilde{u} + \tilde{v}}{\tilde{w}}\frac{(c^{th} - c)}{c^{th}}, \qquad \beta_2 = R_A\frac{\tilde{u} + \tilde{v}}{\tilde{w}}\frac{(b - b^{th})}{b}. \tag{2.8}$$

Let us start considering $c > c^{th}$, which implies that P_0 is stable. Notice now that, if $b < b^{th}$ (nonaggressive tumor), then $\beta_1, \beta_2 < 0$ and all the coefficients a_i in (2.7) are positive. So, by Descartes' Rule of Signs, the unique non-negative equilibrium is the tumor-free state.

Now, let us analyze the case in which $b > b^{th}$ and $c > c^{th}$, or equivalently, an aggressive tumor in a healthy host. In this situation $a_0, a_3 > 0$ and $\beta_1 < 0$, so the number of tumor states are determined by the signal of the coefficients a_1 and a_2.

Notice that, even for $b > b^{th}$, if b is close to b^{th} then a_1 and a_2 may be positive and, in this case, there is no nontrivial equilibrium, or tumor states. However, as we increase b, these coefficients become negative and, according to the Descartes'Rule of Signs, there are 0 or 2 tumor states. On the other hand, the killing rate β appears in the positive terms of both coefficients, so the higher β, the lower the risk of tumor onset.

To illustrate the appearance of the tumor states, we present in Figure 2.6 a bifurcation diagram using the parameter set in Table 2.2. The vertical axis represents the positive roots $\bar{A}$ of polynomial (2.7) varying the tumor aggressiveness b for different values of β, considering a fixed value $c > c^{th}$. The stability analysis was done by the eigenvalues of Jacobian matrix of system (2.1)-(2.2), the blue color represents the stable points, while the red color represents the unstable points.

Figure 2.6 – Bifurcation diagram for the strong tissue response case, $c > c^{th}$. Stable states are in blue, and unstable states in red.

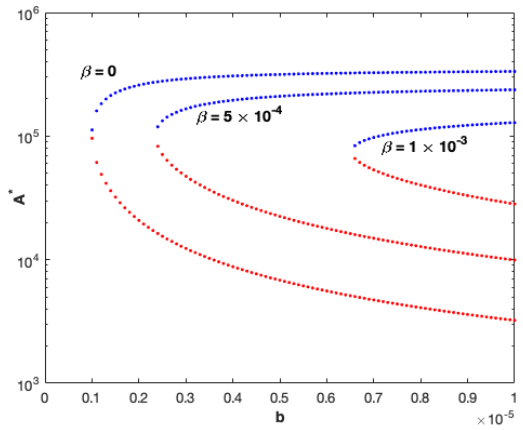

From Figure 2.6, while $b < b^{th}$ there is no tumoral state and the solutions go to the tumor-free state. However, for $b > b^{\tilde{th}}$ ($b^{\tilde{th}} > b^{th}$), two tumoral states appear, one stable and the other unstable, being $b^{\tilde{th}}$ the value of b for which the nontrivial equilibrium appears. In this case, there is bistability between the stable tumor-state and the tumor-free state. The introduction of the immune response, by the parameter β, displaces $b^{\tilde{th}}$ forward, reduce tumor population size and also the basin of attraction of the tumor state. Thus, the better the immune response, the more aggressive the tumor must be to establish itself in the host.

Now, let us consider the case $c < c^{th}$, which means that the tumor-free state P_0 is unstable, so tumor cells can not be totally eliminated. Also, in polynomial (2.7) we have that $a_0 < 0$ and $a_3 > 0$, which implies that there will always be at least one signal alternation, and consequently at least one tumor state.

Firstly, consider $b < b^{th}$, which implies $\beta_2 < 0$ and $a_2 > 0$, so regardless of the a_1 signal, there is a single signal alternation and a single tumor state P^*. Therefore, the combination of a nonaggressive tumor with a weak tissue response guarantees the existence of a unique tumoral state.

Let us consider now an aggressive tumor, $b > b^{th}$. We already show the existence of at least one tumor state, notice now that, if $a_1 > 0$ and $a_2 < 0$ the there are three signal alternations among the coefficients, so by Descartes' Rule of Signs, there are one or three tumor states. To analyse this possibility, let γ_1 and γ_2 be

$$\gamma_1 = \frac{\tilde{u}\mu_d R_A(b - b^{th})}{\tilde{w}\mu_n(\beta - \beta_1)} \qquad \gamma_2 = \frac{\tilde{u}\mu_d b(r_a/K)}{\tilde{w}b(\beta_2 - \beta)},$$

with β_1 and β_2 defined in (2.8). Notice that, if $\beta_1 < \beta < \beta_2$ and $\gamma > \max\{\gamma_1; \gamma_2\}$, than we have $a_1 > 0$ and $a_2 < 0$. However, $\beta_1 < \beta < \beta_2$ makes sense only if $\beta_1 < \beta_2$, or equivalently

$\beta_2 - \beta_1 > 0$, which can be written as

$$\beta_2 - \beta_1 = \frac{c(\tilde{u}+\tilde{v})R_A}{c^{th}\tilde{w}}\left(1 - \frac{b^{th}c^{th}}{bc}\right).$$

Then, to obtain $a_1 > 0$ and $a_2 < 0$ the following conditions must be satisfied: (i) $(b^{th}c^{th})/bc < 1$, (ii) $\gamma > \max\{\gamma_1; \gamma_2\}$ and (iii) $\beta_1 < \beta < \beta_2$.

To confirm the existence of three nontrivial equilibrium points, we performed numerical simulations considering satisfied the conditions (i) and (ii) and varying β. We expect that the three tumor states must appear in a subset of $[\beta_1; \beta_2]$, for instance for $\beta \in [\beta_1^c; \beta_2^c] \subseteq [\beta_1; \beta_2]$.

Figure 2.7 presents a bifurcation diagram representing the situation described above, the vertical axis corresponds to the positive roots of polynomial (2.7) as we vary β for a fixed value $b > b^{th}$ and $c < c^{th}$. The blue color corresponds to the stable points and the red color to the unstable ones. The tumor-free state P_0 was omitted in Figure 2.7 since it is unstable.

Figure 2.7 – Bifurcation diagram for weak tissue response case, $c < c^{th}$. Stable states are in blue, and unstable states in red

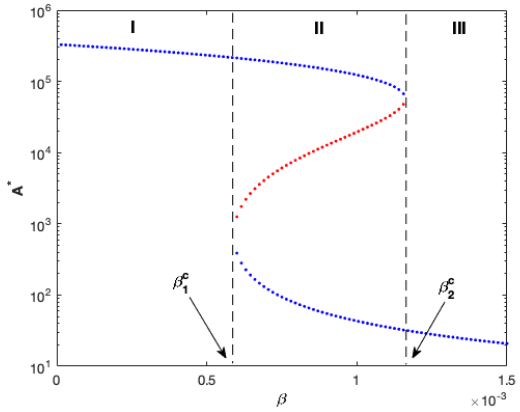

In Figure 2.7, three different regimes occur as we increase the killing rate β. In regime I, with a low killing rate $\beta < \beta_1^c$, there is a single stable tumor state (denoted by P^{up}) with a high tumor burden. As we increase the killing rate, the model goes to regime II, for $\beta_1^c < \beta < \beta_2^c$, in which other two tumor states appear, a stable one with low tumor burden, P^{dw}, and an unstable one; so there is bistability between two different tumoral states: P^{up} and P^{dw}. Finally, in the third regime with $\beta > \beta_2^c$, there is a single stable tumoral state P^{dw} with low tumor burden. So, as we increase β the model transit from a regime with a huge tumor population (I) to a regime in which cancer can be controlled (III), passing through a transient region with two stable tumoral states (II). This bifurcation phenomena is called hysteresis.

The appearance of hysteresis indicates a resistance of the tumor to be eliminated by CTLs. Nonaggressive tumors are more easily controlled since the tumor burden decreases

continuously as we increase β. For the aggressive ones, however, the tumor burden remains high (P^{up}) while $\beta < \beta_2^c$, and only when $\beta > \beta_2^c$, it jumps down from P^{up} to P^{dw}, that is, the parameter β needs to be bigger than β_2^c to reduce the tumor population to the tumor control state.

Summing up, the tumor elimination (P_0 stable) is only possible in a healthy host with a good tissue response ($c > c^{th}$), and the tumor onset is determined by the relation between tumor aggressiveness (b) and CTLs killing rate (β). In the case of a weak tissue response ($c < c^{th}$), tumor onset can not be prevented, but can be controlled by the immune system, which in turn, finds resistance to eliminate aggressive tumors due to the hysteresis.

2.C.2 THE EVASION MECHANISMS IN THE TUMOR-IMMUNE CYCLE MODEL

In this section, we analyze how the tumor evasion mechanisms affect the dynamic described in previous subsection. So, let us consider now that $\nu, \rho \neq 0$, bit keeping $\theta_h = \theta_c = 0$.

Let $\bar{P} = \left(\bar{N}, \bar{A}, \bar{C}, \bar{D}, \bar{D_a}, \bar{D_{al}}, \bar{H_v}, \bar{H_l}, \bar{C_v}, \bar{C_l}\right)$ be an arbitrary equilibrium point. The expressions for $\bar{N}$, $\bar{D}$, $\bar{D_a}$, $\bar{D_{al}}$, $\bar{H_v}$, $\bar{H_l}$, $\bar{C_v}$, $\bar{C_l}$ and $\bar{C}$ can be written as a function of $\bar{A}$, which, in this case, is a root of the following 5th degree polynomial :

$$a_0 + a_1\bar{A} + a_2\bar{A}^2 + a_3\bar{A}^3 + a_4\bar{A}^4 + a_5\bar{A}^5, \tag{2.9}$$

whose coefficients are given by

$$\begin{cases} a_0 &= \tilde{u}\mu_c\mu_d(\mu_{da} + \phi_d)r_n(c - c^{th}) \\ a_1 &= k_1\gamma + k_2 \\ a_2 &= k_3\gamma + k_4 \\ a_3 &= k_5\gamma + k_6 \\ a_4 &= k_7\gamma + k_8 \\ a_5 &= \gamma\rho\nu b(r_a/K)\tilde{u} \end{cases} \tag{2.10}$$

being $\tilde{u} = \mu_c\mu_{cv}\mu_{dal}\mu_h\mu_{hv}(\mu_{cl} + \phi_c)(\mu_{da} + \phi_d)$, $\tilde{v} = p\sigma_h r_d\mu_c\phi_d(\mu_{cl} + \phi_c)(\sigma_c r_h + \mu_{cv}\mu_h)$,

$\tilde{w} = pq\sigma_h\sigma_c r_d r_c r_h \phi_c \phi_d$ and the terms k_i given by

$$\begin{aligned}
k_1 &= \tilde{w}\mu_n(\beta - \beta_1) \\
k_2 &= -\tilde{u}\mu_c\mu_d(\mu_{da} + \phi_d)R_A(b - b^{th}) - (\rho(\mu_{da} + \phi_d) + \nu\mu_c)\tilde{u}\mu_d r_n(c^{th} - c) \\
k_3 &= \tilde{w}b(\beta - \tilde{\beta}_2) \\
k_4 &= -\nu\mu_d\tilde{u}(\mu_c R_A(b - b^{th}) + \rho r_n(c^{th} - c)) + \tilde{u}\mu_d R_A(b - b^{th})(\tilde{\rho} - \rho) \\
k_5 &= -\nu\tilde{u}(\mu_c R_A(b - b^{th}) + \rho r_n(c^{th} - c)) + (\tilde{u}(\mu_{da} + \phi_d) + \tilde{v})R_A(b - b^{th})(\tilde{\rho} - \rho) \\
k_6 &= \nu\tilde{u}\mu_d R_A(b - b^{th})(\tilde{\rho} - \rho) + \rho b(r_a/K)\mu_d\tilde{u}(\mu_{da} + \phi_d) \\
k_7 &= \nu\tilde{u}R_A(b - b^{th})(\tilde{\rho} - \rho) + \rho b(r_a/K)(\tilde{u}(\mu_{da} + \phi_d) + \tilde{v}) \\
k_8 &= \nu\rho b(r_a/K)\mu_d\tilde{u}
\end{aligned} \tag{2.11}$$

where

$$\tilde{\rho} = \frac{br_a\mu_c}{KR_A(b - b^{th})} \text{ and } \tilde{\beta}_2 = \beta_2 + \frac{\rho r_n(\tilde{u}(\mu_{da} + \phi_d) + \tilde{v})(c^{th} - c) - \nu\mu_c\tilde{u}r_n(c^{th} - c)}{\tilde{w}b}.$$

Firstly, let us consider a strong tissue response, $c > c^{th}$. When $b < b^{th}$, notice that $\beta_1, \beta_2, \tilde{\rho} < 0$, therefore $a_i > 0$, $i = 1, \ldots, 5$. So, the tumor-free state is the only one biological-feasible equilibrium point, and It is also a stable equilibrium point. This is the same situation we found when there is no tumor evasion. On the other hand, when $b > b^{th}$, due to complexity of coefficients (2.10) we can not analytically determine the existence of tumor states. Therefore, we assess the effect of tumor evasion for $c > c^{th}$ by numerical simulations. Figure 2.8 presents the existence of tumor states according to b for different values of ν(a) and ρ (b). Again, let us denote by $b^{\tilde{th}}$ the value of b for which the tumor states appear.

Figure 2.8 – Bifurcation diagram for strong tissue response considering the tumor evasion mechanisms.

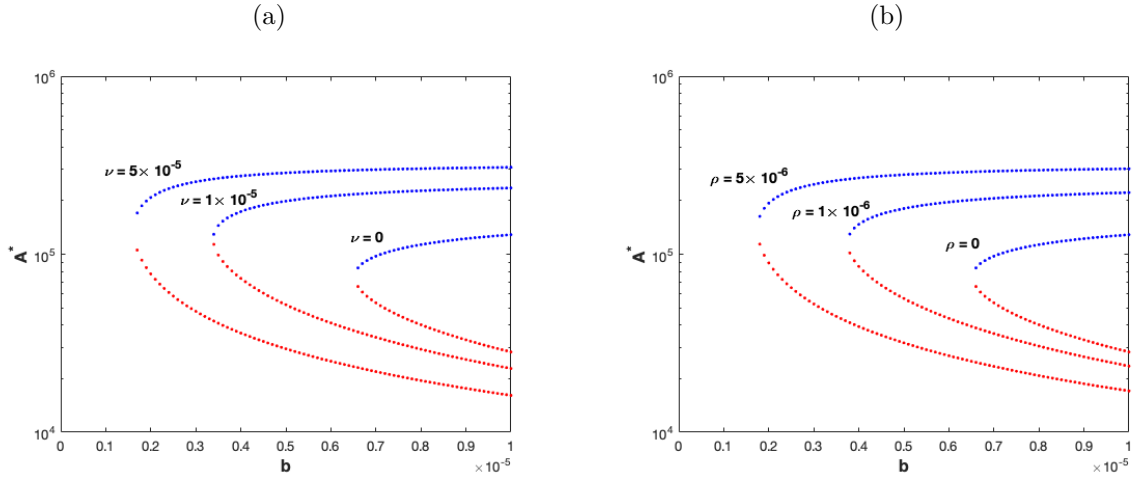

While the immune response displace $b^{\tilde{th}}$ forward and decreases the tumor state basin of attraction (see Figure 2.6), the evasion mechanisms do the opposite: the critical

value $\tilde{b^{th}}$ is displaced backward and the tumor state basin of attraction is increased, that is, the evasion parameters facilitate tumor onset. So, the inclusion of parameters ν and ρ for case $c > c^{th}$ do not change the qualitative behavior of system (2.1)-(2.2), but they allow tumor onset to lower b values, that is, less aggressive tumors may settle down in host body.

From now on, we use $\nu = 1 \times 10^{-5}$ and $\rho = 5 \times 10^{-5}$ in the simulations where these parameters are fixed.

Now, let us deal with the case $c < c^{th}$. Firstly, consider $b < b^{th}$, which implies $\beta_2, \tilde{\rho} < 0$ and consequently $a_0 < 0$ and $a_4, a_5 > 0$. We show that, in this situation, when any evasion mechanisms is included, there is a single tumor state regardless of the value of β, however, notice that if $\nu \neq 0$ and $\rho \neq 0$, then there are one or three signal alternations, so the hysteresis phenomena may happens even for nonaggressive tumor as consequence of the evasion mechanisms. To illustrate it, we perform a bifurcation diagram in Figure 2.9, varying the killing rate β for different values of ν and ρ. The stable states are in blue and the unstable states in red, and for simplicity we use $\nu = \rho$.

Figure 2.9 – Bifurcation diagram for weak tissue response case considering the tumor evasion mechanisms.

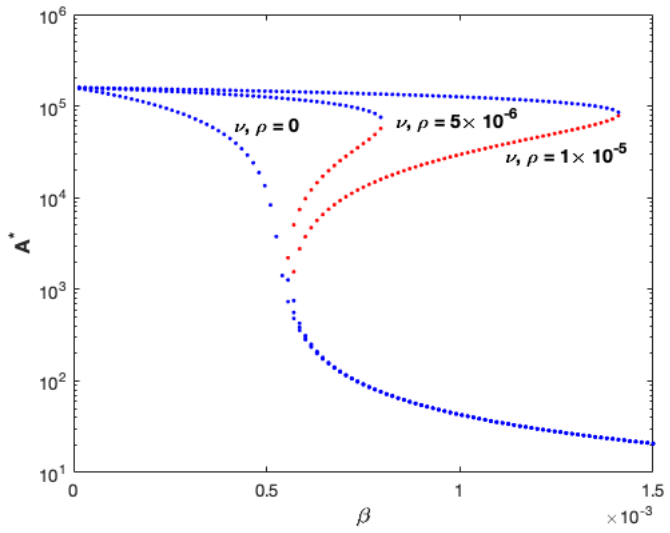

When $\nu = \rho = 0$, there is a single tumor state, whose tumor population decreases as we increase β. Notice that if $\beta > 0.015$, the tumor population is close to zero, which means that the tumor onset is under control. Introducing tumor evasion, the shape of the curve change, and another two tumoral states appear, generating the same hysteresis effect discussed in Figure 2.7. Thus, the evasion mechanisms allow hysteresis even for nonaggressive tumors, which is not possible when $\nu = \rho = 0$. In other words, nonaggressive tumors also show resistance to be eliminated by the immune system, which in turn, needs to be more effective to lead the tumor mass to the tumor control state.

Finally, consider now an aggressive tumor, $b > b^{th}$. From section 2.C.1 , if $\nu = \rho = 0$ and $\beta_1 < \beta < \beta_2$, then there are three tumoral states. Let us analyse how the parameters ν and ρ affect the coefficients in (2.10).

Firstly, notice that k_7 can be written as $k_7 = \dfrac{k_6}{\mu_d} + \dfrac{\rho b r_a \tilde{v}}{K}$, so $k_7 < 0$ implies that

$$\begin{aligned} k_7 < 0 \quad &\Rightarrow \quad \frac{k_6}{\mu_d} + \frac{\rho b r_a \tilde{v}}{K} < 0 \\ &\Rightarrow \quad k_6 < -\frac{\mu_d \rho b r_a \tilde{v}}{K} < 0, \end{aligned}$$

thus, $k_7 < 0 \Rightarrow k_6 < 0$. Moreover, since $b - b^{th} > 0$ and $c^{th} - c > 0$, notice that

$$k_5 < (\tilde{u}(\mu_{da} + \phi_d) + \tilde{v}) R_A (b - b^{th})(\tilde{\rho} - \rho). \tag{2.12}$$

The expression $R_A(b - b^{th})(\tilde{\rho} - \rho)$ appears in k_7 and substituting it in (2.12) the above relation, we obtained that

$$k_5 < \frac{(\tilde{u}(\mu_{da} + \phi_d) + \tilde{v})}{\nu \tilde{u}} (k_7 - \rho b (r_a/K)(\tilde{u}(\mu_{da} + \phi_d) + \tilde{v}))$$

and then, $k_7 < 0 \Rightarrow k_5 < 0$.

Notice now that, since $k_8 > 0$, then $a_4 < 0$ only if $k_7 < 0$, which in turn implies $k_6, k_5 < 0$ and consequently $a_3 < 0$. So, if in the particular case where $b > b^{th}$ and $c < c^{th}$, we conclude that $a_4 < 0 \Rightarrow a_3 < 0$ and there is no signal alternation between these coefficients, which guarantee that there is no possibility of five signal alternations or five tumoral states. Therefore, similar to the previous cases, there are one or three tumoral states.

Let us consider first that $\rho < \tilde{\rho}$. In this case, $k_6 > 0$, consequently $k_7 > 0$ and $a_4 > 0$. Also, note that

$$k_5 = \underbrace{-\nu \tilde{u}(\mu_c R_A (b - b^{th}) + \rho r_n (c^{th} - c))}_{<0} + \underbrace{(\tilde{u}(\mu_{da} + \phi_d) + \tilde{v}) R_A (b - b^{th})(\tilde{\rho} - \rho)}_{>0},$$

look that ν appears in the negative term, so if It is small, then $k_5 > 0$ and $a_3 > 0$, otherwise, $k_5 > 0$ and the coefficient a_3 may turn into negative. So, if ν and ρ are small, the existence of three signal alternations is restrict to the case when $a_1 > 0$ and $a_2 < 0$. Since $k_2 < 0$, β must be greater than β_1 to ensure that $a_1 > 0$. Similarly, to ensure $a_2 < 0$ we need $\beta < \tilde{\beta}_2$, and then, the possibility of three tumoral states occurs if $\beta_1 < \beta < \tilde{\beta}_2$. This situation is similar to that described in the model with absence of evasion mechanisms, but here we can see that $\tilde{\beta}_2 > \beta_2$, so the interval in which there are three tumoral states is increased by the parameters ν and ρ.

As we increase ν and when $\rho > \tilde{\rho}$, the coefficient a_3 becomes negative. In this case, regardless a_4 signal, there always be one signal alternation among a_3, a_4, and a_5, so

there are more signal combinations among the coefficients a_i allowing the existence of three tumoral states. To confirm these results, we perform numerical simulations considering $\rho < \tilde{\rho}$ and $\rho > \tilde{\rho}$ for several values os ν. The diagrams obtained are similar to presented in Figure 2.7 and Figure 2.9, and for this reason they will not be presented here. In all the simulations we observed the hysteresis phenomena previously described, that is, a single tumor state P^{up} for low β, followed by bistability between the tumor state P^{up} (with high tumor population) and the tumor control state P^{dw} (low tumor population) when $\beta_1 < \beta < \tilde{\beta}_2$, and finally a single stable tumor control state P^{dw} for high β. Also, we observe that increasing ν and ρ, the value of $\tilde{\beta}_2$ is also increased, that is, the evasion mechanisms increase the region with bistability, equivalently, increase the hysteresis, so tumor control can only be achieved with higher killing rate β.

Summing up, the tumor evasion mechanisms may affect the model dynamics, increasing tumor state basin of attraction and facilitating its onset. For weak tissue response, hysteresis and tumor resistance can be observed in both, aggressive and nonaggressive tumors. Also, the better the tumor evasion, the more efficient the immune response needs to be to control tumor population.

2.C.3 THE CLONAL EXPANSION IN TUMOR-IMMUNE DYNAMICS

In this section, we discuss the effect of the clonal expansion in the dynamics. Due to the complexity of system (2.1)-(2.2) when the clonal expansion is included, we are not able to write the equilibrium state variables as a function of $\bar{A}$ and determine a polynomial $p(\bar{A})$ like in the other sections, so we use numerical methods to obtain the equilibrium points of system (2.1)-(2.2) and to establish their stabilities. Therefore, to investigate the effect in the model dynamics, we rebuild the bifurcation diagrams in Figure 2.8, for strong tissue response, and in Figure 2.9, for weak tissue response, for different values of $\theta = \theta_h = \theta_c$, but keeping fixed values for ν and ρ.

STRONG TISSUE RESPONSE

Firstly, let us start considering the strong tissue response case, $c > c^{th}$. Figure 2.10 presents a bifurcation diagram considering different cloning rates θ, as we vary parameter b.

In Figure 2.10a the left curve consider no cloning rate, so the dynamics is the same presented in figure 2.6, that is, there is bistability between the tumor state, the blue curve from above, and the tumor-free state, which do not appear in this figure due to logarithmic scale. The red curve in the middle corresponds to the unstable state, which divides the basins of attraction. As we increase the cloning rate, the red curve is displaced up, increasing the tumor-free state's basin of attraction. However, at a certain point, the

Figure 2.10 – The effect of the cloning rate θ in tumor dynamics considering $c > c^{th}$.

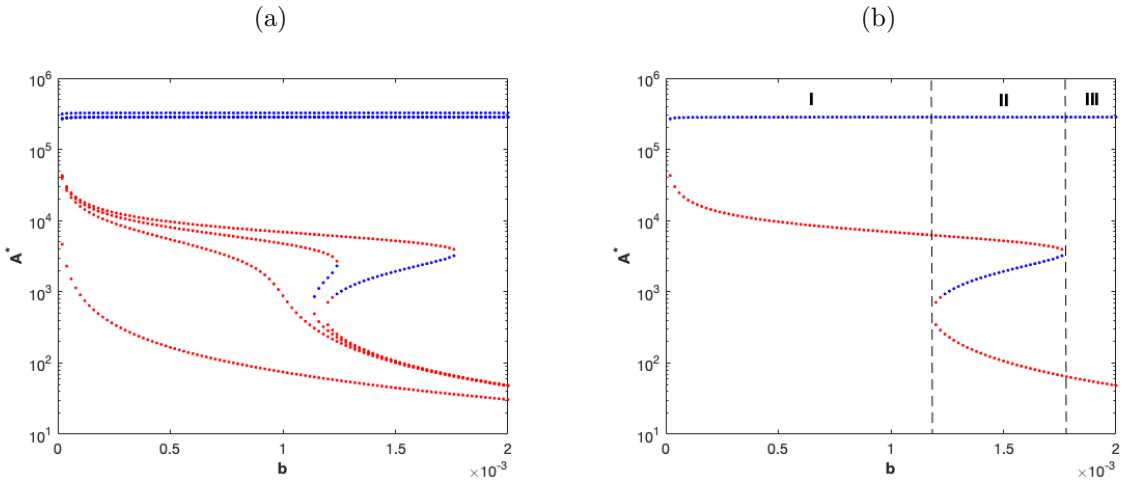

cloning rate is no more able to displace the unstable curve, and starts to deform it, creating two more equilibrium points.

In figure 2.10b, we observe in details the deformed curve. In region I the red line corresponds to the unstable tumor state, separating the stable states's basins of attraction. Therefore, in this state tumor and immune response are in balance, any disturbance favorable to the tumor leads the system to tumor equilibrium, while disturbances favorable to the immune response lead to the tumor-free state.

In region II the clonal expansion deformed the curve and two more states appear, one stable and the other unstable. The upper unstable state is similiar to the one in region I, perturbations around this state will lead the system to the tumor state from above, or to the intermediary tumor state. Therefore, although the cloning rate is not able to increase the tumor-free basin of attraction, it creates an intermediary state with less tumor cells in a certain range of tumor aggressiveness. Moreover, notice that there is a small interval in which the intermediary tumor state is unstable, in this case the dynamics approach to this state initially, but after some time goes away since it is unstable.

On the other hand, the lower unstable state, which appear in regions II and III, behaves differently. This state no longer divides the basins of attractions of the nearby stable states. In fact, any unfavorable disturbance to the tumor leads directly to the tumor-free state, however, favorable disturbances do not always lead to one of the tumor balances. In Figure 2.11 we illustrate the behavior of the upper unstable branch (a) and the lower one (b), fixing $b = 0.0015$ and perturbing the tumor population.

In Figure 2.11a a perturbation of a single cell in the unstable state leads to the tumor state ($A_0 = A^* + 1$), or to the tumor-free state ($A_0 = A^* - 1$), as expected. However, in figure 2.11b the lower unstable state behaves differently: any negative perturbation leads to the tumor-free state, but taking the initial condition above the equilibrium, for

Figure 2.11 – Numerical simulations perturbing the tumor population around the equilibrium points in figure 2.10

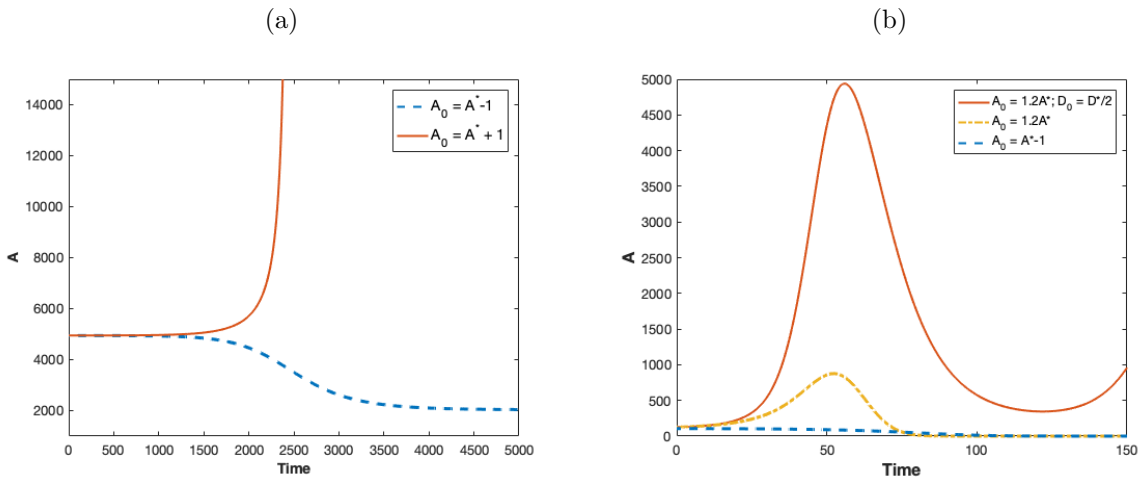

instance $A_0 = 1.2A^*$, the tumor population increases initially and then decreases to zero. If we also consider $D_0 = D^*/2$, the tumor decrease and then increasing again, reaching the intermediary tumor state. In fact, all the performed simulations have the same behavior, tumor increases at the beginning, then decreases; and, according to the initial condition, it decreases to tumor-free state or recover and grow to one of the tumor states. To understand why it happens, we need to analyse each variable of the unstable states, which are presented in Table 2.3

Table 2.3 – State variable values at the equilibrium points in figure 2.10

	Tumor-free state	Lower Unstable State	Upper Unstable State
A	0	107	5204
N	700000	330004	12580
D	50000	19218	632
D_a	0	335	534
D_{al}	0	7527	12006
H_v	10000	5705	4544
H_l	0	2805	7817
H	0	63	332
C_v	10000	7809	5612
C_l	0	296	690
C	0	246	555

In the lower unstable state, there is a small tumor mass and only a few effector lymphocytes, joining this to the high tumor aggressiveness, the cells rapidly proliferate and tumor mass increase. However, the immune response is not completely triggered, there are a lot of DCs which will be activated when tumor increases, starting the immune response. Also, due to the high cloning rates, the number of effector lymphocytes rapidly increases and, consequently, reduce the tumor mass. According to the combination of the initial

condition of each variable, this immune response may be effective and eliminate tumor cells, or the tumor evade and growth to one of the tumor states.

WEAK TISSUE RESPONSE

Now, let us consider the weak tissue response case, $c > c^{th}$. In Figure 2.12 we rebuild the bifurcation diagram of figure 2.7 considering different values for the parameters θ_h and θ_c to investigate how the cloning affects the model dynamics.

Figure 2.12 – The effect of cloning in the weak tissue response diagram, being $\theta_h = \theta_c = \theta$.

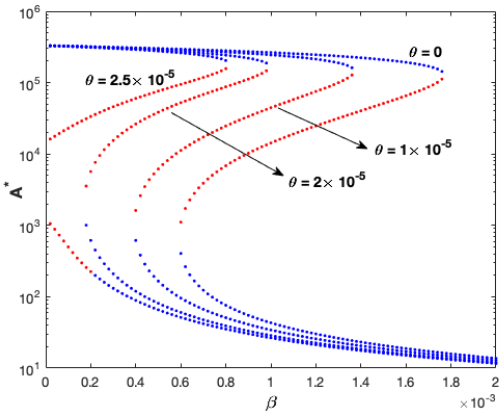

As we increase cloning, the curves are displaced to the left, so that the value of β required for the immune system to be able to control tumor growth becomes smaller and smaller and, consequently, becomes more difficult for the tumor to establish itself in the body host.

Also, when we have $\theta = 2.5 \times 10^{-5}$ the corresponding curve crosses the vertical axis and the hysteresis starts to disappear. Note also that in this case the lower branch of the curve, representing the control or remission state, has an unstable region (in red), while in the other curves it was always stable (in blue). To further investigate this, we present in Figure 2.13 the diagrams of two distinct values of cloning rate, representing the above-described situation.

In figure 2.13a we can see that the hysteresis still remains: in region II we have the existence of the tumor state and also the control/remission state; while in regime III there is only the remission state. In the figure 2.13b the bifurcation diagram has crossed the vertical axis and the hysteresis starts to disappear. In fact, if we further increase the value of the cloning rates, region II will disappear and there will only be the remission state, for any value of β.

Now notice that in both figures the lower branch (representing the remission equilibrium) becomes unstable when $\beta < \beta^*$. For instance, taking $\beta = 1 \times 10^{-4}$ in the figure 2.13a the tumor state is the only stable one, in the figure 2.13b, for $\beta = 4 \times 10^{-4}$, there is no stable equilibrium point. Let us discuss it.

Figure 2.13 – Bifurcation diagrams considering high cloning rate for the weak tissue response case. The blue color corresponds to stable states, while the red color represents the unstable ones.

(a) $\theta = 2.4 \times 10^{-5}$ (b) $\theta = 4 \times 10^{-5}$

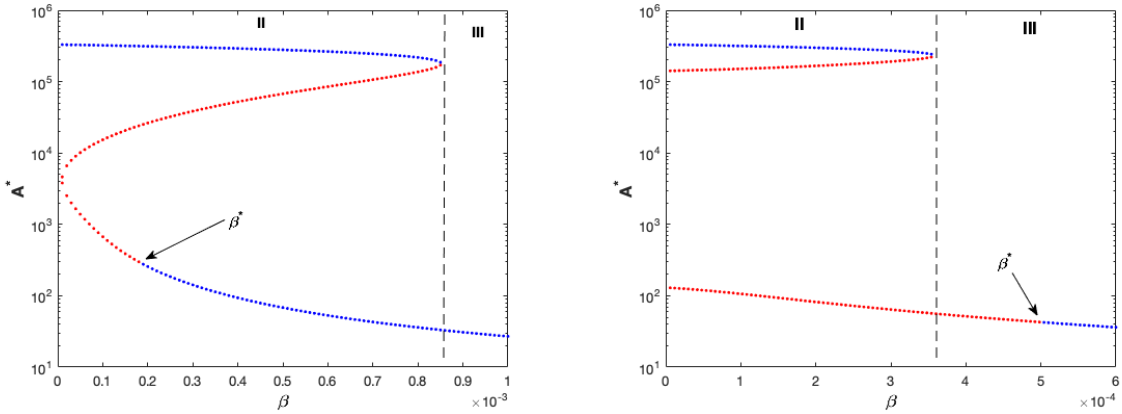

At $\beta = \beta^*$ a Hopf bifurcation was observed: the remission state has a pair of complex eigenvalues whose real part becomes positive for $\beta < \beta^*$, and a periodic solution (or limit cycle) arises around the remission state. In Figure 2.14 we present two trajectories to illustrate the appearance of the periodic solution when $\beta < \beta^*$. Figure 2.14a contains the $A \times C$ plane in which the black squares represent the initial point of each trajectory and the asterisk $(*)$ corresponds to the remission state. Figure 2.14b contains the time evolution of the tumor for each trajectory.

Figure 2.14 – Numerical simulations of system (2.2)-(2.1) considering $\theta = 2.4 \times 10^{-5}$, $\beta = 1.8 \times 10^{-4}$.

(a) Dynamical trajectories in $A \times C$ plane. (b) Tumor temporal evolution.

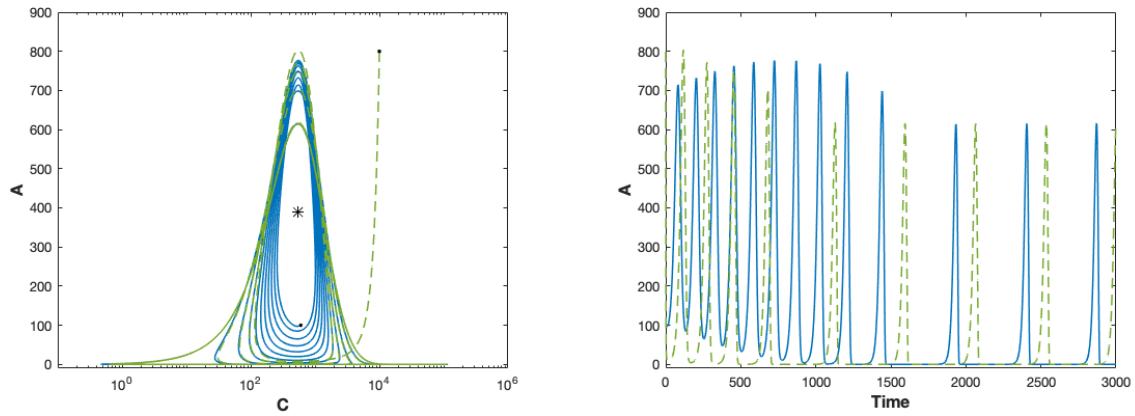

In the blue trajectory, we take an initial condition close to the remission state, where all the state variables are at the equilibrium value, excepts A. In this simulation, we observe that the trajectory oscillates around the equilibrium and approaches the limit cycle. Taking an initial condition outside the limit cycle, the solution may also approaches

the periodic solution, like in the green trajectory. So, the limit cycle is stable. On the other hand, if the initial condition is far from the remission state, the trajectory may approach tumor state. Therefore, there is bistability between the limit cycle and the tumor state.

The amplitude and period of the limit cycle are related to the value of β. The smaller this parameter, the greater the amplitude of the solutions and the greater the time between the peaks, consequently, as β approaches β^* the amplitude of the limit cycle decreases until it collapses in the equilibrium point exactly at $\beta = \beta^*$, from then on the remission state becomes stable.

To illustrate this, we present in figure 2.15 simulations considering different values for the parameter β.

Figure 2.15 – Effect of killing rate β on amplitude and periodicity of the limit cycles.

(a) Dynamical trajectory in $A \times C$ plane

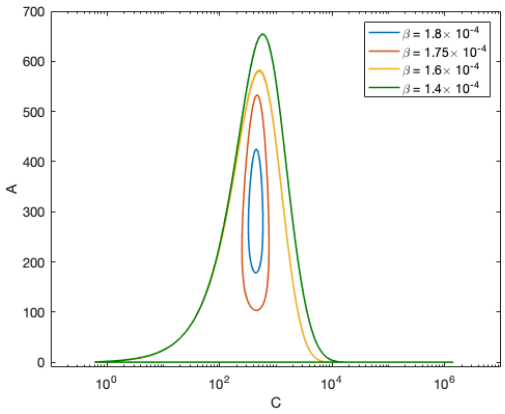

(b) Tumor temporal evolution

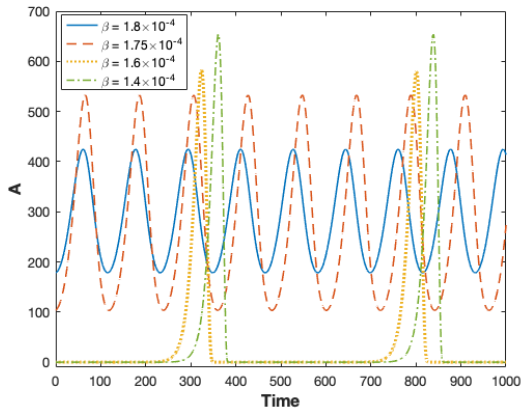

This same behavior occurs in the figure 2.13b: the emergence of the limit cycle for $\beta < \beta^*$. Note that in this case there is a region where the remission equilibrium is the only one that exists. In this case, for any initial condition used, the trajectories always approach the limit cycle, no matter how far they are from the remission state, since tumor equilibrium does not exist in this region. Figure 2.16 illustrates the behavior of the system in this situation.

Remember that both, clonal expansion and antigen presentation, only occur in the presence of tumor cells, so the more tumor cells, the greater the antigen presentation and lymphocytes activation, or equivalently, the fewer tumor cells, the lesser the activation of lymphocytes. The existence of periodic solutions can be biologically interpreted as follows: tumor cells trigger an immune response, which contains a huge number of CTLs due to unlimited clonal expansion. These CTLs decrease the tumor population, remaining only a few cells. As a consequence, the clonal expansion and antigen presentation decrease, since there are only a few tumor cells, and CTLs start to dye by apoptosis. Decreasing the number of immune cells makes TME favorable to tumor progression, so tumor cells

Figure 2.16 – Numerical simulations of the limit cycle for $\theta = 4 \times 10^{-5}$ and $\beta = 4 \times 10^{-4}$.

(a) Dynamical trajectory in $A \times C$ plane.

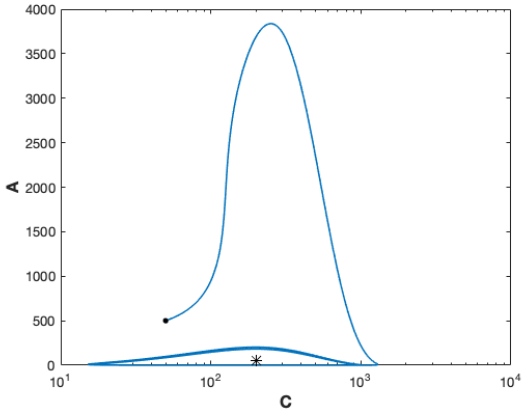

(b) Tumor temporal evolution.

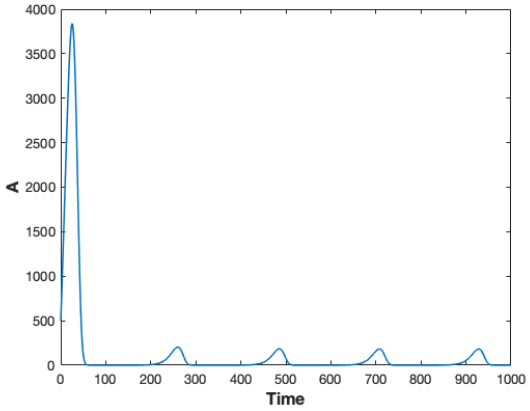

start to proliferating again, which, in turn, trigger a new immune response and restart the cycle, characterizing the periodic solutions.

Conclusão e Perspectivas Futuras

Nesta tese foram propostos e analisados modelos matemáticos para a interação tumor-hospedeiro-imunidade considerando diversos aspectos da resposta imune antitumoral além dos mecanismos usados pelos tumores para evadir o sistema imune. Os modelos, apensar de teóricos e generalistas, podem servir de base para uma melhor compreensão da resposta imunológica contra tumores, além de gerar perspectivas sobre o uso de imunoterapias e abrir caminhos para futuras pesquisas abordando tipos específicos de neoplasias com suas particularidades e tratamentos.

No Capítulo 1 propomos um modelo simplista que aborda a resposta do hospedeiro à presença de tumor contendo dois tipos diferentes de células, diferenciadas pela carga mutacional: as células do tipo 1 acumulam mutações ao longo do tempo e assim passam a ser definidas como células do tipo 2. Por meio da análise deste modelo, determinos as condições sob as quais teremos a formação de um tumor heterogêneo, com ambas células existindo, ou homogêneo, quando a célula do tipo 2 é capaz de deslocar a primeira. Inicialmente observamos que, ao considerar que o fenótipo mais mutado possui um fitness melho, isto é, maior taxa de replicação e menos mortalidade natrual, então estas células sempre irão deslocar as demais e ocorrerá sempre a formação de um tumor homogêneo. Por outro lado, quando as células do tipo 1 possuem melhor fitness elas podem se estabelecer no hospedeiro a depender principalmente da taxa de acúmulo de mutações α. Quando o acúmulo de mutações ocorre de maneira rápida, α elevado, então sempre ocorrerá o desaparecimento das células menos mutadas e uma sobreposição das células do tipo 2. Por outro lado, quando a mutação ocorre de maneira bastente lenta as células do tipo 1 sempre irão de estabelecer, formando assim uma massa tumoral composta pelos dois tipos celulares. Por fim, a região transiente determinado por um valor de α intermediário permite ambas situações: uma relação entre b e c passa a determinar se a massa tumoral será homogênea ou heterogênea.

No Capítulo 2 propomos um modelo matemático considerando a formação da resposta imune antitumoral, desde o reconhecimento dos neoantúgenos pelas células dendríticas, até a ativação dos linfócitos efetores $CD4^+$ e $CD8^+$ no linfonodo regional.

Com base nas análises qualitativas e de simulações numéricas foi possível caracterizar regiões do espaço paramétrico em que ocorrerão cura, progressão, remissão ou mesmo recidiva tumoral. Quando a resposta tecidual do hospedeiro é forte e a agressividade tumoral é baixa então o próprio corpo do hospedeiro será capaz de eliminar as células tumorais, por outro lado se o tumor for agressivo então ele poderá progredir a depender a massa tumoral inicial. No caso de uma resposta tecidual fraca do hospedeiro, a cura não é mais uma possibilidade, no entanto as células imunes podem levar o tumor à remissão, mantendo o número de células anormais em níveis baixos e não perceptíveis. Ainda nesta situação, observamos que o tumor apresenta uma resistência natural á resposta imune, que necessita atingir um valor específico para poder derrubar a defesa das células neoplásicas. Os mecanismos de evasão tumoral desempanham um papel crucial e se mostraram o ponto chave para progressão do tumor. Quanto maiores os valores destes parâmetros, maior é a resistência do tumor à ação imune e mais eficiente precisa ser a resposta antitumoral para que a remissão seja alcançada. Inclusive tumores pouco agressivos apresentam tal resistência quando a evasão tumoral é incluída no modelo, mostrando que esta ainda é a principal barreira enfrentada pelo hospedeiro no controle da progressão. Também avaliamos algumas características da expansão clonal dos linfócitos, como isto afeta a dinâmica do modelo e suas implicações biológicas e matemáticas.

Por fim, usamos o modelo de resposta imune proposto no capítulo 2 para simular o uso de tratamentos imunoterápicos em pacientes. Especificamente, simulamos que a aplicação de certas drogas, como os inibidores de checkpoints imunológico, podem inibir os mecanismos de evasão temporariamente. Ao fazer isso, um paciente que se encontra em uma situação de progressão tumoral pode ser "levado"a um regime de remissão, sendo assim o número de células tumorais começa a diminiur enquanto o tratamento é aplicado. Se o tratamento durar tempo suficiente para que a população tumoral atinja o nível crítico, então mesmo após seu interrompimento o tumor não mais continuará crescendo, por outro lado se o tratamento for interrompido antes deste ponto crítico, as células tumorais voltam a progredir. Além disso, pacientes com baixa resposta tecidual ou um sistema imune comprometido podem não responder ao tratamento, independende da sua duração, conforme simulações realizadas.

Ao longo do trabalho percebemos como a dinâmica tumoral pode se apresentar complexa, com diversas particularidades que devem ou não ser abordadas dependendo dos objetivos de estudo, do tumor a ser analisado, dentre outros fatores. Ainda que os modelos apresentados aqui sejam teóricos, foi possível extrair informação a cerca do papel da resposta imune que poderão dar luz a diversas questões além de abrir caminhos para estudos futuros, especialmente no que tange á imunoterapia e combinações de diferentes tratamentos como quimioterapia e terapia alvo.

Na próxiuma sessão abordaremos alguns assuntos que foram levantados ao

longo do desenvolvimento deste trabalho mas não devidamente concluídos, sendo assim de interesse para trabalhos futuros e contiação direta dos estudos que foram desenvolvidos nesta tese.

CÉLULAS T REGULADORAS NA DINÂMICA TUMOR-IMUNIDADE

As células T reguladoras (Tregs) compreendem um conjunto de células imunosupressoras que desempenham um papel importante na manutenção da homeostase, auxiliando no controle da autominudade, processos inflamatórios, tolerância materno-fetal, controlando assim a ação do sistema imune contra o próprio organismo (68).

A atividade supressora das Tregs pode ocorrer por contato célula-célula, ou de maneira independente. Os principais mecanismos utilizados por estas células para o controle das repostas imunes incluem a secreção de citocinas supressoras, checkpoints imunológicos, citotoxidade, de forma a causar a lise de células inflamatórias, dificultar a atividade dos linfócitos T atuando na exaustão dessas células e/ou consumindo IL-2, citoncina envolvida na proliferação dos linfócitos (69, 70).

As células tumorais secretam uma série de quimiocinas que recrutam Tregs ao microambiente tumoral, onde são capazes de suprimir a resposta imune e contribuir para o desenvolvimento de um microambiente imunossuprimido, promovendo assim a evasão das células tumorais e facilitando o desenvolvimento do tumor (71). Além disso, células $CD4^+$ normais podem ser convertidas em Tregs no microambiente tumoral. Deste modo, grandes infiltrados de células Tregs normalmente estão associados a prognósticos ruins.

Nesta seção apresentaremos brevemente o efeito destas céluas na dinâmica tumor-imunidade descrita no capítulo 2. Para isto, iremos considerar que parte das linfócitos efetores $CD4^+$ presentes no linfonodo (denotados por H_l) irão migrar para o microambiente tumoral, se apresentando como células T reguladoras, denotadas por H. Esta migração, como já mencionado, é dependente do estímulo gerado pelas células tumorais, de modo que o fluxo de H_l para H será representado pela expressão $\phi_r A/(g+A)$. Uma vez no linfonodo as Tregs irão atrapalhar a ação citotóxica dos linfócitos efetores C por meio da taxa de supressão denotada pelo parâmetro ξ. As equações que representam as variáveis H_l, H e C estão apresentadas abaixo, todas as demais variáveis possuem as mesmas equações apresentadas no modelo 2.1-2.2.

$$\begin{cases} \dfrac{dH_l}{dt} &= \sigma_h H_v D_{al} + \theta_h H_l D_{al}\left(1-\dfrac{H_l}{Q_h}\right) - \mu_h H_l - \dfrac{\phi_r A}{g+A} H_l \\ \dfrac{dR}{dt} &= r\dfrac{\phi_r A}{g+A} H_l - \mu_r H \\ \dfrac{dC}{dt} &= q\phi_c C_l - \rho_1 A_1 C - \rho_2 A_2 C - \xi H C - \mu_c C + \tau C_d \end{cases} \tag{2.13}$$

Para analisar o efeito das células Tregs nós reconstrímos os diagramas de bifurcação apresentados no capítulo anterior para diferentes valores dos parâmetros ϕ_r e ξ, que correspondem respectivamente ao fluxo de Tregs para o microambiente tumoral e o efeito supressor destas células sobre os linfócitos T citotóxicos. No geral, pôde-se observar que o efeitos destas células na dinâmica do modelo são similares aos mecânismos de evasão representados por ν e ρ. No caso de resposta tecidual forte, ficou evidente que aumentar tanto ϕ_r, quanto ξ, diminui a agressividade tumoral necessária para que o tumor se estabeleça, de maneira similar ao que foi mostrado no diagrama 2.8, sendo assim tumores menos agressivos podem se estabelecer no hospedeiro. De modo semelhante, para uma fraca resposta tecidual, observou-se que as Tregs facilitam o surgimento da histerese, além de aumentar o valor de β necessário para que o sistema imune consiga levar o tumor à remissão. Os grágicos obtidos ao aumentarmos o valor da taxa de supressão ξ é similar ao caso apresentado em 2.9 e por isso não será mostrado aqui.

A principal consequência decorrente da inclusão de tais células no modelo foi observada quando aumentamos as taxas de clonagem ϕ_c e ϕ_h dos linfócitos efetores. Uma vez que assumimos que uma parcela das células $CD4^+$ migra para o linfonodo como Tregs, a expansão clonal passa a ter um efeito ambiguo: ela aumenta a população de linfócitos efetores e por consequência a população de CTLs no microambiente tumoral, mas por outro lado aumenta também a população de Tregs que inibe o funcionamento dos CTLs, assim impulsionando e suprimindo a resposta imune simultâneamente.

Para o caso de resposta tecidual forte, ao simularmos diferentes combinações dos parâmetros ξ, θ_h, θ_c e β, encontramos a possibilidade de mais de uma histerese, isto é, poderão surgir mais regiões com três pontos de equilíbrio tumoral ou mesmo regiões com cinco pontos de equilíbrio. Para ilustrar tal situação apresentamos na Figura 2.17 a existência e estabilidade dos pontos de equilíbrio á medida que aumentamos β, fixados ξ, θ_h e θ_c

Figure 2.17 – Efeito das Tregs na dinâmica tumoral considerando alta taxa de clonagem e resposta tecidual forte.

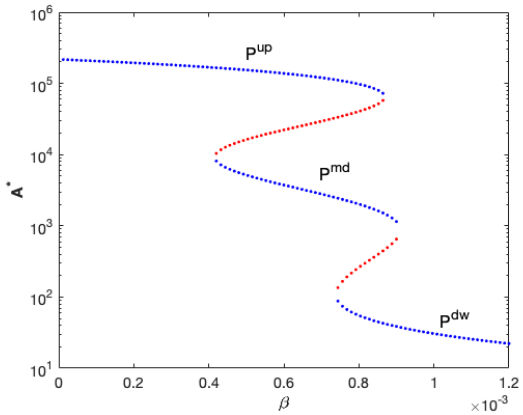

Veja que, inicialmente, para valores baixos de β, o único ponto de equilíbrio existente é P^{up}, com uma alta carga tumoral. Á medida que aumentamos a taxa de morte pelos CTLS (β), observamos o surgimento de um segundo ponto de equilíbrio tumoral P^{md}, neste caso h;a bistabilidade entre os pontos, e podemos inferir que o sistema imune é capaz de reduzir a população tumoral para um estágio menor, mas ainda não o suficiente para controlá-lo. Aumentando ainda mais β o ponto de equilíbrio de controle P^{dw} surge na dinâmica. Note que para um determinado intervalo os três pontos de equilíbrio podem coexistir. Quando β se torna grande P^{dw} se torna o único equilíbrio existente e portanto o sistema imune é capaz de controlar o tumor.

Portanto, quando incluímos as células Tregs, o sistema imune não é capaz de levar o tumor ao estágio de controle de forma direta, mas antes disso precisa passar por um equilíbrio intermediário, no qual a massa tumoral está presente, porém reduzida em comparação ao equilíbrio superior P^{up}.

Este comportamento pode afetar o uso de tratementos baseados em imuno terapia. No capítulo 2 abordamos como o uso de tal tratamento poderia ser simulado, usando o fato de que a terapia deslocaria as curvas apresentadas. Aqui o mesmo pode ser feito, no entanto, uma vez que existêm mais pontos de equilíbrio, mais desfechos possíveis podem ser observados, além da remissão ou progressão tumoral.

A depender da combinação dos parâmetros as regiões de existência de cada equilíbrio tumoral pode mudar, aumentando ou reduzindo as regiões de histerese a depender de ξ, β e da taxa de clonagem. Sendo assim, mais análises e simulações devem ser feitas para melhor caracterizar a dinâmica do sistema proposto.

MODELANDO DIFERENTES IMUNOGENICIDADES NA RESPOSTA CELULAR ANTITUMORAL

No Capítulo 1 propomos um modelo simples descrevendo a dinâmica tumor-hospedeiro considerando duas populações tumorais, diferenciadas pelo acúmulo de mutações. A partir da análise do modelo e de simulações numéricas verificamos que, a depender do fitness de cada fenótipo tumoral e da relação tumor-hospedeiro, a célula com maior carga mutacional poderia deslocar a menos mutada e extingui-la do hospedeiro, ou então ambas poderiam coexitir, formando um tumor heterogêneo neste aspecto.

No segundo capítulo, por outro lado, analisamos um modelo para a interação tumor-hospedeiro-imunidade, considerando um único tipo de célula tumoral. Através de simulações numéricas nós caracterizamos as possibilidades de cura, remissão e recidiva a partir das repostas imunes.

É de se saber que a carga mutacional de um tumor pode ser utilizada para

predizer a reposta a um tratamento imunoterápico pois, espera-se que o sistema imune seja capaz de encontrar e eliminar tais células com maior ou menor facilidade. Deste modo, a pressão exercida pelo sistema imune pode alterar a seleção das células mais ou menos mutadas no microambiente tumoral que estudamos no primeiro capítulo. Com base nisso, propomos aqui um modelo unificando os capítulos 1 e 2, isto é, um modelo que incorpora duas populações tumorais diferenciadas pelo acúmulo de carga mutacional juntamente com a resposta imune do hospedeiro. A ideia é modelar que cada população tumoral apresenta uma imunogenicidade diferente, ou seja, iremos assumir que tumores que carregam mais mutações desencadeiam mais resposta imune e são eliminados mais facilmente.

As variáveis incluídas no modelo são apresentadas na tabela 2.4

Table 2.4 – Variáveis do modelo unificado 2.14-2.15

	Description	Unit
TME Variables		
A_1	Tumor cells	$cell/vol_t$
A_2	Mutated Tumor cells	$cell/vol_t$
N	Healthy tissue cells	$cell/vol_t$
C	Cytotoxic T Lymphocytes (CTLs)	$cell/vol_t$
C_d	Disabled CTLs	$cell/vol_t$
H	Regulatory T cells (Tregs)	$cell/vol_t$
D	Dendritic cells	$cell/vol_t$
D_a	Activated dendritic cells	$cell/vol_t$
LN Variables		
H_v	Naïve $CD4^+$ cells	$cell/vol_{ln}$
H_l	Effector $CD4^+$ cells in LN	$cell/vol_{ln}$
C_v	Naïve $CD8^+$ cells	$cell/vol_{ln}$
C_l	Effector $CD8^+$ cells in LN	$cell/vol_{ln}$
D_{al}	Activated dendritic cells in LN	$cell/vol_{ln}$

Na figura abaixo apresentamos um diagrama que ilustra a dinâmica do sistema. Veja que o modelo é essencialmente o mesmo apresentado no capítulo 2, porém incluindo duas populações tumorais, A_1 e A_2 de modo que o acúmulo de mutações diferencia as células do tipo 1 para o tipo 2. Além disso, consideramos também o recrutamento de células T reguladoras para o microambiente tumoral, conforme foi discutido na seção anterior.

Baseado neste diagrama, apresentamos abaixo as equações que descrevem a dinâmica do modelo.

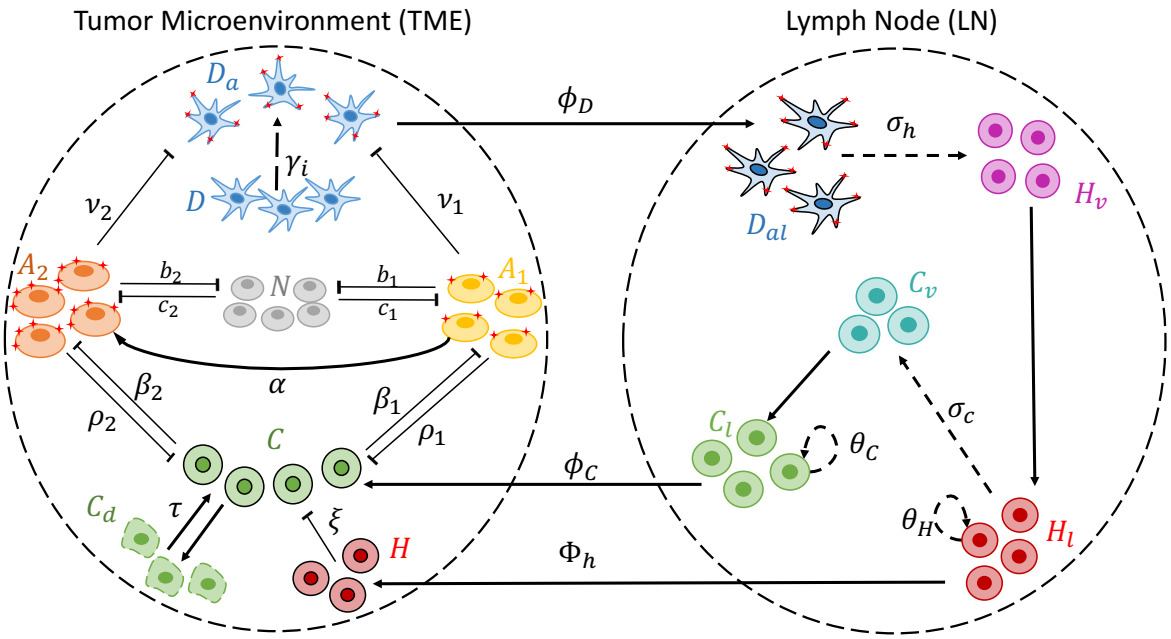

Figure 2.18 – Diagrama ilustrativo da dinâmica celulas proposta no modelo unificado 2.14-2.15

$$
\text{TME}\begin{cases}
\dfrac{dN}{dt} &= r_n - b_1 N A_1 - b_2 N A_2 - \mu_n N \\
\dfrac{dA_1}{dt} &= r_1 A_1 \left(1 - \dfrac{A_1 + A_2}{K}\right) - \alpha A_1 - c_1 A_1 N - \beta_1 A_1 C - \mu_1 A_1 \\
\dfrac{dA_2}{dt} &= r_2 A_2 \left(1 - \dfrac{A_1 + A_2}{K}\right) + \alpha A_1 - c_2 A_2 N - \beta_2 A_2 C - \mu_2 A_2 \\
\dfrac{dC}{dt} &= q\phi_c C_l - \rho_1 A_1 C - \rho_2 A_2 C - \xi H C - \mu_c C + \tau C_d \\
\dfrac{dC_d}{dt} &= \rho_1 A_1 C + \rho_2 A_2 C + \xi H C - (\tau + \mu_c) C_d \\
\dfrac{dR}{dt} &= r \dfrac{\phi_r A}{g + A} H_l - \mu_r H \\
\dfrac{dD}{dt} &= r_d - \gamma_1 A_1 D - \gamma_2 A_2 D - \mu_d D \\
\dfrac{dD_a}{dt} &= \gamma_1 A_1 D + \gamma_2 A_2 D - \nu_1 A_1 D_a - \nu_2 A_2 D_a - (\phi_d + \mu_{da}) D_a
\end{cases} \tag{2.14}
$$

$$
\text{LN}\begin{cases}
\dfrac{dD_{al}}{dt} &= p\phi_d D_a - \mu_{dal} D_{al} \\
\dfrac{dH_v}{dt} &= r_h - \sigma_h H_v D_{al} - \mu_{hv} H_v \\
\dfrac{dH_l}{dt} &= \sigma_h H_v D_{al} + \theta_h H_l D_{al} \left(1 - \dfrac{H_l}{Q_h}\right) - \mu_h H_l - \dfrac{\phi_r A}{g + A} H_l \\
\dfrac{dC_v}{dt} &= r_c - \sigma_c C_v H - \mu_{cv} C_v \\
\dfrac{dC_l}{dt} &= \sigma_c C_v H + \theta_c C_l H \left(1 - \dfrac{C_l}{Q_c}\right) - (\phi_c + \mu_{cl}) C_l
\end{cases} \tag{2.15}
$$

Os parâmetros usados na modelagem estão descritos na tabela 2.4.

Table 2.5 – Parâmetros do modelo unificado 2.14-2.15

Parameter	Description	Value	Reference
r_n	Recruitment rate of Normal cells	10^5	(50, 51, 52)
r_d	Recruitment rate of DCs	5×10^2	(53)
r_c, r_h	Recruitment rate of Naive lymphocytes	10^3	(53)
r_1 (r_2)	Tumor intrinsic growth rate	4.3×10^{-1}	(54)
μ_1 (μ_2)	Tumor natural death rate	0.02	Assumed
μ_n	Normal cells natural death rate	0.143	(55)
μ_d	Immature DCs natural death rate	0.01	(53)
μ_{da}, μ_{dal}	Mature DCs natural death rate	0.02	(53)
μ_{hv}, μ_{cv}	Naive lymphocytes natural death rate	0.1	(53)
μ_h, μ_c	Effector lymphocytes natural death rate	0.3	(53, 56)
K	Tumor carrying capacity	0.75×10^6	Assumed
b_1, b_2	Tumor cells aggressiveness		Variable
c_1, c_2	Tissue response to tumor cells		Variable
α	Mutation rate		Variable
γ_1 (γ_2)	Antigen presentation coefficient	10^{-4}	(54)
ϕ_d	DCs flux to lymph node	0.9	(57, 58)
ϕ_c	Effector $CD8^+$ flux to TME	0.9	(53)
ϕ_r	Tregs flux to TME	0.9	(53)
p, q, r	Density fitness coefficients	0.5	(57, 58)
σ_h,	Naïve $CD4^+$ activation rate	10^{-3}	(59)
σ_c	Naïve $CD8^+$ activation rate	10^{-3}	(59)
w	Proportion of Treg cells	0.1	
θ_h, θ_c,	Effector $CD4^+$ and $CD8^+$ cloning rates		Assumed
θ_r	Treg cloning rate		Assumed
Q_h, Q_c	$CD4^+$ and $CD8^+$ carrying capacity in LN	10^4	(60)
ξ	CTLs suppression by Tregs		Assumed
τ	Disabled CTLs recovery rate	0	-
β	Tumor killing rate by CTLs		Variable
ρ	CTLs blocking coefficient by tumor cells		Assumed
ν	DCs disruption coefficient by tumor cells		Assumed

Devido a alta complexidade das equações em 2.14-2.15, o modelo unificado será estudado por meio de simulações numéricas. A ideia é que em trabalhos futuros possamos explorar o impacto da diferença de imunogenicidade nas populações tumorais na formação de tumores heterogêneos e como a pressão exercida pela resposta imune pode selecionar um fenótipos tumorais ou então permitir a formação de tumores heterogêneos pois, enquanto as células mais mutadas possuem um melhor fitnees, como assumimos no capítulo 1, elas também são mais facilmente reconhecidas e eliminadas pelo sistema imune, deste modo ao mesmo tempo que elas se beneficiam por um lado, perdem pelo outro, o que pode mudar os perfis tumorais quye observamos no capítulo 1. Além disso, nesta nova situação a imunoterapia pode apresentar resultas interessantes e diferentes das simulações realizadas no capítulo 2, pois ao impulsionarmos a resposta imune iremos consequentemente eliminar mais células tumorais com alta carga mutacional, enquanto que as demais podem passar

despercecibas, o que irá interferir no resultado do tramamento ou mesmo na alteração da dinâmica inerente do modelo proposto.

Assim, os modelos apresentados nesta tese além de gerarem informações relevantes e insights teóricos acerca da imunidade contra tumores, também abre espaço para o desenvolvimento de outros estudos relevantes para o tema.

Referências

1 BRAY, F.; LAVERSANNE, M.; WEIDERPASS, E.; SOERJOMATARAM, I. The ever-increasing importance of cancer as a leading cause of premature death worldwide. *Cancer*, Wiley Online Library, v. 127, n. 16, p. 3029–3030, 2021. Citado na página 13.

2 (WHO), W. H. O. *Global Health Estimates 2020: Deaths by Cause, Age, Sex, by Country and by Region, 2000-2019*. 2020. Available at: who.int/data/gho/data/themes/mortality-and-global-health-estimates/ghe-leading-causes-of-death. Accessed at december 16, 2021. Citado na página 13.

3 LESTERHUIS, W. J.; HAANEN, J. B.; PUNT, C. J. Cancer immunotherapy–revisited. *Nature reviews Drug discovery*, Nature Publishing Group, v. 10, n. 8, p. 591–600, 2011. Citado na página 13.

4 HEPPNER, G. H. Tumor heterogeneity. *Cancer Research*, American Association for Cancer Research, v. 44, n. 6, p. 2259–2265, 1984. ISSN 0008-5472. Disponível em: <https://cancerres.aacrjournals.org/content/44/6/2259>. Citado na página 15.

5 MARUSYK, A.; POLYAK, K. Tumor heterogeneity: causes and consequences. *Biochimica et Biophysica Acta (BBA)-Reviews on Cancer*, Elsevier, v. 1805, n. 1, p. 105–117, 2010. Citado na página 15.

6 BURRELL, R. A.; MCGRANAHAN, N.; BARTEK, J.; SWANTON, C. The causes and consequences of genetic heterogeneity in cancer evolution. *Nature*, Nature Publishing Group, v. 501, n. 7467, p. 338–345, 2013. Citado na página 15.

7 SWANTON, C. Intratumor heterogeneity: evolution through space and time. *Cancer research*, AACR, v. 72, n. 19, p. 4875–4882, 2012. Citado 2 vezes nas páginas 15 e 37.

8 MERLO, L. M.; PEPPER, J. W.; REID, B. J.; MALEY, C. C. Cancer as an evolutionary and ecological process. *Nature reviews cancer*, Nature Publishing Group, v. 6, n. 12, p. 924–935, 2006. Citado 2 vezes nas páginas 15 e 37.

9 REITER, J. G.; MAKOHON-MOORE, A. P.; GEROLD, J. M.; HEYDE, A.; ATTIYEH, M. A.; KOHUTEK, Z. A.; TOKHEIM, C. J.; BROWN, A.; DEBLASIO, R. M.; NIYAZOV, J. et al. Minimal functional driver gene heterogeneity among untreated metastases. *Science*, American Association for the Advancement of Science, v. 361, n. 6406, p. 1033–1037, 2018. Citado na página 16.

10 CHEN, D. S.; MELLMAN, I. Oncology meets immunology: the cancer-immunity cycle. *Immunity*, Elsevier, v. 39, n. 1, p. 1–10, 2013. Citado 2 vezes nas páginas 16 e 41.

11 COLLI, L. M.; MACHIELA, M. J.; MYERS, T. A.; JESSOP, L.; YU, K.; CHANOCK, S. J. Burden of nonsynonymous mutations among tcga cancers and candidate immune checkpoint inhibitor responses. *Cancer research*, AACR, v. 76, n. 13, p. 3767–3772, 2016. Citado 2 vezes nas páginas 16 e 60.

12 SNYDER, A.; MAKAROV, V.; MERGHOUB, T.; YUAN, J.; ZARETSKY, J. M.; DESRICHARD, A.; WALSH, L. A.; POSTOW, M. A.; WONG, P.; HO, T. S. et al. Genetic basis for clinical response to ctla-4 blockade in melanoma. *New England Journal of Medicine*, Mass Medical Soc, v. 371, n. 23, p. 2189–2199, 2014. Citado na página 16.

13 ALLEN, E. M. V.; MIAO, D.; SCHILLING, B.; SHUKLA, S. A.; BLANK, C.; ZIMMER, L.; SUCKER, A.; HILLEN, U.; FOPPEN, M. H. G.; GOLDINGER, S. M. et al. Genomic correlates of response to ctla-4 blockade in metastatic melanoma. *Science*, American Association for the Advancement of Science, v. 350, n. 6257, p. 207–211, 2015. Citado na página 16.

14 RIZVI, N. A.; HELLMANN, M. D.; SNYDER, A.; KVISTBORG, P.; MAKAROV, V.; HAVEL, J. J.; LEE, W.; YUAN, J.; WONG, P.; HO, T. S. et al. Mutational landscape determines sensitivity to pd-1 blockade in non–small cell lung cancer. *Science*, American Association for the Advancement of Science, v. 348, n. 6230, p. 124–128, 2015. Citado na página 16.

15 HANAHAN, D.; WEINBERG, R. A. Hallmarks of cancer: the next generation. *cell*, Elsevier, v. 144, n. 5, p. 646–674, 2011. Citado 3 vezes nas páginas 16, 17 e 43.

16 SPENCER, S. L.; BERRYMAN, M. J.; GARCÍA, J. A.; ABBOTT, D. An ordinary differential equation model for the multistep transformation to cancer. *Journal of Theoretical Biology*, Elsevier, v. 231, n. 4, p. 515–524, 2004. Citado na página 16.

17 ENDERLING, H.; CHAPLAIN, M. A.; ANDERSON, A. R.; VAIDYA, J. S. A mathematical model of breast cancer development, local treatment and recurrence. *Journal of theoretical biology*, Elsevier, v. 246, n. 2, p. 245–259, 2007. Citado na página 16.

18 GENTRY, S. N.; JACKSON, T. L. A mathematical model of cancer stem cell driven tumor initiation: implications of niche size and loss of homeostatic regulatory mechanisms. *PloS one*, Public Library of Science, v. 8, n. 8, p. e71128, 2013. Citado na página 16.

19 FASSONI, A. C.; YANG, H. M. Modeling dynamics for oncogenesis encompassing mutations and genetic instability. *Mathematical medicine and biology: a journal of the IMA*, Oxford University Press, v. 36, n. 2, p. 241–267, 2019. Citado na página 16.

20 ALVAREZ, R. F.; BARBUTO, J. A.; VENEGEROLES, R. A nonlinear mathematical model of cell-mediated immune response for tumor phenotypic heterogeneity. *Journal of theoretical biology*, Elsevier, v. 471, p. 42–50, 2019. Citado na página 16.

21 GENTRY, S.; ASHKENAZI, R.; JACKSON, T. A maturity-structured mathematical model of mutation, acquisition in the absence of homeostatic regulation. *Mathematical Modelling of Natural Phenomena*, EDP Sciences, v. 4, n. 3, p. 156–182, 2009. Citado na página 16.

22 TELLO, J. I. On a mathematical model of tumor growth based on cancer stem cells. *Mathematical Biosciences & Engineering*, American Institute of Mathematical Sciences, v. 10, n. 1, p. 263, 2013. Citado na página 16.

23 ENDERLING, H.; HAHNFELDT, P. Cancer stem cells in solid tumors: Is 'evading apoptosis'a hallmark of cancer? *Progress in biophysics and molecular biology*, Elsevier, v. 106, n. 2, p. 391–399, 2011. Citado na página 16.

24 DUNN, G. P.; OLD, L. J.; SCHREIBER, R. D. The three es of cancer immunoediting. *Annu. Rev. Immunol.*, Annual Reviews, v. 22, p. 329–360, 2004. Citado na página 16.

25 SCHREIBER, R. D.; OLD, L. J.; SMYTH, M. J. Cancer immunoediting: integrating immunity's roles in cancer suppression and promotion. *Science*, American Association for the Advancement of Science, v. 331, n. 6024, p. 1565–1570, 2011. Citado na página 16.

26 SIMONS, B. D.; CLEVERS, H. Strategies for homeostatic stem cell self-renewal in adult tissues. *Cell*, Elsevier, v. 145, n. 6, p. 851–862, 2011. Citado 2 vezes nas páginas 17 e 42.

27 FACCIABENE, A.; MOTZ, G. T.; COUKOS, G. T-regulatory cells: key players in tumor immune escape and angiogenesis. *Cancer research*, AACR, v. 72, n. 9, p. 2162–2171, 2012. Citado 2 vezes nas páginas 17 e 43.

28 GATENBY, R. A.; GAWLINSKI, E. T.; GMITRO, A. F.; KAYLOR, B.; GILLIES, R. J. Acid-mediated tumor invasion: a multidisciplinary study. *Cancer research*, AACR, v. 66, n. 10, p. 5216–5223, 2006. Citado 2 vezes nas páginas 17 e 43.

29 ARAUJO, A. L. de; FASSONI, A. C.; SALVINO, L. F. An analysis of a mathematical model describing acid-mediated tumor invasion. *Mathematical Methods in the Applied Sciences*, Wiley Online Library, v. 42, n. 18, p. 6686–6705, 2019. Citado 2 vezes nas páginas 17 e 43.

30 FEDI, P.; TRONICK, S.; AARONSON, S. Growth factors. *Cancer medicine*, Williams and Wilkins, Baltimore, MD, p. 41–64, 1997. Citado na página 17.

31 ANDERSON, B.; JACKSON, J.; SITHARAM, M. Descartes' rule of signs revisited. *The American Mathematical Monthly*, Taylor & Francis, v. 105, n. 5, p. 447–451, 1998. Citado na página 22.

32 FASSONI, A. C.; YANG, H. M. An ecological resilience perspective on cancer: insights from a toy model. *Ecological Complexity*, Elsevier, v. 30, p. 34–46, 2017. Citado 4 vezes nas páginas 23, 24, 41 e 59.

33 WORLD Health Organization. 2018. Accessed 22-09-2020. Citado na página 40.

34 ABBAS, A. K.; LICHTMAN, A. H.; PILLAI, S. *Cellular and molecular immunology E-book*. [S.l.]: Elsevier Health Sciences, 2014. Citado 3 vezes nas páginas 40, 41 e 43.

35 TIAN, T.; OLSON, S.; WHITACRE, J. M.; HARDING, A. The origins of cancer robustness and evolvability. *Integrative Biology*, Oxford University Press, v. 3, n. 1, p. 17–30, 2010. Citado na página 40.

36 BURNET, M. Cancer—a biological approach: Iii. viruses associated with neoplastic conditions. iv. practical applications. *British medical journal*, BMJ Publishing Group, v. 1, n. 5023, p. 841, 1957. Citado na página 41.

37 ROMERO, P.; CEROTTINI, J.-C.; SPEISER, D. E. The human t cell response to melanoma antigens. *Advances in immunology*, Elsevier, v. 92, p. 187–224, 2006. Citado na página 41.

38 GERLONI, M.; ZANETTI, M. Cd4 t cells in tumor immunity. In: SPRINGER. *Springer seminars in immunopathology*. [S.l.], 2005. v. 27, n. 1, p. 37–48. Citado na página 41.

39 VESELY, M. D.; KERSHAW, M. H.; SCHREIBER, R. D.; SMYTH, M. J. Natural innate and adaptive immunity to cancer. *Annual review of immunology*, Annual Reviews, v. 29, p. 235–271, 2011. Citado na página 41.

40 MOTZ, G. T.; COUKOS, G. Deciphering and reversing tumor immune suppression. *Immunity*, Elsevier, v. 39, n. 1, p. 61–73, 2013. Citado na página 41.

41 LIU, V. C.; WONG, L. Y.; JANG, T.; SHAH, A. H.; PARK, I.; YANG, X.; ZHANG, Q.; LONNING, S.; TEICHER, B. A.; LEE, C. Tumor evasion of the immune system by converting cd4+ cd25- t cells into cd4+ cd25+ t regulatory cells: role of tumor-derived tgf-β. *The Journal of Immunology*, Am Assoc Immnol, v. 178, n. 5, p. 2883–2892, 2007. Citado na página 41.

42 LIPPITZ, B. E. Cytokine patterns in patients with cancer: a systematic review. *The lancet oncology*, Elsevier, v. 14, n. 6, p. e218–e228, 2013. Citado na página 41.

43 PILLIS, L. G. de; RADUNSKAYA, A. E.; WISEMAN, C. L. A validated mathematical model of cell-mediated immune response to tumor growth. *Cancer research*, AACR, v. 65, n. 17, p. 7950–7958, 2005. Citado 2 vezes nas páginas 41 e 59.

44 MAHASA, K. J.; OUIFKI, R.; ELADDADI, A.; PILLIS, L. de. Mathematical model of tumor–immune surveillance. *Journal of theoretical biology*, Elsevier, v. 404, p. 312–330, 2016. Citado na página 41.

45 ARCIERO, J.; JACKSON, T.; KIRSCHNER, D. A mathematical model of tumor-immune evasion and sirna treatment. *Discrete & Continuous Dynamical Systems-B*, American Institute of Mathematical Sciences, v. 4, n. 1, p. 39, 2004. Citado 2 vezes nas páginas 41 e 60.

46 ROBERTSON-TESSI, M.; EL-KAREH, A.; GORIELY, A. A mathematical model of tumor–immune interactions. *Journal of theoretical biology*, Elsevier, v. 294, p. 56–73, 2012. Citado na página 41.

47 COLETTI, R.; LEONARDELLI, L.; PAROLO, S.; MARCHETTI, L. A qsp model of prostate cancer immunotherapy to identify effective combination therapies. *Scientific reports*, Nature Publishing Group, v. 10, n. 1, p. 1–18, 2020. Citado na página 42.

48 KERBEL, R. S. Tumor angiogenesis. *New England Journal of Medicine*, Mass Medical Soc, v. 358, n. 19, p. 2039–2049, 2008. Citado na página 43.

49 YANG, H. M. Mathematical modeling of solid cancer growth with angiogenesis. *Theoretical Biology and Medical Modelling*, BioMed Central, v. 9, n. 1, p. 2, 2012. Citado na página 43.

50 HOLT, P.; SCHON-HEGRAD, M. Localization of t cells, macrophages and dendritic cells in rat respiratory tract tissue: implications for immune function studies. *Immunology*, Wiley-Blackwell, v. 62, n. 3, p. 349, 1987. Citado 2 vezes nas páginas 46 e 86.

51 HOLT, P. G. Antigen presentation in the lung. *American journal of respiratory and critical care medicine*, American Thoracic Society New York, NY, v. 162, n. supplement_3, p. S151–S156, 2000. Citado 2 vezes nas páginas 46 e 86.

52 HOLT, P. G.; STUMBLES, P. A. Regulation of immunologic homeostasis in peripheral tissues by dendritic cells: the respiratory tract as a paradigm. *Journal of allergy and clinical immunology*, Elsevier, v. 105, n. 3, p. 421–429, 2000. Citado 2 vezes nas páginas 46 e 86.

53 MARINO, S.; KIRSCHNER, D. E. The human immune response to mycobacterium tuberculosis in lung and lymph node. *Journal of theoretical biology*, Elsevier, v. 227, n. 4, p. 463–486, 2004. Citado 2 vezes nas páginas 46 e 86.

54 UNNI, P.; SESHAIYER, P. Mathematical modeling, analysis, and simulation of tumor dynamics with drug interventions. *Computational and mathematical methods in medicine*, Hindawi, v. 2019, 2019. Citado 2 vezes nas páginas 46 e 86.

55 BOWDEN, D. H. Cell turnover in the lung. *American Review of Respiratory Disease*, American Lung Association, v. 128, n. 2P2, p. S46–S48, 1983. Citado 2 vezes nas páginas 46 e 86.

56 SPRENT, J.; BASTEN, A. Circulating t and b lymphocytes of the mouse: Ii. lifespan. *Cellular immunology*, Elsevier, v. 7, n. 1, p. 40–59, 1973. Citado 2 vezes nas páginas 46 e 86.

57 PENG, H.; ZHAO, W.; TAN, H.; JI, Z.; LI, J.; LI, K.; ZHOU, X. Prediction of treatment efficacy for prostate cancer using a mathematical model. *Scientific reports*, Nature Publishing Group, v. 6, n. 1, p. 1–13, 2016. Citado 2 vezes nas páginas 46 e 86.

58 COLETTI, R.; LEONARDELLI, L.; PAROLO, S.; MARCHETTI, L. A qsp model of prostate cancer immunotherapy to identify effective combination therapies. *Scientific reports*, Nature Publishing Group, v. 10, n. 1, p. 1–18, 2020. Citado 2 vezes nas páginas 46 e 86.

59 MOORE, H.; LI, N. K. A mathematical model for chronic myelogenous leukemia (cml) and t cell interaction. *Journal of theoretical biology*, Elsevier, v. 227, n. 4, p. 513–523, 2004. Citado 2 vezes nas páginas 46 e 86.

60 YOUNG, A. J. The physiology of lymphocyte migration through the single lymph node in vivo. In: ELSEVIER. *Seminars in immunology*. [S.l.], 1999. v. 11, n. 2, p. 73–83. Citado 2 vezes nas páginas 46 e 86.

61 MURRAY, J. D. *Mathematical biology. I, volume 17 of Interdisciplinary Applied Mathematics*. [S.l.]: Springer-Verlag, New York,, 2002. Citado 2 vezes nas páginas 47 e 49.

62 INSTITUTE, N. C. *NCI Dictionary of Cancer Terms*. 2021. Available at: https://www.cancer.gov/publications/dictionaries/cancer-terms. Accessed at december 16, 2021. Citado na página 50.

63 SCHUMACHER, T. N.; SCHREIBER, R. D. Neoantigens in cancer immunotherapy. *Science*, American Association for the Advancement of Science, v. 348, n. 6230, p. 69–74, 2015. Citado na página 56.

64 COUZIN-FRANKEL, J. *Cancer immunotherapy*. [S.l.]: American Association for the Advancement of Science, 2013. Citado na página 56.

65 RIBAS, A.; WOLCHOK, J. D. Cancer immunotherapy using checkpoint blockade. *Science*, American Association for the Advancement of Science, v. 359, n. 6382, p. 1350–1355, 2018. Citado na página 56.

66 PARDOLL, D. M. The blockade of immune checkpoints in cancer immunotherapy. *Nature Reviews Cancer*, Nature Publishing Group, v. 12, n. 4, p. 252–264, 2012. Citado na página 56.

67 JUNE, C. H.; O'CONNOR, R. S.; KAWALEKAR, O. U.; GHASSEMI, S.; MILONE, M. C. Car t cell immunotherapy for human cancer. *Science*, American Association for the Advancement of Science, v. 359, n. 6382, p. 1361–1365, 2018. Citado na página 56.

68 SAKAGUCHI, S.; YAMAGUCHI, T.; NOMURA, T.; ONO, M. Regulatory t cells and immune tolerance. *cell*, Elsevier, v. 133, n. 5, p. 775–787, 2008. Citado na página 81.

69 SHEVACH, E. M. Mechanisms of foxp3+ t regulatory cell-mediated suppression. *Immunity*, Elsevier, v. 30, n. 5, p. 636–645, 2009. Citado na página 81.

70 SCHMIDT, A.; OBERLE, N.; KRAMMER, P. H. Molecular mechanisms of treg-mediated t cell suppression. *Frontiers in immunology*, Frontiers, v. 3, p. 51, 2012. Citado na página 81.

71 CHAUDHARY, B.; ELKORD, E. Regulatory t cells in the tumor microenvironment and cancer progression: role and therapeutic targeting. *Vaccines*, Multidisciplinary Digital Publishing Institute, v. 4, n. 3, p. 28, 2016. Citado na página 81.